Data-assimilation studies of marine, nitrogen based, ecosystem models in the North Atlantic Ocean

Dissertation

zur Erlangung des Doktorgrades

der Mathematisch-Naturwissenschaftlichen Fakultät

der Christian-Albrechts-Universität

zu Kiel

vorgelegt von

Markus Schartau

Kiel

2001

Referent:	Prof. Dr. Jürgen Willebrand
Korreferentin:	Prof. Dr. Karin Lochte
Tag der mündlichen Prüfung:	10. Mai 2001 (Disputation)
Zum Druck genehmigt:	Kiel, ...

Contents

Zusammenfassung

Das übergreifende Ziel dieser Arbeit ist es, die Leistungsfähigkeit von Ökosystem-Modellen zu evaluieren und die Ergebnisse der Modelle für den Nordatlantik mit Beobachtungsdaten zu vergleichen. Um Abweichungen zwischen den Modellergebnissen und den Beobachtungsdaten zu minimieren, werden die Modellparameter mit Hilfe von Assimilationsverfahren optimiert. Zur Optimierung der Parameter werden die adjungierte Methode und ein mikro-genetischer Algorithmus (μGA) eingesetzt. Die Assimilationsexperimente werden mit Modellen durchgeführt welche auf Stickstoff basieren und drei bis vier Zustandsvariablen enthalten (NPZ- und NPZD Modelle): gelöster anorganischer Stickstoff (N), Phytoplankton (P), herbivores Zooplankton (Z) und Detritus (D). Das NPZ Modell simuliert mittlere Konzentrationen dieser Variablen innerhalb der oberen durchmischten Schicht des Ozeans, während das NPZD Modell die Verteilung der Variablen in der Wassersäule vertikal auflöst. Die physikalischen Randbedingungen werden aus Ergebnissen eines dreidimensionalen Ozean-Zirkulationsmodells des Nordatlantiks übernommen, welches mit täglichen atmosphärischen ECMWF-Reanalyse Daten angetrieben wurde.

Um das NPZ-Modell zu optimieren, werden zunächst Assimilationsexperimente durchgeführt mit Beobachtungsdaten der Studie "Bermuda Atlantic Time-series Study (BATS)". Unter Anwendung der adjungierten Methode werden unterschiedliche Lösungen gefunden, sobald von verschiedenen Anfangsschätzungen der Parameter die Optimierung gestartet wird. Es wird gezeigt, daß für die Parameteroptimierung eines Ökosystem-Modells die Anwendung eines μGA besser geeignet ist als ein Gradientenverfahren, einschließlich der adjungierten Methode.

Desweiteren werden simultane Assimilationsexperimente mit dem NPZD Modell durchgeführt, die auf Beobachtungsdaten aus drei verschiedenen Gebieten im Nordatlantik zurückgreifen: BATS, dem Gebiet des "North Atlantic Bloom Experiment (NABE)" und der Station des "Ocean Weather Ship-India (OWS-INDIA)". Die simultane Optimierung liefert einen optimalen Parametersatz, welcher für die beckenweite Simulation gekoppelter physikalisch-biologischer Modelle des Nordatlantiks genutzt werden kann. Die modellierten biogeochemischen Flüsse, die sich mit dem Parametersatz aus den simultanen Optimierungen ergeben, unterscheiden sich deutlich von Modellergebnissen, welche mit früheren Parameterwerten aus der Literatur berechnet werden. Im Gegensatz zu früheren Untersuchungen weisen die Modellergebnisse auf eine schnelle Remineralisierung von organischer Substanz zur Auf-

rechterhaltung der Primärproduktion hin. Systematische Abweichungen zwischen den ^{14}C-Fixierungsraten und der modellierten Primärproduktion werden aufgezeigt. Es wird vorgeschlagen, daß die kohlenstoffbasierte Primärproduktion nicht adäquat von Ökosystem-Modellen simuliert werden kann, wenn ein konstanter Faktor für die Umrechnung von Stickstoff zu Kohlenstoff verwendet wird.

Die erhaltenen physikalischen Randbedingungen sind ausreichend, um die biogeochemischen Flüsse bei BATS und NABE adäquat zu simulieren. Für hohe Breitengrade (wie bei OWS-INDIA) ist die physikalisch-biologische Kopplung im Modell jedoch nicht in der Lage, die im Frühling beobachtete Tiefenverteilung von Chlorophyll darzustellen. Es wird vorgeschlagen, daß zu dieser Zeit ein Wechsel zwischen kurzfristiger Stratifizierung der oberen Wassersäule, eine schnelle biologische Reaktion darauf und eine darauf folgende tiefe Durchmischung des Phytoplanktons für die beobachteten Chlorophyllkonzentrationen in Tiefen von 150 bis 200 Metern verantwortlich sind.

Abstract

The overall goal of this work is to investigate the performance of ecosystem models and to relate their results to existing observations in the North Atlantic. Therefore different data assimilation methods are applied. A variational adjoint technique and a micro-generic algorithm (μGA) are utilized to estimate model parameters, such that the misfit between model results and observations is minimised. Data assimilation experiments are performed with nitrogen based ecosystem models, comprising three and four state variables (NPZ- and NPZD models): dissolved inorganic nitrogen (N), phytoplankton (P), herbivorous zooplankton (Z) and detritus (D). The NPZ-model simulates mean concentrations of the different variables within the upper mixed layer, while the NPZD-model has a vertically resolved grid. Physical boundary conditions are obtained from three-dimensional simulations of the ocean's circulation in the North Atlantic, with daily mean atmospheric forcing from ECMWF-reanalysis data.

First, data assimilation experiments are conducted with observations from the Bermuda Atlantic Time-series Study (BATS) in order to optimise the NPZ-model. While applying the adjoint method different optimal parameter sets are obtained when starting from different initial parameter sets. It is shown that for parameter optimisation of an ecosystem model, the application of the μGA is superior to the performance of the adjoint method.

Second, simultaneous assimilation experiment are performed with the NPZD-model using observational data from three locations in the North Atlantic: BATS, the site of the North Atlantic Bloom Experiment (NABE) and the Ocean Weather Ship-India (OWS-INDIA). The simultaneous optimisation yields a best parameter set, which can be utilized for basin wide simulations in coupled physical-biological (general circulation) models of the North Atlantic.

The parameter set retrieved from the simultaneous optimisations produces substantial differences in the biogeochemical fluxes when compared with model results using previously published parameters. In contrast to earlier models the rapid cycling of organic matter for sustaining primary production is emphasized. Furthermore, systematic discrepancies between ^{14}C-fixation rates and modelled primary production are identified. It is suggested that carbon based primary productivity may not be adequately represented by ecosystem models when a constant nitrogen to carbon conversion factor is assumed.

The chosen physical boundary conditions are adequate to simulate the biogeochemical fluxes at the BATS and NABE sites. At high latitudes (OWS-INDIA), however, the physical-biological interactions in the model cannot represent the observed chlorophyll distribution in spring. It is suggested that during this period short-termed alterations of stratification, rapid biological response and deep mixing of phytoplankton are necessary in order to reproduce chlorophyll concentrations at depths of 150-200m.

"*In our endeavor to understand reality we are somewhat like a man trying to understand the mechanism of a closed watch. He sees the face and the moving hands, even hears its ticking, but he has no way of opening the case. If he is ingenious he may form some picture of a mechanism which could be responsible for all the things he observes, but he may never be quite sure his picture is the only one which could explain his observations.*"
—Albert Einstein and Leopold Infeld, *The Evolution of Physics*

Abbreviations

BATS	Bermuda Atlantic Time-series Study
BBSR	Bermuda Biological Station of Research
BODC	British Oceanographic Data Center
BS	Bootstrap method
CHL	Chlorophyll a
CO_2	Carbon dioxide
DCM	Deep chlorophyll maximum
DIC	Dissolved inorganic carbon
DIN or N	Dissolved inorganic nitrogen
DOM	Dissolved organic matter
DON	Dissolved organic nitrogen
ECMWF	European Center for Medium Range Weather Forecast
EP85	Phytoplankton light limited growth function according to Evans and Parslow 1985
FDM-model	Ecosystem model according to Fasham, Ducklow and McKelvie 1990
GA	Genetic algorithm for optimisation
GCM	General circulation model
GFDL	Geophysical Fluid Dynamics Laboratory
HA-model	Ecosystem model with allometric parameterisation proposed by Hurtt and Armstrong 1996
JGOFS	Joint Global Ocean Flux Study
mGA or μGA	Micro-genetic algorithm for optimisation
MPDCD	Multidimensional positive definite centered differences advection scheme
MLD	Mixed layer depth
MOM	Modular Ocean Model

NABE	North Atlantic Bloom Experiment
NADR	North Atlantic Drift Region
NAO	North Atlantic Oscillation
NO_2	Nitrite
NO_3	Nitrate
NPZ-model	Ecosystem model with dissolved inorganic nitrogen (N), phytoplankton- (P) and zooplankton biomass (Z)
NPZD-model	Ecosystem model with dissolved inorganic nitrogen (N), phytoplankton- (P), zooplankton biomass (Z) and detritus (D)
NPZD-wW	NPZD-model with vertical advective velocities
NPZD-nW	NPZD-model with no vertical advective velocities regarding sinking of detritus only.
OG-model	Coupled physical-biological ocean circulation model of the North Atlantic according to Oschlies and Garcon 1999
OWS-INDIA	Ocean weather ship INDIA
PAR	Photosynthetic available radiation
PDF	Probability density function
POC	Particulate organic carbon
POM	Particulate organic matter
PON	Particulate organic nitrogen
PRIME-project	Phytoplankton Reactivity In the Marine Environment project
SA	Simulated annealing algorithm for optimisation
SARC	Atlantic Subarctic Province
SMS	Biological source minus sink terms in advective-diffusive equation
TKE	Turbulent kinetic energy
VM	Variable metric algorithm for optimisation
W-NAST	Western part of the North Atlantic Subtropical Gyre Province
0D	Zero-dimensional, here used for ecosystem models of the upper mixed layer with varying box sizes
1D	one-dimensional, here used for ecosystem models with vertical resolution

1

Introduction

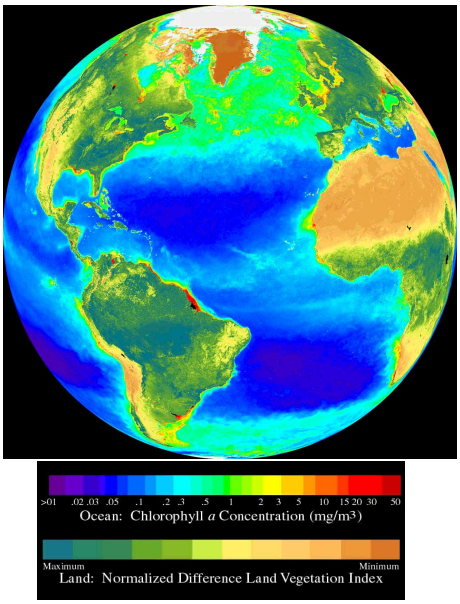

Figure 1.1: Seawifs false color picture of the ocean surface *cholorphyll a* concentration in the Atlantic Ocean, averaged over a period of 10 months (September 1997 to July 1998). Picture source: `http://seawifs.gsfc.nasa.gov/SEAWIFS/IMAGES/SEAWIFS_GALLERY.html`.

To date there is no doupt that the earths atmosphere is considerably affected by human activities. This is particularly true for the atmospheric content of carbon dioxide (CO_2) which has risen proportional to industrial emmissions from pre-industrial values of 280 ppm to 360 ppm in 1994 (Keeling et al. 1995). The natural atmospheric CO_2 content has an impact on the earth's radiation budget since it considerably absorbs, along with water vapour, long-wave infrared radiation. For this ability it is regarded as being one of the greenhouse gases. Hence, the atmospheric CO_2 concentration is of general scientific interest and its possible effect on climate changes is extensively investigated, covering several fields of research.

The ocean's role is crucial because its interface with the atmosphere allows for

a CO_2 gas exchange. CO_2 dissolves chemically in seawater and can be transported into the oceans interior through deep water formation. For instance, at high latitudes cold surface waters can pick up CO_2 and as soon as those water parcels start to sink they carry dissolved carbon to depth which can then be transported over the hemisphere by ocean circulation (Broecker and Peng 1992). This process is called physical oceanic carbon pump. Besides these physical-chemical interactions the carbon pump is influenced by biological processes. Marine phytoplankton assimilate dissolved inorganic carbon into particulate organic carbon (POC), which is remineralized by heterotrophic organisms or eventually exported to deep waters through sedimentation (Eppley and Peterson 1979, Volk and Hoffert 1985), known as biological pump (or "organic matter pump"). The upper ocean's chlorophyll concentration indicates that the formation of POC by phytoplankton is large, Figure (1.1). Nevertheless, there are large uncertainties about the extent of the biological carbon pump and estimates range from 4 to 20 Gt yr^{-1}. Due to high temporal and spatial variability the biological carbon uptake and its sequestration is difficult to determine. Biological productivity in the ocean fundamentally depends on the ocean's physics and chemistry. Therefore large-scale estimates of the biological pump rely on biological (ecosystem) models embedded in general ocean circulation models.

1.1 Marine ecosystem models

The biological variations of the dissolved inorganic carbon concentration in the ocean are relatively small and difficult to detect against high background values. For the determination of carbon fluxes most ecosystem models are based on nitrogen. This is justified by a theory based on several concepts. First, a reciprocal interaction between the elemental composition of marine biota and their dissolved nutrition resources is assumed, whereby the nutrient elements are taken up and released in fixed proportions of C:N:P of 106:16:1 (Redfield et al. 1963). Second, it is assumed that the biological production in the ocean is principally limited by the availability of nitrogen, meaning that the supply of nitrogen also determines the amount of carbon incorporated into biomass. Production based on nitrogen (e.g. nitrate), which newly enters the euphotic zone, where light availability is sufficient for net growth, is referred to as new production and is differentiated from production based on the remineralized compounds of nitrogen (Dugdale and Goering 1967). According to Eppley and Peterson (1979) the export flux of organic material from this upper oceanic layer equals the new production. Thus, to understand the cycling of nitrogen is a necessary prerequisite to modelling the biological carbon cycle (Fasham and Evans 1995).

The aim of simulating relevant biological processes of the nitrogen cycle has led to the development of relatively simple nitrogen-based models of marine ecosystems. Such models were coupled to basin-scale general circulation models of the North Atlantic (Sarmiento et al., 1993, Oschlies et al., 2000). One could argue whether these models really simulate ecosystems or should rather be named biogeochemical

models. That is, because such models simply transfer mass from an inorganic reservoire into organic pools and may lack, for instance, important ecological processes. Nevertheless, the terminology "ecosystem model" is commonly used for those biological models that include parameterisations mostly describing mass exchange rates. In general the model parameters are considered to be constant in time. Hence, the model solutions strongly depend on the choice of the corresponding biological parameters which, in addition, need to represent a diversity of individual organisms, grouped into compartments of, for example, phytoplankton and herbivorous zooplankton. Since the model parameters should represent a complex system in such a simple way, their appropriate estimate remains a major challenge.

1.2 Reliability and associated problems

Concept for data-assimilative approach

One long term interest of biogeochemical modelers is to first check relatively simple models for consistency and thereby discover the most important processes that need to be considered for large–scale predictions of biogeochemical fluxes. If these most prevailing processes are recovered and correctly parameterised, such a basic model could then be gradually modified and be extended for local process studies as well. The model of Fasham et al. (1990), hereafter named FDM-model, was the first attempt to include all essential processes, yielding a model with seven state variables (a seven compartment model).

For ecosystem modelling it is inevitable to validate the applied model equations and to justify the associated complexity. Many marine ecosystem models consist of parameterisations which are believed to describe certain biogeochemical processes within the ocean. Only few parameterisations are based upon measurements, conducted in laboratories and in the open ocean. This is in strong contrast, for example, to physical models of the ocean circulation, which are mainly build on the sound theory of the Navier-Stokes equation. Yet, there is, apart from the conservation of the number of atoms, no such fundamental theoretical framework for the marine biological environment. As a consequence, it becomes necessary to study the discrepancies between model results and observations with great care. Such investigations can be subject to three major questions:

1. Are the model's equations and their spatial discretization appropriate?

2. Are the model's parameter values optimally chosen?

3. Are the model's derived variables comparable with *in situ* observations?

In practice all the questions above cannot be handled separately, making a systematic approach more troublesome. For example, it is difficult to distinguish between the errors which are related with the model equations and those which are due to the

improper choice of parameter values. If one seeks for the most appropriate prognostic equations or model resolution one must answer, or at least discuss, the second and third question in advance.

With respect to the second question, data-assimilation techniques are generally used to find an optimal combination of parameter values that minimise a function which describes the misfits between observation and model results, mostly named objective- or cost function. But finite data sets can only constrain a limited number of degrees of freedom of any given model. For instance, a highly complex ecosystem model, perhaps containing several phytoplankton species or size fractions, would need more measurements than available from the recent time series stations in order to be sufficiently constrained. On the other hand, if the dimensionality (the number of equations and parameters) of an ecosystem model is increased it becomes more likely to find an optimal set of parameters, which produces a best model fit to the available observations. But this "blessing of dimensionality" can be misleading since the number of possibilities to produce a particular result for certain modelled state variables has also increased. In other words:

There might be an apparently good fit of the model result to the available observation but perhaps for the wrong dynamical reason.

A conservative approach is to start with a relatively simple ecosystem model and to increase complexity only when it is required by model-data misfits, in order to overcome the above mentioned difficulty. After a parameter optimisation the remaining misfits between observations and the optimal model results can be tested, analyzing the plausibility of the applied equations. Evans (1999) suggested that an improvement of biogeochemical models could result from careful investigations of the model-data misfits, and that data assimilation may iteratively help to discover processes which are insufficiently resolved by the model.

The third question deals with the interpretation of biogeochemical measurements and the associated terminology. For the optimisation one usually presumes that the model counterparts to the observations are correctly calculated. It means that the applied diagnostics for the conversion of the nitrogen based model results to e.g. *chlorophyll a* concentrations and carbon assimilation rates are considered to be accurate. In some cases it is still discussed whether a certain measurement, or its procedure, represents a specifically defined biogeochemical process sufficiently well or not [1]. In contrast, the model's counterparts to the observations are mathematically clearly defined. Consequently, the inconsistency between a model output and a measurement result must not automatically imply that the model equations are wrong but could be subject to the inadequacy of comparing the model's diagnostic result with the measurement.

[1] For example, the measurement of primary production with labeled ^{14}C may not be comparable with phytoplankton biomass production because the cells can release carbon under certain physiological conditions.

Parameter optimisation

Many different methods for parameter estimation exist, such as statistical and variational analysis methods (e.g. Smedstad and O'Brien 1991 and Navon 1997). The estimation of an optimal set of parameter values for a specified model is mostly concomitant with the aim of finding the global extremum of an objective function [2]. Unfortunately, the definition of an objective function does not automatically give a single objective criterium for the optimisation procedure. Additional problems arise within the context of optimisation which are subject to recent investigations in many fields of research. The dominating difficulties are:

1. *Constraints*: Does the available set of observations suffice to estimate all the model's parameters?

2. *Multi-objective criteria*: How do the individual terms of the cost function contribute to the overall cost function value?

3. *Robustness*: Is the optimisation procedure able to find the same combination of optimal parameter values when started from different initial values?

4. *Computing power*: Is the applied optimisation algorithm capable of finding the optimal parameter solution within moderate computational time?

To date many minimization algorithms have been proposed. Some minimization algorithms are considered as unique since they can be utilized for a variety of different optimisation problems. Nevertheless, it is not straightforward to apply any of these algorithms since they need to be tuned as well. In general the algorithms search for coefficients or parameters to make a function extremal, being either maximal or minimal (hereafter the minimum of a data-model misfit function will be referred to). In practice this can become a nontrivial task, in particular for nonlinear objective functions which may contain more than one minimum. With regard to the overall performance, all methods need some compromise between accuracy and computational expense.

1.3 Motivation

There are two main intentions with this thesis. First is to investigate the overall applicability of data-assimilation methods for parameter estimation of ecosystem models, relying on real observational data. The second intention regards the optimisation of parameter values to be adopted for improved large-scale simulations in the North Atlantic.

In the following chapter observational data from a time-series study near Bermuda is assimilated into a simple ecosystem model of the upper ocean's mixed layer. Observations and model results are compared at the dates of measurement, covering a

[2] For the parameter optimisation of a biogeochimcal model it is mostly the minimum of a well defined least square misfit function.

period from 1989 through 1993. Furthermore, two different algorithms for optimisation are compared under realistic conditions and it is attempted to determine which one is superior to the other.

The last chapter builds upon the conclusions drawn from the preceeding chapter, mainly with respect to the optimisation method. The better of the two testet methods is adopted for assimilating observations into a vertically resolved ecosystem model whose physical boundary conditions are obtained from a three-dimensional ocean circulation model of the North Atlantic. Optimal parameter values are estimated when assimilating observational data into an ecosystem model at three different biogeochemical provinces simultaneously. This is particularly attempted in order to provide an optimal estimate of parameter values for an existing basin-wide ecosystem model of the North Atlantic.

2

Data-assimilation into 0D-ecosystem models

2.1 Introduction

For the improvement of biological models it is, of course, recommendable to compare the model's solutions with observations and to learn from the analysis of the remaining errors. Beforehand, it is expedient to reduce those model errors which are associated with ambiguities other than the formulation of the equations itself. For instance, parameter values are vaguely known for some models. An improper choice of the model's parameters may induce model errors that could be avoided if their accurate values were known. One effort to overcome such uncertainties is to apply data-assimilation methods which yield optimal parameter estimates with respect to minimal data-model misfits. In general it is attempted not to violate the model dynamics. The appropriate data-assimilation technique for such a problem can be regarded as strong-constraint method. It simply means that the model results should only be altered by variations of its parameter values while the model dynamics are "strongly" preserved.

Harmon and Challenor (1997) tested a Monte Carlo method to recover parameter means and standard errors. Although their method was successful, many iterations ($O(10^6)$) were needed to find one optimal set of parameter values. Another computationally expensive method is to apply a stochastic simulated annealing algorithm (SA) for the minimization of the data-model misfit, a brief overview and some test results are given in the Appendix (A.3.1). The SA was applied to seek for optimal parameter values of biological models by Matear (1995) and Hurtt and Armstrong (1996, 1999).

Information about the gradients in parameter space of the cost function greatly reduces the computational time for finding the optimal set of parameter values. The gradients can be computed using the chain rule, applying some perturbation technique (Prunet et al. 1996) or the adjoint technique. The adjoint method is very efficient (particularly for high-dimensional parameter spaces), because it provides a complete gradient vector after a single prognostic- and adjoint model integration. Lawson et al. (1996) introduced the adjoint method for data assimilation in marine

ecosystem models. Performing optimisations with synthetically produced data, they investigated necessary sampling rates in order to recover the model's parameter values. Spitz et al. (1998) successfully extended this technique to assimilate real data of the Bermuda Time-series Study (BATS) into a pelagic seven-compartment model. They noticed remaining model deficiencies which were attributed to the lack of interannual variability because their observations to be assimilated were folded into one single year, similar to the approach of Hurtt and Armstrong (1996, 1999).

In this study, it is attempted to fully account for interannual variability at the BATS location. The assimilation experiments are performed with relatively simple ecosystem models. Otherwise, if the ecosystem was too complex it would become more likely to find an optimal set of parameters which could make the model simulate the observational data apparently well but perhaps for wrong dynamical reasons. It is expected that major model deficiencies are better exhibited when the model's complexity is kept low and the ratio of the number of observational data to the number of model state variables becomes maximal. The results of the assimilation, among two different sets of model equations, are compared with observations within the upper mixed layer near the Bermuda islands, applying two different strong-constraint assimilation methods. In this chapter, the three main aims are:

- The applicability of the adjoint method needs to be analysed[1]. Effects on parameter estimates and hence on the model results should be evaluated.
- Prevailing model errors of two slightly different models should be determined from the best model fits to observations.
- It is attempted to investigate whether the adjoint method is really superior to a stochastic search algorithm for data-assimilation into a typical ecosystem model.

2.2 Method

2.2.1 NPZ–Model

Model prognostics

The chosen nitrogen-based ecosystem model has only three state variables, phytoplankton (P), herbivorous zooplankton (Z) and dissolved inorganic nitrogen (N), as originally proposed by Evans and Parslow (1985). It resembles the three compartment model of Fasham (1995) for the upper mixed layer, see Figure (2.1). The complete model equations are listed in the Appendix (A.1). A corresponding list of thirteen model parameters (p_ν), for the variational analysis, is given in Table (2.1).

For this study the parameterisation of the turbulent flux of deep nutrients into the mixed layer is changed, which will be explained in section (2.2.1). Further, additional

[1] As it could be shown in Chapter 1 if either plateaus or local minima exist a gradient method can become ineffective in search for the global minimum.

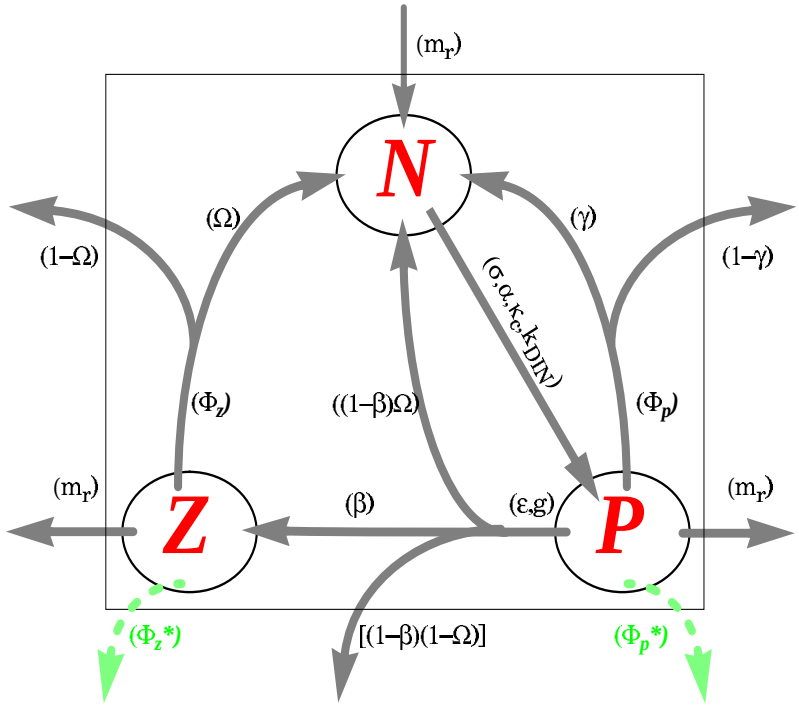

Figure 2.1: Structure of the nitrogen-based ecosystem model with three state variables, phytoplankton (P), herbivorous zooplankton (Z) and dissolved inorganic nitrogen (N). The arrows that point outside of the mean square box indicate a loss of mass out of the mixed layer, yielding the non-conservative property of the model. The greek letters (in brackets) are the parameters that are involved in the processes represented by the arrows.

quadratic mortalities for phytoplankton and zooplankton are optional (dashed lines in Figure (2.1)). These additional sinks can be added or neglected, depending on the experiment. The quadratic mortalities account for possible sinks, such as a phytoplankton loss due to aggregation and enhanced sinking out of the mixed layer, while for zooplankton it represents carnivorous feeding on herbivorous zooplankton in a simple way.

The model allows the recycling of nutrients via zooplankton (Steele and Henderson 1992) in addition to the recycling of phytoplankton losses. Zooplankton losses could be fecal pellets or particulate material due to sloppy feeding, which are partly remineralized. The remineralization of phytoplankton losses could be referred to as microbial decomposition of suspended particles, the so-called “microbial loop” (e.g. Ducklow 1983). The growth function of Evans and Parslow (1985) is used. They introduced an analytical function for daily phytoplankton growth, depending on photosynthetically available irradiance (PAR), mixed layer depth (M), maximum growth rate, and on the initial slope of the photosynthesis versus light (P-$\mathcal{I}$) relation. A Holling Type III function with a prey capture rate and a maximum grazing rate, represents the grazing by the herbivores. A Beer’s law formula with attenuation coefficients due to seawater (κ_w) and chlorophyll (κ_c) is considered to simulate the mean

p_ν	Symbol	Parameters of interest	Unit
p_1	μ_m	Growth rate parameter	[d^{-1}]
p_2	α	Slope of (P-$\mathcal{I}$)-relationship	[m^2 W^{-1} d^{-1}]
p_3	Φ_p	Phytoplankton linear loss	[d^{-1}]
p_4	k_{DIN}	Half saturation of N uptake rate	[mmol N m^{-3}]
p_5	g	Maximum grazing rate	[d^{-1}]
p_6	ϵ	Prey capture rate	[m^6 mmol N^{-2} d^{-1}]
p_7	Φ_z	Zooplankton linear loss	[d^{-1}]
p_8	β	Zooplankton assimilation efficiency	[dimensionless]
p_9	m_r	Turbulent mixing rate	[m d^{-1}]
p_{10}	γ	Phytoplankton remineral. fraction	[dimensionless]
p_{11}	Ω	Zooplankton remineral. fraction	[dimensionless]
p_{12}	Φ_p^*	**Phytoplankton quadr. loss**	**[m^3 mmol N^{-1} d^{-1}]**
p_{13}	Φ_z^*	**Zooplankton quadr. loss**	**[m^3 mmol N^{-1} d^{-1}]**

Table 2.1: The model's parameters which are used for optimisation. The rendered bold parameters for quadratic losses of phyto- and zooplankton are optional.

light field within the mixed layer. Both attenuation coefficients remain constant in time, κ_w=0.04 m^{-1} and κ_c=0.048 m^2 mg^{-1}. The total attenuation coefficient becomes $\kappa = \kappa_w + \kappa_c \cdot CHLa$. The resulting value of κ is comparable with the empirical relationship of Morel (1988) for a mixed layer mean chlorophyll concentration of ≈ 0.1mg CHL a m^{-3}.

The astronomical formulae of Brock (1981) are used for the calculation of day-length and the noon irradiance at the top of the atmosphere. For the atmospheric transmittance of solar radiation the empirical function derived from Reed (1977) has been applied with a cloudiness of four oktas. The PAR just below the ocean surface is assumed to be 43% of the irradiance at the ocean surface. Either the empirically derived noon radiation, as described before, or daily averaged surface radiation data from ECMWF reanalysis (Oschlies and Ferry, personal communication) can be taken as forcing for the model.

The chlorophyll concentration of the model is determined from a variable CHL:N ratio multiplied by the modelled phytoplankton biomass. Cloern et al. (1995) suggested an empirically derived relationship for the conversion factor of carbon to chlorophyll that is based on a collection of a variety of experimental results. This CHL:C ratio depends on temperature, PAR and nutrient availability. A molar carbon to nitrogen ratio of 6.625 is assumed which yields a factor of 0.0126 for the conversion of milligram carbon to millimol nitrogen.

For the integration an Euler forward scheme is chosen with a time-step of τ=36 min. Such a time-step is significantly shorter than the internal time-scale of the resolved ecosystem dynamics. The mixed layer depths are kept fixed for a 24 h period (40 time-steps). This is consistent with the assumptions made for a daily averaged light limited growth rate (μ) which remains unchanged within one day of integration as well. A total period of seven years is integrated of which the first two years corresponded to an initial spin-up time. During these spin-up years the seasonal changes in mixed layer depths are identical to those of the year 1989.

Mixed layer variability

From weekly mean temperatures of a three-dimensional model simulation with realistic daily forcing (heat flux, wind stress and sea surface temperature SST), taken from the ECMWF reanalysis data (Oschlies and Ferry, personal communication), the mixed layer depths M_{week} were determined from a temperature difference of $\triangle T = 0.2^o$C between surface and depth for the years 1989 to 1993 at the BATS location. For comparision the same $\triangle T$-criterion has been applied to observed data. CTD temperature profiles, averaged over night and day casts in the depth range of $z = 1\text{m} - 400\text{m}$, were obtained for each cruise. Figure (3.5) shows the simulated and observed temperature evolution for the years 1989 to 1993 at the BATS location.

Turbulent flux of dissolved inorganic nitrogen

The turbulent flux of N at the bottom of the mixed layer ($z = M$) is calculated as

$$\mathcal{F}_N = \frac{m_r + w_e}{M} \cdot \triangle N \tag{2.1}$$

with a constant mixing rate m_r and $\triangle N = (N_D - N_i)$, the difference between the dissolved nitrogen concentrations of the mixed layer N_i and of the layer below N_D. The entrainment velocity is defined as $w_e = max(\frac{dM}{dt}, 0)$. It denotes entrainment with mass conservation when the mixed layer deepens and a conservation of the nitrogen concentration when stratification occurs. The strength of the nitrate flux into the mixed layer is determined by the rate multiplied by the concentration difference.

Many studies have shown that the parameterisations for the deep dissolved nitrogen concentrations N_D strongly affect the model results (e.g. Steele and Henderson 1993, Fasham 1995, Hurtt and Armstrong 1996, Spitz et al. 1998). A constant concentration of N_D, down to a defined depth and a constant gradient below that depth, has been assumed by Fasham (1995) following Steele and Henderson (1993). Hurtt and Armstrong (1996) preferred a deep concentration that resulted from a constant vertical $NO_2 + NO_3$ gradient multiplied by the mixed layer depth. Their constant gradient was determined from BATS observations within the upper 500 meters, assuming a permanent $NO_2 + NO_3$ concentration of zero at the surface.

In the optimisations using Hurtt and Armstrong's approach, very high mixing rates m_r were necessary to fit the observed winter/spring concentrations of N within

the mixed layer. This had some adverse effect, because in the model m_r is considered to be constant in time and the turbulent fluxes were unrealistically large during the summer periods. To avoid such model behavior a different deep nutrient parameterisation is formulated. In principle, an approach is seeked that increases the turbulent nitrogen flux for deep mixing events but not for the shallow summer mixed layer. First, a concentration difference is defined

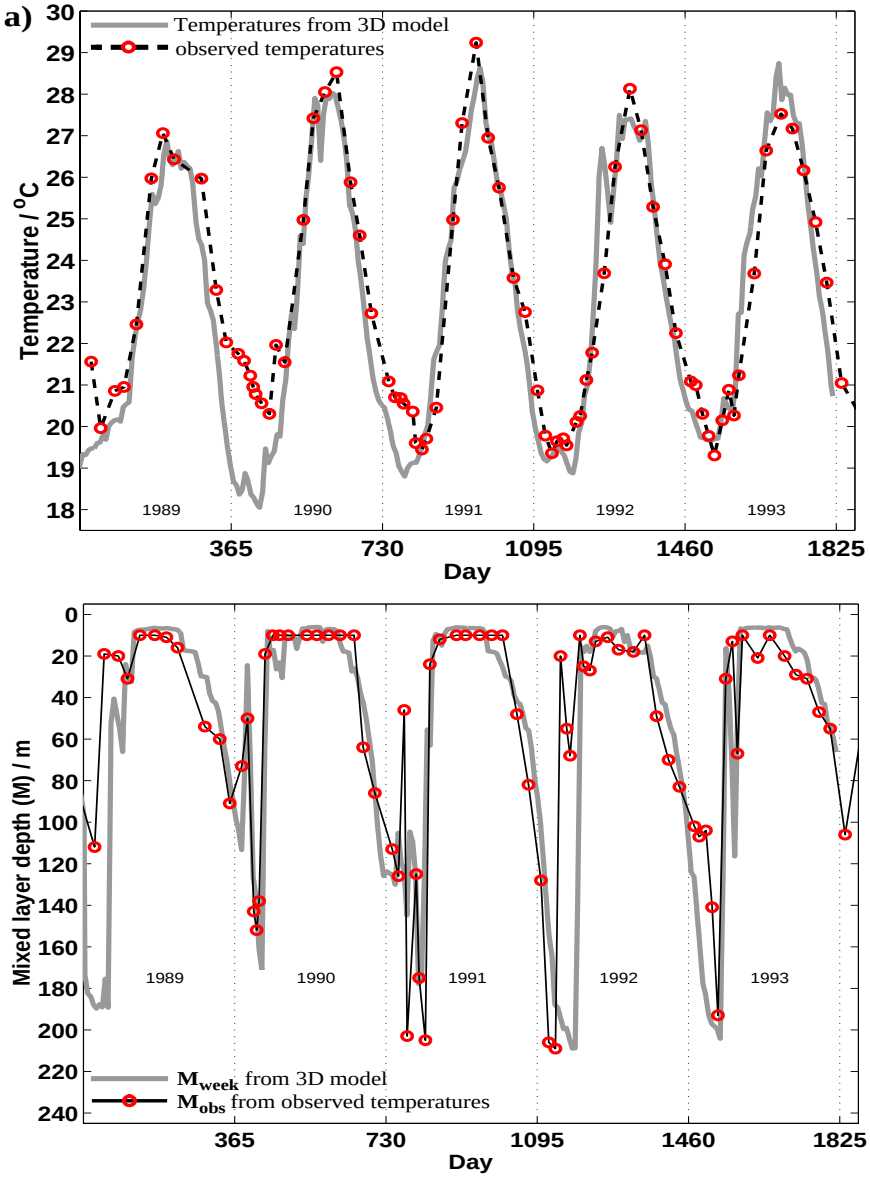

Figure 2.2: TOP: Weekly mean temperatures near Bermuda of the upper ocean layer from a general circulation model of the North Atlantic, under realistic forcing taken from the ECMWF reanalysis and the observed temperatures from averaged CTD profiles (BATS: biweekly-monthly measurements). BOTTOM: The resulting mixed layer depths M_{obs} and M_{week} when a 0.2^{o}C temperature criterion is applied.

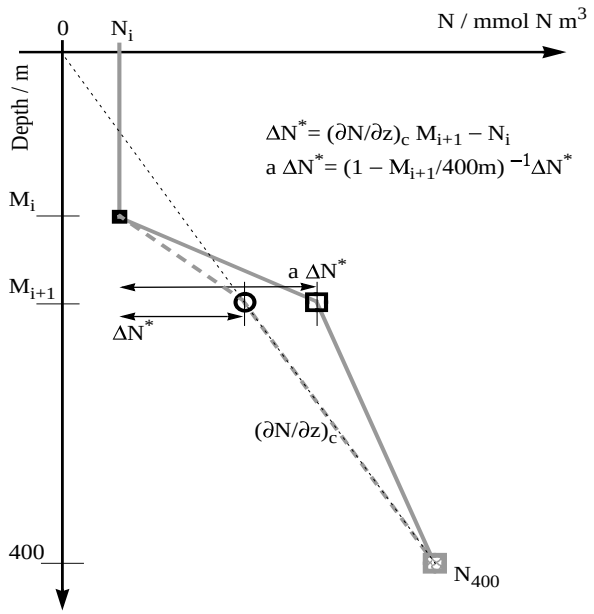

Figure 2.3: Sketch to illustrate the effect of the parameterisation with increased deep nutrient N_D availability. N_i is the modelled concentration at timestep i at depth M_i. To calculate N_{i+1} the turbulent flux of N needs to be determined when the mixed layer deepens from M_i to M_{i+1}. The gray dashed line represents the background, assuming a constant vertical gradient, $N_D^* = (\frac{\partial N}{\partial z})_c \cdot M_{i+1} = 0.0125$ mmol N$^{-4} \cdot M_{i+1}$. The gray solid line shows the associated vertical profile for the modified parameterisation with $\triangle N = a \cdot (N_D^* - N_i)$

$$\triangle N^* = \left[\left(\frac{\partial N}{\partial z} \right)_c \cdot M - N_i \right] = \left[0.0125 mmol N m^{-4} \cdot M - N_i \right] \tag{2.2}$$

identical to Hurtt and Armstrong (1996), with c subscribing a constant gradient of inorganic nitrogen. In order to increase the turbulent flux during winter mixing, the nitrogen difference $\triangle N^*$ is modified by

$$\triangle N = a \cdot \triangle N^* = \left(1 - \frac{M}{400m} \right)^{-1} \cdot \triangle N^*. \tag{2.3}$$

In winter the mixed layer deepens down to approximately $M \approx 200$m, Figure (3.5). Hence, the turbulent flux is maximal increased by a factor of about 2 in winter. But during the summer periods, when the mixed layer is very shallow and the modelled concentrations N_i are close to zero, $\triangle N$ approaches $\triangle N^*$, see Figure (2.3).

2.2.2 The cost function: Definition of a least square misfit function

Let $\mathbf{z}_t^{obs}$ denote a vector of observations at a time t with the components of nitrate (together with nitrite), chlorophyll and ^{14}C-primary production measured at BATS. At a discrete integration step i the ecosystem model, which depends on biological parameters p_ν, predicts the state vector $\mathbf{y}_i = (N_i, P_i, H_i)$. Not every state variable of the model can be directly compared with observational data. For example, a function for the conversion of nitrogen based phytoplankton biomass to chlorophyll concen-

trations is needed. Thus, a function $f(\mathbf{y})$ transforms the state variable to a model counterpart to the observations. For the optimisation a least square misfit function (hereafter named cost function) is defined as:

$$\begin{aligned} J &= J^{obs} + J^{prior} = \left(J^{N} + J^{CHL} + J^{\mathcal{PP}} + J^{ZOO}\right) + J^{prior} \\ &= \frac{1}{2}\sum_{j=1}^{j=4}\sum_{t=1}^{\mathcal{N}_j}\frac{1}{\mathcal{N}_j\sigma_{jt}^2}\left(f_j - z_j^{obs}\right)_t^2 + J^{prior} \end{aligned} \tag{2.4}$$

The index j denotes the different data types while t accounts for each individual observation with $\mathcal{N}_j$ indicating the total number of each type. A Gaussian error distribution for the observations z_{jt}^{obs} is assumed and therefore their corresponding root mean square (rms) standard deviations σ_{jt}^{obs} are prescribed. Minimising J, an optimal parameter set is determined which is most likely to produce a best model output when compared with observations. The data-assimilation covers a period of 5 years. Temporal correlations of the used data are not considered. Actually, the data is treated as if there were no cross variable correlations in addition. Hence, the observational least-square terms in equation (2.4) are simply scaled by their total numbers $\mathcal{N}_j$ combined with weights given by the inverse variances of observations.

The second term J^{prior} in equation (2.4) accounts for the a priori parameter values and their estimated standard deviations $p_\nu^{prior} \pm \sigma_{p_\nu}$. This term in the cost function avoids final parameter estimates far beyond a biologically credible range. The standard form

$$J^{prior} = \frac{1}{2}\sum_{\nu=1}^{11}\frac{1}{\sigma_\nu^2}\left(p_\nu^{est} - p_\nu^{prior}\right)^2 \tag{2.5}$$

contains a priori information considering the initial guess p_ν^{prior} to be an estimate with given variance σ_ν^2, as used in optimisations by Matear (1995) and Gunson et al. (1999). This standard form assumes a Gaussian error distribution and induces a strong constraint on the estimated parameter values. Because of systematic model errors and large uncertainties on initial parameter values such a probability distribution is not always a good assumption. Therefore, an alternative type of constraint is applied in this study. It does not penalize parameter estimates within a parameter range with upper and lower limits, p_ν^u and p_ν^l respectively, and is of the form

$$\begin{aligned} J^{prior} = \frac{1}{8}\sum_{\nu=1}^{P}[&\frac{1}{\left(\sigma_\nu^l\right)^2}\left(|p_\nu^{est} - p_\nu^l| - \left(p_\nu^{est} - p_\nu^l\right)\right)^2 \\ &+ \frac{1}{\left(\sigma_\nu^u\right)^2}\left(|p_\nu^{est} - p_\nu^u| + \left(p_\nu^{est} - p_\nu^u\right)\right)^2] \end{aligned} \tag{2.6}$$

with P being the number of parameters for variation. This means that the parameter estimates within these limits are only constrained by the observational cost function term, $J^{obs} > 0$, while $J^{prior} = 0$. If the optimisation procedure leads to values outside the limits equation (2.6) becomes $J^{prior} > 0$. Note that, with equal upper and lower variances $\left(\sigma_\nu^l\right)^2 = \left(\sigma_\nu^u\right)^2 = \sigma_\nu^2$ and when the lower and upper boundary values are chosen to be identical $p_\nu^l = p_\nu^u = p_\nu^{prior}$ then equation (2.6) reduces to equation (2.5).

In this study the standard deviations at the limits are assumed to be 100% of their boundary values (Gunson et al.), computing the variances $\left(\sigma_\nu^l\right)^2 = \left(p_\nu^l\right)^2$ and $(\sigma_\nu^u)^2 = (p_\nu^u)^2$.

Observations

All data are taken from the Bermuda Atlantic Time-series Study (BATS) as a part of the U.S. Joint Global Ocean Flux Study (Michaels and Knap 1996), and are provided by the Bermuda Biological Station for Research (BBSR). Three types (nitrate+nitrite, chlorophyll a and ^{14}C-production) of biweekly and monthly data have been accessed. Observations of zooplankton biomass were depicted from Caron et al. (1995). Most observations, zooplankton being the only exception, covered a time-period from January 1989 to December 1993. After a linear interpolation onto a 1 meter vertical grid, the mean observed values within the mixed layer were calculated for all four types of observations.

A total of $\mathcal{N}_1 = 76$ nitrate profile measurements were combined with those of nitrite. The N component of the cost function is :

$$J^N = \frac{1}{2\mathcal{N}_1} \sum_{t=1}^{\mathcal{N}_1} \frac{1}{\sigma_{din}^2} \Big(N - (NO_3 + NO_2)^{\,obs} \Big)_t^2 \tag{2.7}$$

The variance σ_{din}^2 is calculated from the variances $\sigma_{din}^2 = \sigma_{NO_2}^2 + \sigma_{NO_3}^2$, which are $\left(4 \cdot 10^{-4} + 6.4 \cdot 10^{-3}\right)$ μmol^2 l^{-2} $= 6.8 \cdot 10^{-3} \mu$mol^2 l^{-2} of both measurement methods (JGOFS report No.19 1996, Grasshoff et al., 1999). Observed ammonium concentrations fall into the range of nitrate and nitrite errors and were neglected.

For adding chlorophyll data to the cost function a counterpart of simulated chlorophyll is computed from phytoplankton nitrogen, see equation (A.4). The chlorophyll term then becomes

$$J^{CHL} = \frac{1}{2\mathcal{N}_2} \sum_{t=1}^{\mathcal{N}_2} \frac{1}{\left(\sigma_t^{chl}\right)^2} \Big(r_{chl}\,(T, PAR, M, u) \cdot P - CHL^{obs} \Big)_t^2 \tag{2.8}$$

for $\mathcal{N}_2$=76 observations. The variances in chlorophyll concentrations should implicitly account for heterogenous spatial distributions. Errors due to this kind of patchiness are mostly described as relative errors and were here taken into account by σ_t^r=0.15$\cdot CHL_t^{obs}$. But these proportional errors lead to apparent discrepancies in the residuals between observations and model counterparts, as shown by Prunet et al. (1996). To avoid too small errors for low chlorophyll measurements, an absolute error of σ_a=0.01 mg CHL was added, derived from replicate analysis of (Herbland et al. 1985). Hence, the variances are $(\sigma_t{}^{chl})^2 = (\sigma_a)^2 + (\sigma_t^r)^2$.

^{14}C-production data are used according to Michaels and Knap (1996). In order to approximate net primary production, the dark measurements are subtracted from the observations with light. A total of $\mathcal{N}_3$=66 profiles enter the optimisation.

$$J^{\mathcal{PP}} = \frac{1}{2\mathcal{N}_3} \sum_{t=1}^{\mathcal{N}_3} \frac{1}{\left(\sigma_t{}^{\mathcal{PP}}\right)^2} \Big(R \cdot \mu u P - \mathcal{PP}^{obs} \Big)_t^2 \tag{2.9}$$

The ratio R transforms the modelled photosynthetically fixed nitrogen to primary produced carbon by R=79.52 mg C mmol N^{-1}. Following Richardson (1991), we prescribe an absolute error of σ_a=0.46 mg C m^{-3} d^{-1}, which results from 12 % of the total mean mixed layer production $\overline{\mathcal{PP}} = 3.83$ mg C m^{-3} d^{-1}). The relative error contribution is very conservatively considered as $\sigma_t^r = 40$ % of the observed value (JGOFS report No.19 1996, Richardson 1991).

Unfortunately, only very few zooplankton observations are available at BATS. Zooplankton measurements which were reported by Caron et al. (1995) fall into the period of model integration (August 1989 and March-April 1990). The number of observational days is $\mathcal{N}_4$=12.

$$J^{ZOO} = \frac{1}{2\mathcal{N}_4} \sum_{t=1}^{\mathcal{N}_4} \frac{1}{\sigma_{zoo}^2} \left(Z - ZOO^{\,obs} \right)_t^2 \tag{2.10}$$

Nitrogen biomass of heterotrophic nanoplankton, together with microplankton is obtained for the assimilation experiment and a constant standard deviation of 0.01 mmol N m^{-3} is assumed.

2.2.3 Procedures for optimisation

The adjoint method

The variational adjoint method can be utilized to find the optimal parameter set of an ecosystem model fitted to measurements. An adjoint model provides the gradient of the cost function with respect to the parameters ($\partial J/\partial \mathbf{p}$). The relatively simple structure of the model allows the derivation of the adjoint equations directly. These equations are calculated from the discrete prognostics of the forward model (e.g. Thacker 1987, Smedstad and O'Brien 1991) and are listed in the Appendix. A routine, based on the so-called variable metric method of Fletcher and Powell (1963), was utilized (see Press et al., 1992) for the minimization. The algorithm was extensively tested, Wagner and Lovelace 1971 and Jung et al., 1998), see also Figure (A.6) in the Appendix. To initialize the minimization procedure, the second derivative of a parabola function is calculated for each parameter, that fits two cost function values J_l and J_u at p_ν^l and p_ν^u respectively, assuming a cost function value of zero somewhere in the range between p_ν^l and p_ν^u. Hence, the square root of the inverse second derivative is assumed as initial error for the corresponding parameter. An error matrix, the square root of the inverse diagonal elements of the Hessian $H_{\nu\nu}^{-1}$ (as it is approximated by the minimization algorithm), also lays down the convergence criterium for the step size vector s_ν. The algorithm stops as soon as $s_\nu \leq 0.1 \cdot \sqrt{H_{\nu\nu}^{-1}}$ is satisfied for all ν parameters.

Figure (2.4) illustrates the optimisation procedure. The search algorithm is initialized with first parameter guesses (*a priori* estimates). Then the NPZ-model is run with that particular set of initial parameter values. The model results as well as the observational data enter the cost function. After the evaluation of the cost function

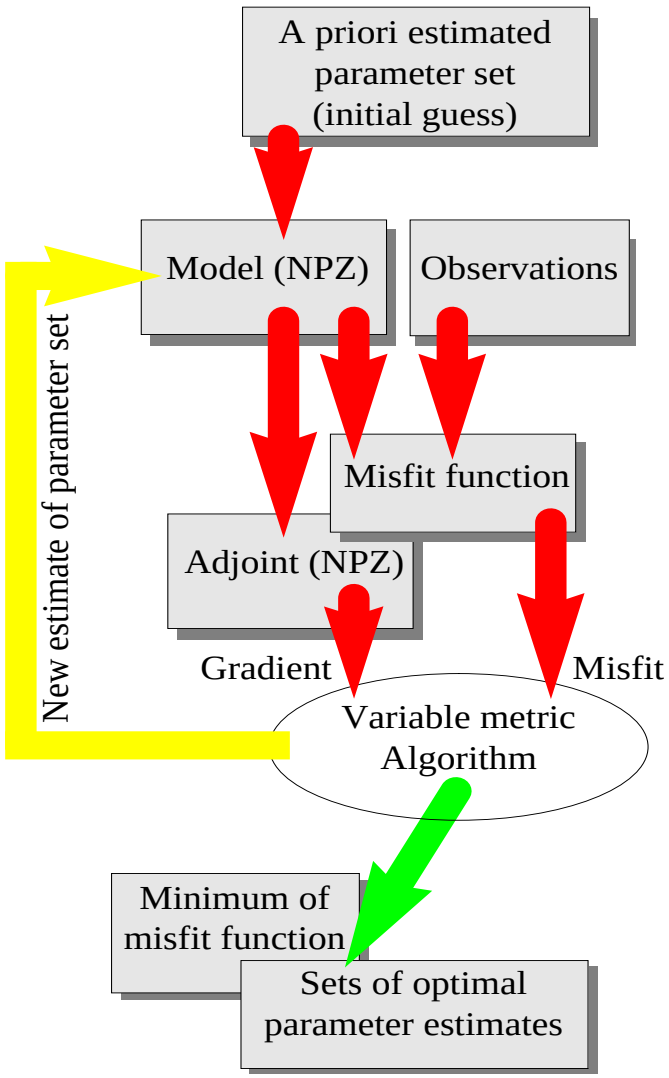

Figure 2.4: Sketch of the optimisation procedure when the adjoint model could be used to determine the derivatives of the misfit- or cost function with respect to the parameters of interest.

the adjoint model is integrated backwards in time, yielding the derivatives of the cost function with respect to the parameters. The algorithm follows a search path which is the opposite gradient direction. Along the search path a new set of parameters is estimated and reenters the NPZ-model. These iterations are repeated until the above mentioned convergence criterium applies and an optimzed parameter can be retrieved.

The micro-genetic algorithm (μGA)

The principle functioning of the μGA is described in the Appendix (A.3.1). Moreover, the configuration of the algorithm is adopted from preliminary studies shown in the Appendix as well. According to the preceding tests a population with 13 individuals turned out to be a trustworthy size. A total number of 2000 generations is prescribed,

yielding 2000*13=26000 iterations. That is, an equal amount of parameter sets will be called up during the optimisation process. Table (2.2) shows the parameter ranges for variation, prescribing upper and lower bounds. Dividing the parameter range by the number of possibilities specifies the increments and vice versa. Each increment reflects the resolution of the corresponding parameter. Hence, it is impossible to achieve a greater accuracy of parameter guesses than the given increments. The parameter symbols are described in Table (2.1).

PARAMETER CONFIGURATION FOR MICRO-GENETIC ALGORITHM				
PARAMETER	**Lower bound**	**Upper bound**	**Increment**	**# of possibilities**
μ_m	0.600	3.775	0.025	128
α	0.025	0.535	0.002	256
Φ_p	0.010	0.137	0.001	128
k_{DIN}	0.100	0.730	0.010	64
g	0.300	1.560	0.020	64
ϵ	2.500	3.760	0.020	64
Φ_z	0.010	0.137	0.001	128
β	0.100	1.045	0.015	64
m_r	0.100	1.370	0.010	128
Ω	0.010	1.030	0.004	256
γ	0.010	1.030	0.004	256
Φ_p^*	0.010	1.030	0.004	256
Φ_z^*	0.010	1.030	0.004	256

Table 2.2: Parameter setup for optimisation with the micro-genetic algorithm.

2.2.4 Analysis

Performance of the optimisation procedure

In order to explore the cost function's geometry and hence the applicability of the adjoint method, hundreds of individual optimisations are performed, using a wide range of first parameter guesses. The application of the adjoint method then yields a large number of optimal parameter estimates, which are considered as independent results of the optimisation processes. The initial guesses, namely the *a-priori* parameter estimates, are randomly generated within a parameter space with lower and upper limits (p_ν^l and p_ν^u), see equation (2.6). The limits are considered as extreme

values for parameter variation, mostly derived from model sensitivity studies (e.g. Fasham 1995) and are listed in Table (2.4).

If there was only one single minimum of the cost function, it is anticipated that this minimum can always be found, independently of the first parameter guesses. Thus, it must be very likely to obtain equally low cost function values after all optimisations. For comparision with our expectations it is helpful to approximate a smoothed probability density function (PDF). For all optimisations performed, the distribution will be assessed according to equation:

$$PDF_i = \frac{1}{M \cdot \sqrt{2\pi}\sigma} \sum_{j=1}^{M} exp\left[-\frac{1}{2\sigma^2}\left(B_i - J_j\right)^2\right] \tag{2.11}$$

with bases B_i and M the total number of optimisations. The bases are discrete with equidistant increments, $B_i(1, 2, 3, \cdots, 1000)$. The weight is prescribed with $\sigma = 1.0$.

In the ideal case, the *a-posteriori* PDF should follow a Chi-square distribution with the minimal cost function ($J_{min} \approx \frac{1}{2} \cdot (1 + 1 + 1 + 1) \approx 2$) as the value of expectation, while the *a-priori* cost function values should be significantly higher.

The application of the genetic algorithm does not yield a large number of independent results, allowing no PDF-analysis as for the adjoint method. Nevertheless, the goodness of the stochastic optimisation procedure will be determined from an intercomparision of the lowest achieved cost function values, found by either of the methods while the assimilated data and model configurations remain identical.

Cost function sensitivities

The sensitivity of the cost function to variations of certain model parameters gives information whether these parameters are important for fitting the observational data or not. The cost function's sensitivity is related to the model's sensitivity, particularly the model's counterparts to observations. Sensitivities can be interpreted by the geometry of the cost function's surface. Plateaus, for instance, indicate very low or no sensitivities, which imply that the associated parameter can be hardly constrained [2]. Such plateau regions of the cost function may have two possible causes. First, the parameter of interest has almost no effect on the model result and therefore it must be considered as redundant. Second, the available observations are insufficient in order to constrain that particular parameter. Note that the second cause does not automatically imply the first one. On the other hand a steep and narrow valley indicates high sensitivity and the parameter is strongly constrained and its optimal value is expected to be easily estimated. Unfortunately, in a high dimensional space it is hardly possible to fully determine the cost function's geometry.

When the adjoint method is applied several hundred times with different starting point in parameter space, then it is possible to analyse all parameter solutions

[2] Plateaus are parameter spaces where the model result is insensitive to variations of one or more parameters, producing no changes in the misfit function.

(best estimates) which should correspond to one or more minima of the cost function. Combining all solutions, they provide useful information on the high dimensional hyper-surface. As a consequence, the function's sensitivity to variations of two or more parameters can be examined. A three-dimensional sketch, Figure (2.5A), should disclose such typical informations for a two-dimensional parameter set (parameter vector). The hyper-surface represents the cost function when two parameters are varied. Any combination of these two parameters produces a cost function value on the hyper-surface. Two orthogonal cross sections (plains) intersect the cost function at the minimum, indicated by the red-green dashed vertical line. The red and green plains belong to parameter one and two, respectively. Each plain intersects the cost function, which reveals functional changes associated with variations of the corresponding parameter, while the other parameter remains fixed at its optimal value, see Figures (2.5B). Parameters can differ in units and may have different ranges of reasonable values for variations. Upper and lower limits of the ranges of

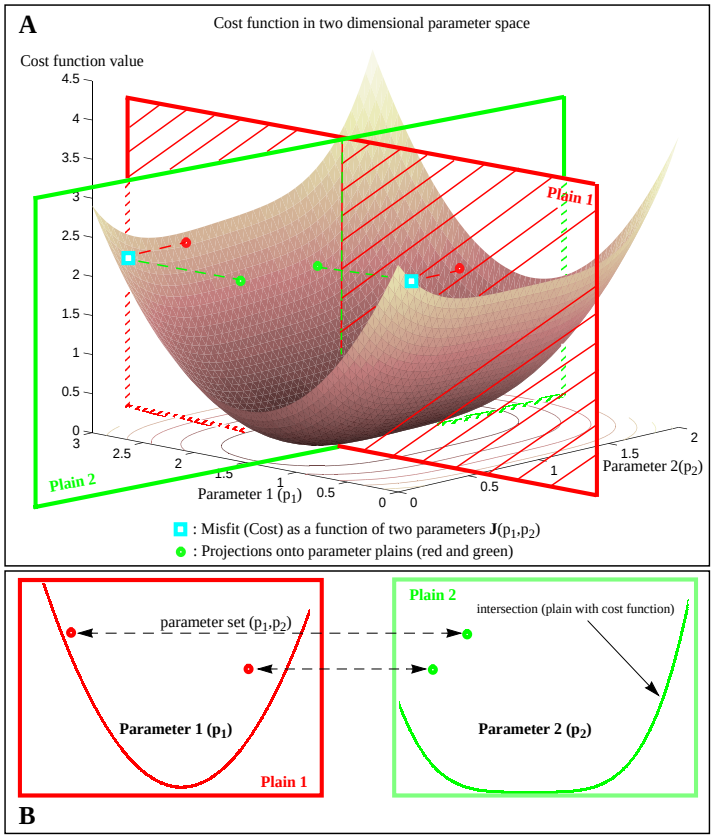

Figure 2.5: Changes in the cost function (J) depend on the variations of two model parameters (p_1 and p_2). Two cross sections intersect at the function's minimum, indicated by the vertical red and green dashed line (A). The squares represent two different sets of parameters and their corresponding cost function values. The circles indicate the projections of these two parameter sets onto the parameter cross sections (Plain1 and Plain2). Each plain then contains information from a higher dimensional parameter space, yielding spots (circles) on the function versus parameter plot (B).

variation need to be resolved within each plot. Comparing both plains, it can be seen how variations of parameter one produce a distinct increase of the cost function, whereas changes in parameter two result in minor increases close to the minimum. The model results are more sensitive to changes in parameter one than to parameter two. Strictly speaking this only holds when the two parameters are uncorrelated. If they are correlated one could probably find combinations of both parameters such that the cost function maintains minor changes.

At this point one major advantage of stochastic search algorithms becomes apparent. A set of model parameters is considered optimal as soon as the global extremum of a defined cost function (here it is the minimum of a least square misfit) is identified. Any stochastic search for this minimum is inevitably linked to a large number of cost function evaluations. Hence, many model runs with different sets of parameter values are needed. Although this is a computational expensive procedure, it allows a better insight to the cost function's sensitivity than hundreds of solutions obtained by the adjoint method. During a stochastic optimisation the entire param-

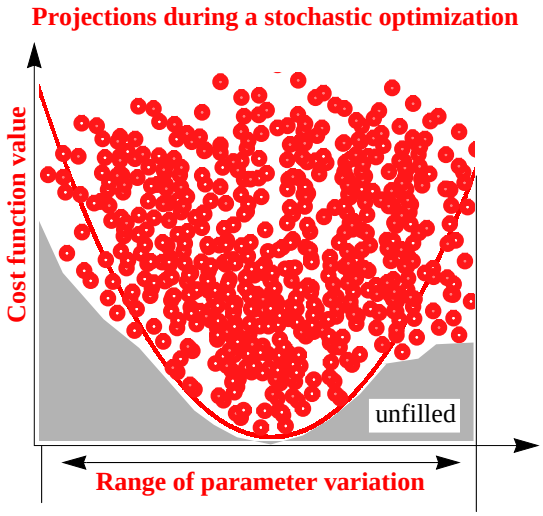

Figure 2.6: Sketch of parameter cross section. The circles indicate the projections of the higher dimensional parameter space onto the cross section (plain) while the parabola represents the intersection of that plain with the cost function's hyper-surface at the global minimum (in a one dimensional case all projections would remain on the intersection line). The vertical lines show upper and lower limits for parameter variation.

eter space is explored. Hence, if all parameter combinations are projected onto the individual cross sections then certain regions or spaces will be filled on the plains, as it can be seen in Figure (2.6).

For any particular parameter there exists a certain range of values within which the cost function has a lower limit. This means, it is unlikely to find a combination of parameters that includes values within this specified range yielding a cost function value lower than the limit. Parameter correlations are accounted for as well. In other words, as soon as the parameter values fall within the specified range the cost

function becomes larger or is equal to that limit.

In this study the parameter sets of interest contain eleven to thirteen parameters and therefore an equal number of projections will be looked at. Applying the adjoint method, as described before, hundreds of parameter sets (solutions) are available from which the projections onto the parameter cross sections can be examined. The stochastic optimisation, on the other hand, provides several thousands of parameter combinations to be projected.

One information is of major interest when the projected plots are analysed. That is to focus on the parameter ranges near the optimal estimate. Compared to the prescribed "allowed" parameter range for variation, a narrow vertical band of filled space (projections) will be noticed when the sensitivity is strong and the parameter is , whereas a wide band yields parameter values that have a weak influence on the cost function. The overall performance of each optimisation procedure can then be compared.

2.3 Experiments

The following experiments are part of a series of optimisations with different ecosystem models, but all consisting of the same three state variables. Preceding assimilation studies have been performed and some additional experiments are described in Schartau et al. (2001). In this work, two distinct model configurations are chosen for data-assimilation at the US-JGOFS Bermuda time series station. Three experiments will be presented, of which two experiments include identical model configurations but different optimisation schemes. Table (2.3) shows all optimisation setups, listing the differences between the experiments. In the first two experiments (Exp. I and II) different model configurations are compared, while the gradient method is utilized for optimisation. In the third experiment the ecosystem model remains identical to the one in Exp. II but a stochastic parameter optimisation is performed. This final experiment tests the applicability of the micro genetic algorithm.

There are three distinctions between the two model configurations. One drastic change includes the phytoplankton and zooplankton loss terms. The loss terms (sinks) in the equations of phyto- and zooplankton comprise linear mortalities which suffice in Exp. I. In Exp. II and III the loss terms of phyto- and zooplankton are expanded. A quadratic term is simply added to the linear mortalities, as already introduced by Doney et al. (1996) for a one-dimensional model at the BATS site. Hence, two additional parameters are implemented (Φ_p^* and Φ_z^*). The quadratic term enhances losses during times with large biomass. The two other distinctions, in surface radiation and growth function, lead to minor differences in model results, if compared to the changes in mortalities. In experiment one (Exp. I) the astronomical formulae of Brock (1981) is applied together with Reed's empirical relationship for atmospheric radiation transfer (Reed 1977) to receive the noon irradiance at the ocean surface. In Exp. II the daily averaged surface radiation data from ECMWF reanalysis (Oschlies and Ferry, personal communication) are taken. The light limited

growth in Exp. I is calculated according to the original analytical function Evans and Parslow (1985), indicated as EP85, and the simplified formula EP85*, as it is published in (Evans and Garçon 1997) [3], is applied in Exp. II and III.

Experiments	**I**	**II**	**III**
Optimisation method	Adjoint	Adjoint	μGA
Surface radiation	Brock81	ECMWF	ECMWF
Light limited growth	EP85	EP85*	EP85*
Mortalities	lin.	lin.+quadr.	lin.+quadr.
Number of parameters for variation	11	11	13
Number of initial parameter sets	600	300	13**

Table 2.3: Experiments: All optimisations with the NPZ-models are performed with an identically defined cost function. The mortalities are labelled as "lin." (linear) and "quadr." (quadratic). (**)The initial generation of the μGA contains a population of thirteen parameter sets.

Beforehand it must be stated that according to the results of Exp. I the remineralization parameters (γ and Ω) turned out to be hardly constrainable. The cost function sensitivities were lowest for these two parameters, (Schartau et al. 2001). Instead of increasing the total number of parameters for variation it is decided to keep these two parameters fixed in Exp. II. Again, eleven parameters entered the variational process again in Exp. II, although two parameters were added the model. Regarding the remineralization rates, being hardly constrainable should not cause any difficulties for the μGA and therefore they reentered the optimisation process in Exp. III .

Due to the nonlinearities of the model and the usage of real observational data there may be several minima or plateaus of the cost function. This suggests that the optimisation with gradient information produces results which depend on the choice of the initial parameter values. As a consequence 600 initial parameter sets in Exp. I and 300 in Exp. II are randomly generated from which the optimisations are started. The rationale behind the numbers of 600 (Exp. I), and then 300 (Exp. II), optimisations is simply computational time. Approximately 30–50 iterations are needed before the convergence criterium stops the minimization algorithm. Each iteration includes one forward- and one adjoint model integration. Hence, up to 100 model runs are necessary until a single set of parameters is estimated. This results in maximal $6{\cdot}10^4$ model runs for Exp. I. In Exp. III the number of model runs is fixed by the number of the population multiplied with the number of generations. The evolutionary micro-genetic algorithm (μGA) will have a population of 13 individuals (parameter sets) and 2000 generations, yielding a total of $2.6{\cdot}10^4$ model runs.

[3] The approximated light limited growth function is the one that is fully consistent with its adjoint version, since it is used for gradient calculations in the adjoint NPZ-model

2.3.1 Results: Experiment I (adjoint method)

In case of an ideal least-square fit there would exist one single minimum and all minimizations should have converged to an expected cost function value of J≈2, corresponding to an error

$$\varepsilon_j^2 = \sum_{t=1}^{\mathcal{N}_j} \frac{1}{\mathcal{N}_j \sigma_{jt}^2} \left(f_j - z_j^{obs} \right)_t^2 \approx 1 \tag{2.12}$$

for each observational term j. This would mean that on average each misfit falls within the range of the given observational error variance. Further, if all data-model misfits were normally distributed, the errors ε_j^2 should follow a Chi-squared distribution. Because of systematic model errors and an imperfect weighting in the cost function, these ideal distributions are not really awaited, as it was already stated in section 2.2.4. Nevertheless, the smoothed probability distribution of the final (minimised) cost function values reveales a completely different picture than expected, Figure(2.7).

The lowest cost function value that could be achieved after all optimisations is J_{min}=J^N+J^{CHL}+$J^{\mathcal{PP}}$+J^{ZOO}+J^{prior}=0.88+8.40+1.06+11.67+0.00=22.01. The zooplankton constraint produced the largest contribution to the finally remaining misfit. The initial cost function values of the first parameter guesses range from $J \approx$30 to $J \approx$1000. The lowest *a priori* cost was J=28.470 In fact, there are as less as $n = 8$ solutions with cost function values lower than any initial value. These eight best solutions are part

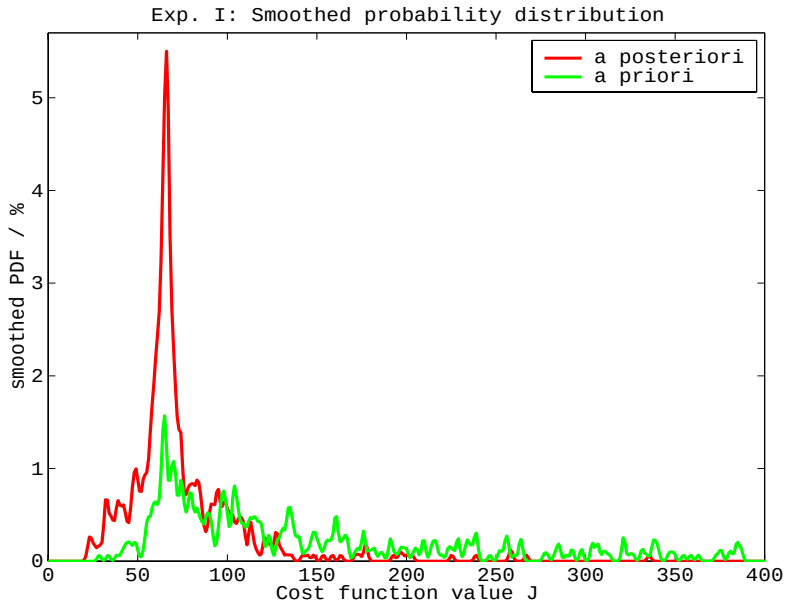

Figure 2.7: The smoothed probability density function expresses the efficiency (*a-posteriori* estimates) of the optimisation procedure when a gradient method is applied, starting from random initial parameter guesses (*a-priori* estimates). According to equation (2.11), the cost function range is binned into △J=1 increments.

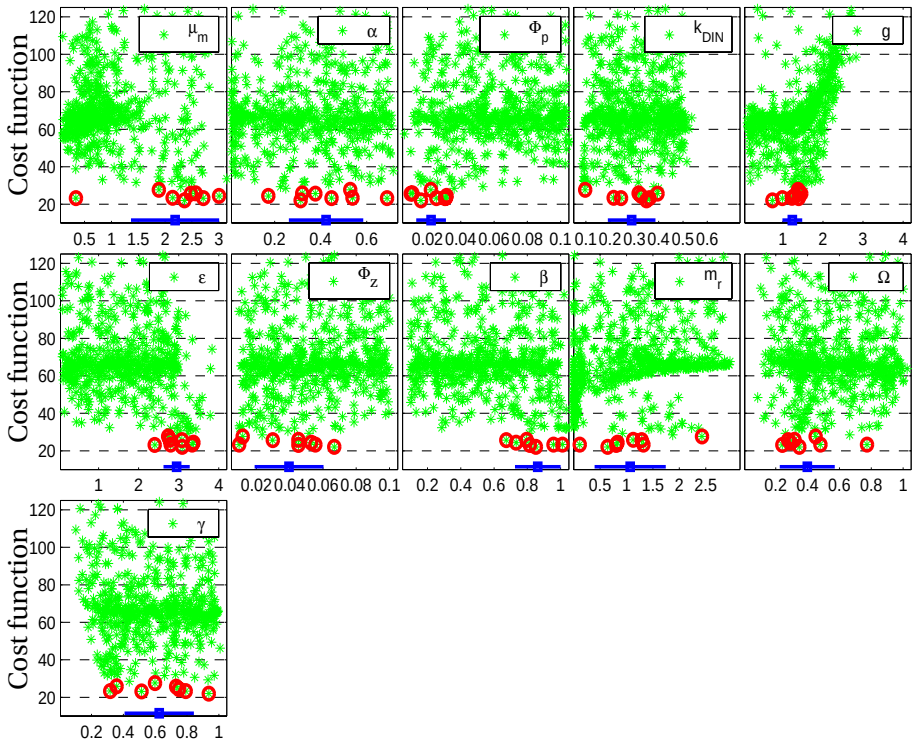

Figure 2.8: This plot shows projections of the model's parameters of interest, as described in section 2.2.4. The declaration of the symbols can be found in Table (2.1). The bold circles (red) mark all parameter estimates that are associated with a cost function value lower than $J < 28.470$. The squared markers (blue) represent the mean values together with their standard deviations.

of the first peak of the smoothed probability density function, see Figure(2.7), and will therefore be considered separately from the other solutions. The first small peak indicates that only little less than 1% of all optimisations produced final cost function values below 30. More than 40% of all optimisations converged to, or rather remained at, values between 60 and 70. At this point, the question becomes: How do the eight best parameter sets differ from those producing cost function values larger than 28? If there was a local minimum (around J=65) then the parameter sets would clearly differ from the estimates associated with the global minimum. On the other hand, if there are saddle points (or plateau regions) of the cost function, than the parameters may not be constrained, yielding a degeneracy of the costs.

This crucial information is retrieved by plotting the cost function values over the parameter solutions, as described in section 2.2.4. In Figure (2.8) the parameter projections whose costs are lower than 28 are emphasized by red bold circles. One important property can be observed. That is, all parameter estimates with costs between 60 and 70 do not seem very well constrained, if at all. The inverse problem becomes locally degenerated with very small gradients (which drastically reduce the step lengths for the next parameter estimation) on the cost function's plateau area.

The search path for the variable metric algorithm is short and may be even incorrect

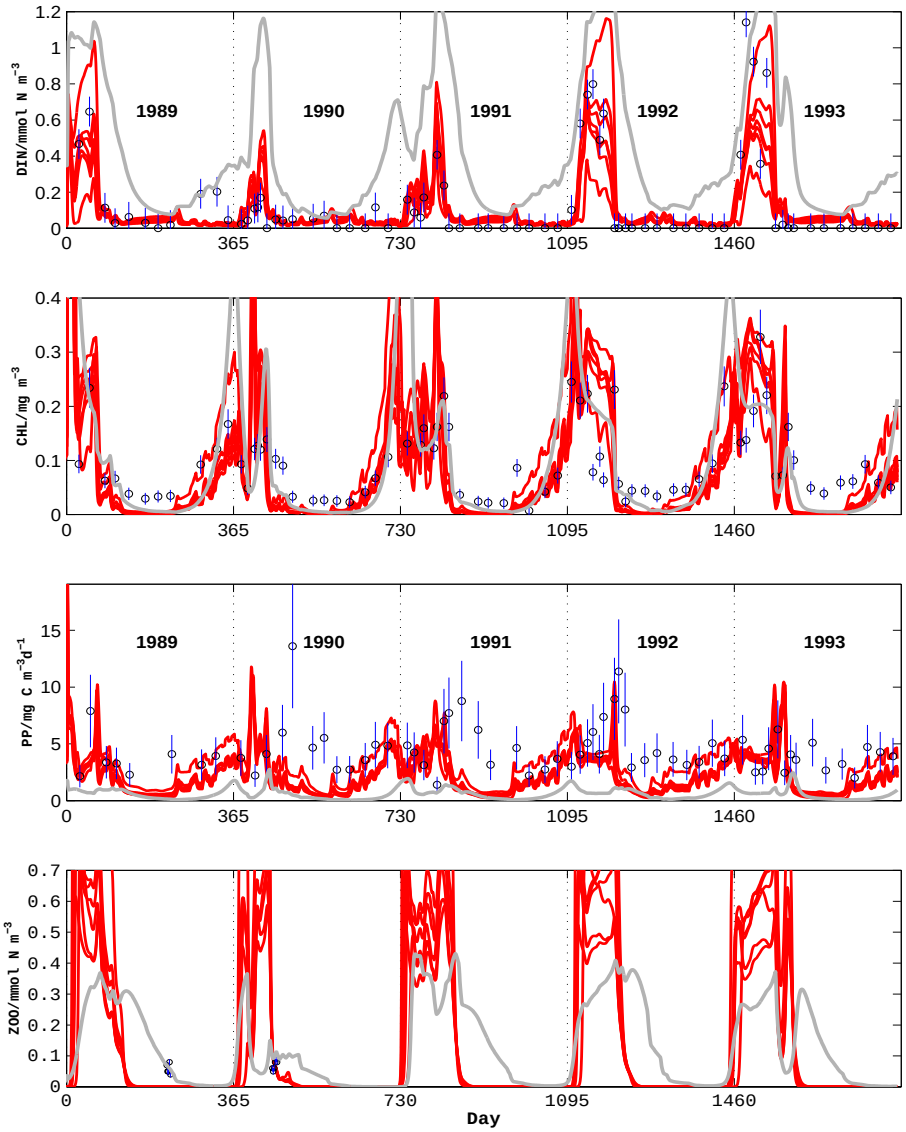

Figure 2.9: Model solutions for the years 1989 through 1993 at the BATS site. The observations (averaged values within the mixed layer) are marked by circles together with their standard deviations. Eight trajectories can be seen (seven red and one gray), of which the bold gray trajectory belongs to the model solution associated with the exceptional parameter set that includes μ_m=0.336d^{-1}.

due to computer precission when the gradients, provided by the adjoint model, become close to zero. Fortunately, the distinction between the best solutions with costs lower than 28 and those with larger costs, seems reasonable since some of the best parameter estimates clearly differ from the others. For instance, the best estimates of the linear phytoplankton mortality parameter are close to $\Phi_p \approx 0.02$ d^{-1}, whereas its other estimates range within its lower and upper limits. Same features can be seen for the zooplankton assimilation efficiency (β) and the prey capture rate (ϵ). Concerning

the phytoplankton's maximum growth rate (μ_m), one of the best solutions seems to be a remarkable exception because its value of μ_m=0.336 d^{-1} is significantly smaller than the other best estimates.

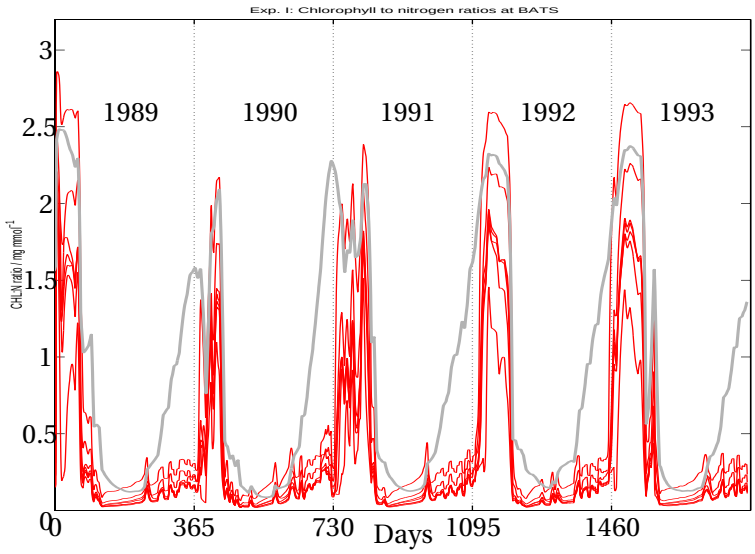

Figure 2.10: The modelled chlorophyll to nitrogen ratios of the eight best model solutions in Exp. I (red). The "low growth solution" (gray line) simulates higher chlorophyll to nitrogen ratios in late autumn and early winter, because of high nutrient availability and low light conditions.

Consequently, all model solutions are looked at, corresponding with the eight best parameter sets. These eight model solutions are presented in Figure (2.9), showing that the parameter set which includes the low estimate of the phytoplankton growth parameter produces completely different model trajectories (the low growth solution) if compared with the others. This is a clear, and the first, indication for a local minimum of the cost function rather than a plateau region. Although having almost equally low cost, the low growth solution shows a bare utilization of the entrained dissolved nitrogen while the primary productivity remains low. Unexpectedly, the low growth solution comprises relatively high chlorophyll concentrations. The only difference to the other chlorophyll trajectories is the early increase in winter. This is due to higher chlorophyll to nitrogen values because of the high nutrient availability during limited light conditions[4].

In all of the eight best ecosystem model fits, phytoplankton was essentially controlled by the grazing of the herbivores. Furthermore, the modelled maxima of zooplankton biomass exceeded the maximal observed values by a factor of more than 5, although the model results remain either close to observations or remain zero at the few dates of observation. Such top-down controlled ecosystems were already obtained in experiments without additional zooplankton constraints in the cost function (Schartau et al. 2001).

[4]The ratio depends on the nutrient uptake rate and PAR.

2.3.2 Results: Experiment II (adjoint method)

As described before, two additional parameters are introduced to the model in Exp. II, namely the quadratic loss parameters of phyto- and zooplankton (Φ_p^* and Φ_z^*). In the second experiment only 300 optimisations have been performed, yielding approximately a maximal number of 30000 model runs. The lowest cost function value found was J=20.24. The PDF-analysis, Figure(2.11, reveals an improved probability distribution if compared with Exp. I. Most minimizations ended within a cost function

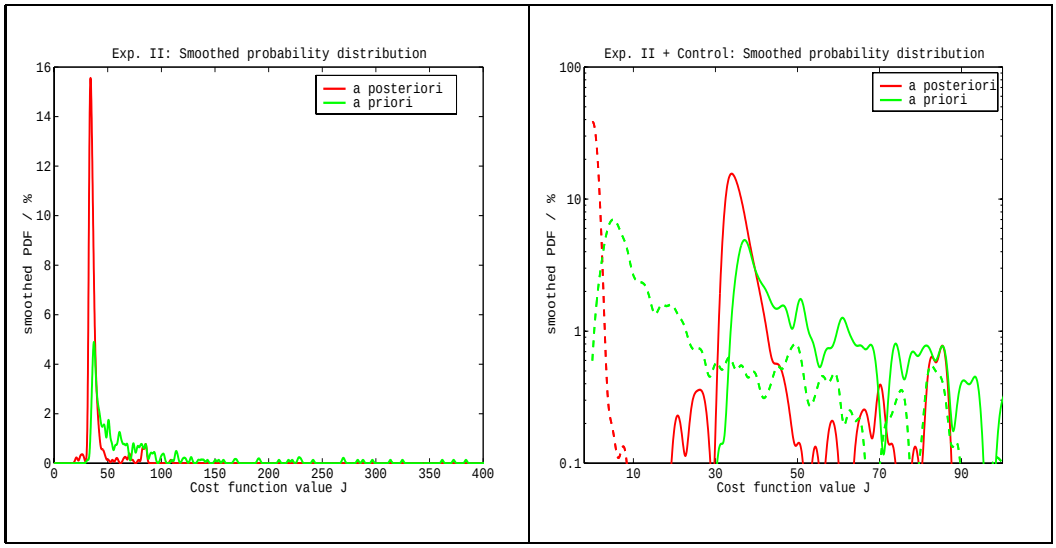

Figure 2.11: The smoothed probability density function for Exp. II, starting from 300 random initial parameter guesses (*a-priori* estimates). LEFT: *A priori* (green) and *a posteriori* (red) distributions. RIGHT: PDF with logarithmic scaling for the cost function values. Results from an identical twin experiment are added for comparision (dashed lines), indicating a maximum of the *a posteriori* (red) distribution close to zero[a].

[a] *In an identical twin experiment the observations are substituted by model results that were produced with a reference parameter set. These reference parameter values should then be recovered during optimisation, testing the general ability of the assimilation scheme and to retrieve the optimal solution under idealized conditions.*

range between J=30 and J=40. This suggests that the modified model is superior to the previous configuration. Nevertheless, three distinct maxima are evident from the PDF. The first two maxima seem to be connected, containing solutions in between. As in Exp. I we now concentrate on the parameter projections. A total of seven estimated parameter sets correspond with cost function values below J=28. A gap between $J \approx$28 and $J \approx$30 can be identified. Therefore, the seven best parameter sets are labelled differently in Figure(2.12). A clear distinction between the seven best parameter combinations and the rest is noticable, especially for the zooplankton parameters. The differences are most obvious for the linear zooplankton mortality Φ_z and the assimilation efficiency β. Another remarkable distinction is associated with

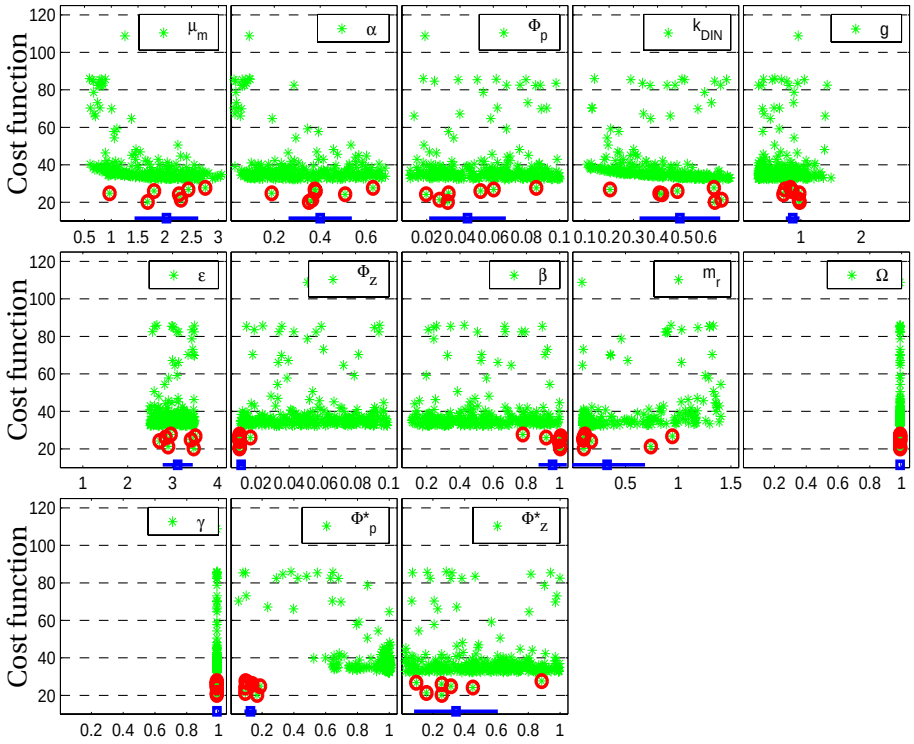

Figure 2.12: Projections of the model's parameters of interest. The bold circles (red) mark all parameter estimates that are associated with a cost function value lower than $J < 27.51$. The squared markers represent the mean values together with standard deviations.

the estimates of the "new" phytoplankton quadratic mortality Φ_p^*. The best estimates correspond to low values (Φ_p^* <0.2 $m^3 mmol\ N^{-1} d^{-1}$) while other estimates clearly exceed 0.5 $m^3 mmol\ N^{-1} d^{-1}$, (neglecting estimates with cost function values beyond J=50). Such a noticable feature suggests that this newly introduced parameter plays a key role for the phytoplankton loss.

The model solutions (trajectories) confirm the relevance of phytoplankton losses for our system of interest. Figure(2.13) shows model solutions which belong to the seven best parameter estimations (gray trajectories). The other six trajectories are depicted from those solutions yielding cost function values in the vicinity of $J \approx 35$ ($34.9 < J < 35.1$). There is evidence that both solutions are different with regard to the zooplankton biomass whereas the other variables remain undistinguishable. In particular the chlorophyll concentrations are comparable, although the fluxes differ significantly. In Figure(2.14 the annually averaged fluxes are illustrated together with their standard deviations due to interannual variabilities. The best solution is associated with the lowest cost function value whereas the "local" solution is represented by one parameter set which produced a cost function value in closest vicinity to J=35. Comparing all trajectories in Figure(2.13, best and local solutions agree fairly well in productivity and the remineralisation of phytoplankton losses. Even

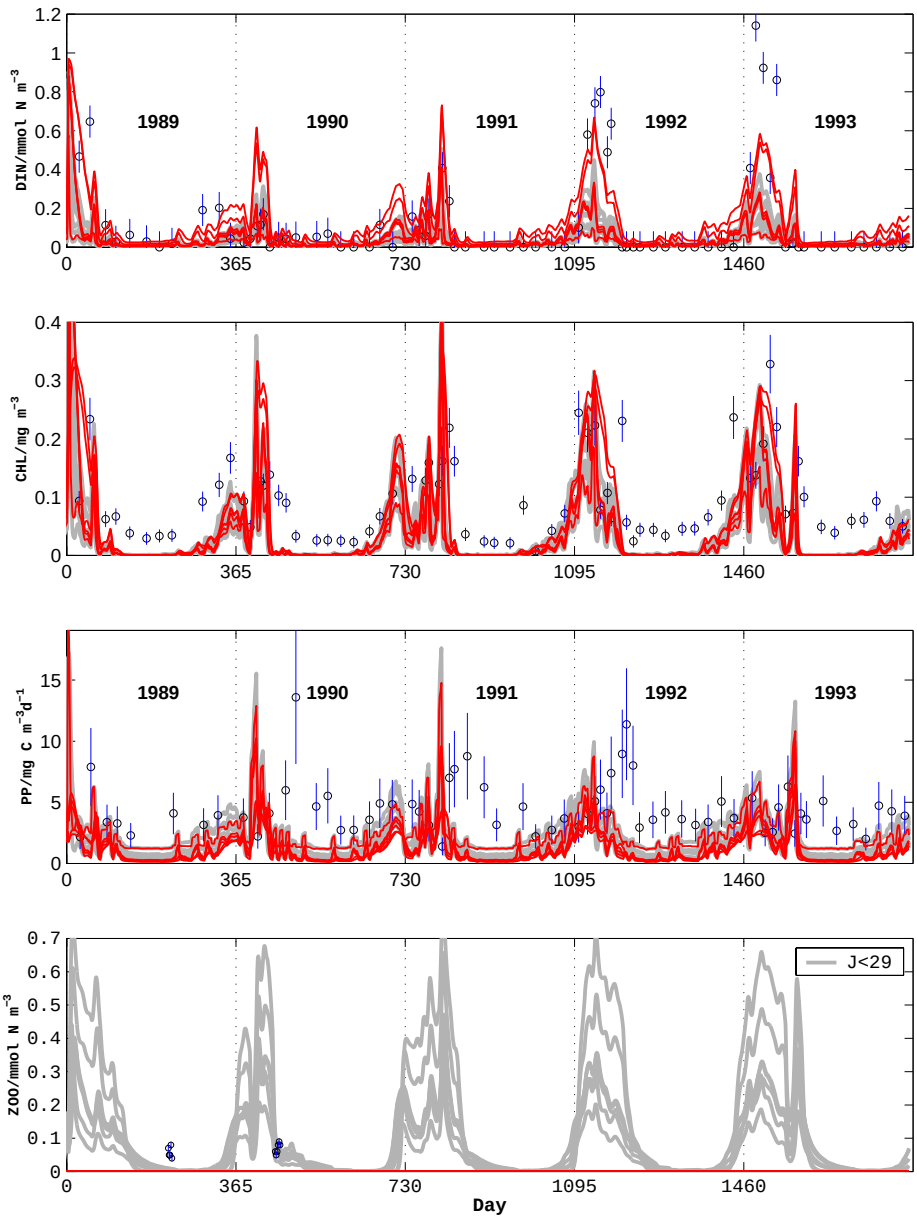

Figure 2.13: Model solutions for the years 1989 through 1993 at the BATS site. The observations (averaged values within the mixed layer) are marked by circles together with their standard deviations. Seven trajectories can be seen which yield cost function values lower than J=27 (gray lines). Six additional trajectories are chosen to representative for the PDF peak around $J \approx 35$ (red trajectories). They are depicted from the precise cost function range ($34.9 < J < 35.1$).

losses due to the dilution effect are almost equivalent[5]. Nevertheless, the major nitrogen flux occurs via zooplankton in the best solution whereas no zooplankton is needed in the local solution. The local solution implies a redundant role of zoo-

[5]Dilution occurs when the mixed layer deepens and then immediately restratifies. This is because mass is conserved during the deepening of the mixed layer while concentrations are conserved during stratification.

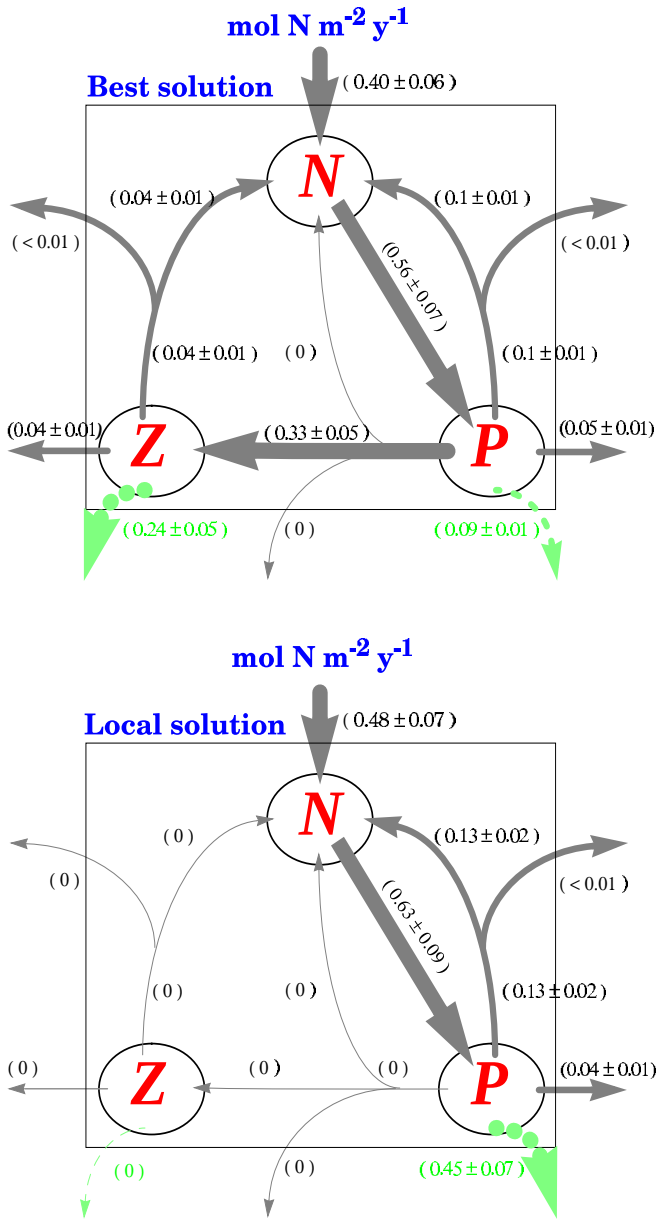

Figure 2.14: Diagram of averaged yearly nitrogen fluxes of the NPZ-model at the BATS site. UPPER: Fluxes of the best model fit to observations as found by the optimisation process. LOWER: Fluxes of the representative local solution (see text), lacking zooplankton biomass.

plankton when nitrogen fluxes are considered at the BATS site. From now on that particular solution will be considered as “no grazing solution” since it does not depend on zooplankton biomass.

2.3.3 Results: Experiment III (μGA)

In Exp. III the same model configuration as for Exp. II is used. The prevailing question deals with the optimisation process itself: How competitive is a stochastic evolutionary optimisation algorithm with the adjoint method? Actually, it is expected from the micro-genetic algorithm (μGA) to recover the global minimum of the cost function, which should be close to the best solution found in Exp. II . The two remineralization parameters (γ and Ω) reenter the optimisation process because the μGA should easily cope with plateaus of the hyper-surfaces of the cost function (implying very low sensitivities). Therefore the number of parameters for variations increases to thirteen. In Figure(2.15) cost function values of all iterations are shown. The minimum found by the μGA is J=18.92. One major advantage of this evolutionary algorithm is obvious. Until the end of all 26000 iterations the entire parameter space is explored. Typical features can be seen when we focus on a small fraction of iterations, as it is presented in Figure(2.15) as well. The red solid lines represent averaged cost function values of one generation which include thirteen individual parameter sets (13 iterations). A saw-toothed structure can be noticed, indicating that after few generations the individual parameter sets converge back to their currently best parameter estimates. After reconvergence the estimations spread out through the entire parameter space again and may then converge to the same or a lower minimum of the cost function.

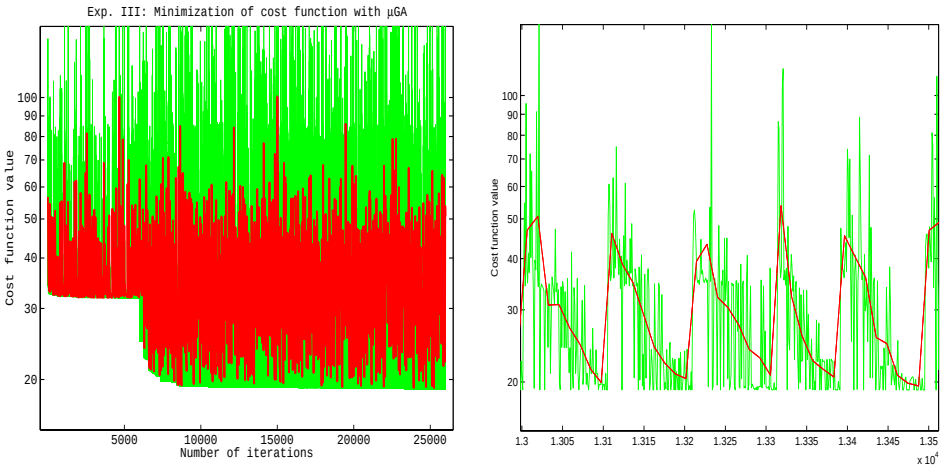

Figure 2.15: Cost function values (green/gray) of each iteration during stochastic evolutionary optimisation with averages of each generation (bold red/black line). LEFT: All 26000 iterations; RIGHT: Focus after about 13000 iterations with saw-toothed structure already visible which assures convergence while the entire parameter space is continuously explored, see also Appendix (A.3.1)

As stated in section 2.2.4 sensitivities can be determined from the parameter projections, as shown in Figure(2.16). Although the model and cost function remain unchanged, the μGA search ends with a cost function value lower than the one found in

Exp. II . But with regard to the parameter projections we can conclude that the minimum found in Exp. III does not fully coincide with the seven best solutions found in Exp. II . In order to emphasize the differences between the best solution and the previously found “no grazing solution” of Exp. II all parameter projections yielding cost function values lower than J=30 are separately labelled in Figure(2.16). The

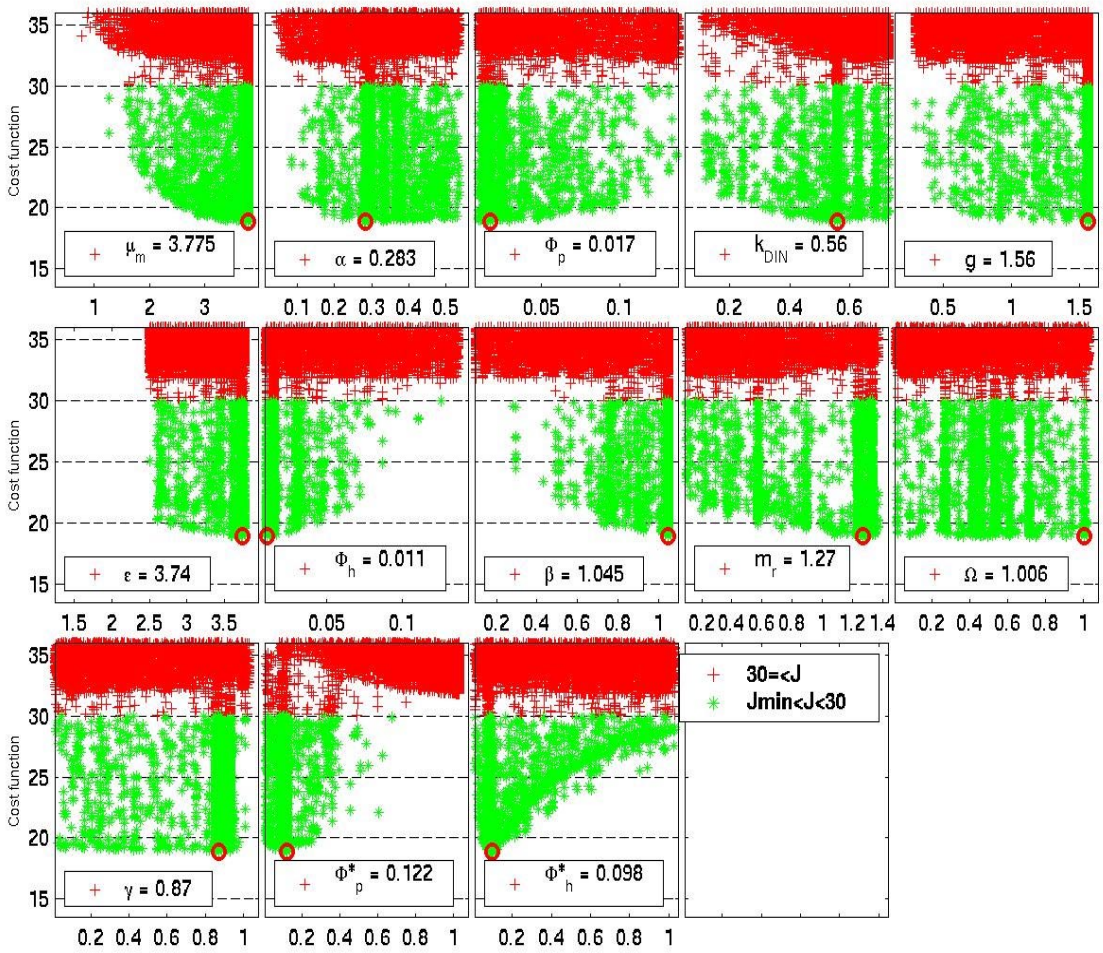

Figure 2.16: Parameter projections of all thirteen parameters as they were estimated during the evolutionary optimisation process. The vertical axis is chosen in accordance to the sensitivity of the cost function. It gives an impression on the cost function's geometry in the vicinity of the minimum.

zooplankton parameters are very well constrained. Lowest sensitivies can be determined for the remineralization parameters γ and Ω, as noticed before. Nevertheless, their best estimates are surprisingly close the fixed values that have been asumed for Exp. II .

2.3.4 Combined results (Exp. I, II and III)

Finally, the trajectories of the three best solutions retrieved from the three experiments are shown in Figure(2.17). The best solution of Exp. I (solid black line) seem to give the best representation of the nitrate concentrations. Furthermore, it also matches chlorophyll concentrations relatively well for the years 1992 and 1993 but produces extraordinary peaks in the previous years which yield large contributions to the cost function. Referring to primary productivities, the solution found in Exp. II shows the lowest rates (dash-dot line) whereas the other solutions are not very different. The few zooplankton observations appear to be better resolved by the solu-

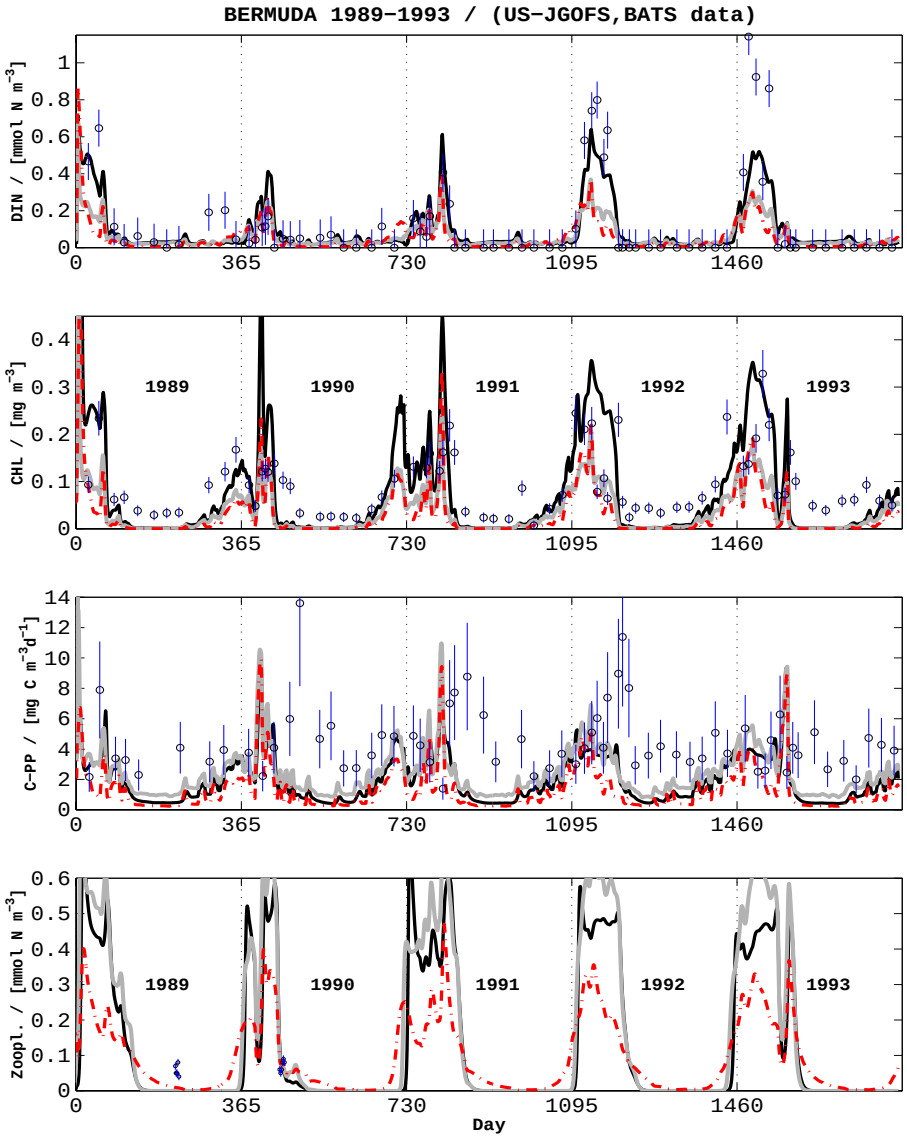

Figure 2.17: Optimised model solutions at the US-JGOFS BATS site. The NPZ-models simulate a five years period (1989-1993). Solid black line: best solution of Exp. I ; Dark red/gray dash-dot line: Exp. II ; Solid gray line: Exp. III .

tion of Exp. II than by the others. Nevertheless, all solutions maintain relatively high abundances of zooplankton. This is not very realistic since such high standing stocks could not be observed. The zooplankton grazing is the major sink for phytoplankton biomass in these model solutions. These solutions are likely to be retrieved because of high productivities together with low chlorophyll concentrations. Hence, the optimised models clearly prefer a solution that is associated with a top down control of the ecosystem which is not really supported by the available zooplankton observations. Eventually, similar cost function values can be obtained by either lowering the models primary production rates while achieving better fits to zooplankton or by increasing productivity but simultaneously increasing the model's misfit to zooplankton.

From all fitted model results identical mismatches can be depicted in primary production at the end of the phytoplankton bloom. The maxima in primary production were measured when chlorophyll concentrations had decreased significantly. These data-model discrepancies are apparent in all years and may therefore be regarded as a systematic deficiency.

2.4 Concluding discussion

One objective of this study is to test the applicability of the adjoint method (or gradient methods in general). Furthermore, the consequences of cost function irragularities on parameter estimates and the corresponding model results are analysed. From these investigations conclusions can be made on the goodness of the assimilation process. Hence, informations on accuracy and reliability of the parameter estimates are obtained.

The experiments presented reveal that the optimised NPZ-model provides results which are not fully consistent with observations. Major misfits can be attributed to the high abundance of zooplankton in the model and to primary production immediately after the chlorophyll drawdown. To date, there exists no reliable ecosystem model simulating the BATS observations consistently. The results presented here are based on an experimental approach which differs from other assimilation studies with BATS data (Hurtt and Armstrong 1996 and Spitz et al., 1998). In this work, only a simple three compartment model has been used for the assimilation of BATS data. Interannual variabilities over a five year period have been included. From other modelling studies we already learned how difficult it is to resolve the most relevant biogeochemical processes correctly at the BATS site and to justify the proposed model complexities (e.g. Fasham et al. 1990, Hurtt and Armstrong 1996, 1999 and Spitz et al. 1998). Our experiments, in addition, demonstrate how data-assimilation can lead to wrong model results although the observed data, which enter the data-model misfit function, may apparently be fitted. Such optimal fits are insufficient to really validate the applied model equations. Having a relatively simple model, we could easily realize that these optimal results were not biological plausible for the BATS site. The detection of such implausible features can quickly become more dif-

ficult in more complex models.

2.4.1 Optimisation and cost function

In the absence of local minima or plateau regions of the cost function the optimally determined parameter set should be associated with one single minimum of the cost function. That particular minimum is generally identified by the minimization algorithm no matter what the *a priori* parameter guesses are. From Exp. I and II it must be concluded that either local minima and plateaus exist. Hence, the parameter solutions found with the adjoint method depend on their initial guesses. Additional evidence for local minima was given by Vallino (2000), who assimilated mesocosm observations into a complex ecosystem model. In his work, a variety of minimization algorithms were tested. During his investigations up to 20 local minima were recovered.

The *a posteriori* error probability function of the optimal parameter estimates were not known when the experiments were started. The parameter projections provide useful information on the errors of the optimisation process. The projections, for instance, show that the optimal parameter values are not always normally distributed. This is especially the case for the phytoplankton maximal growth rate (Φ_p^*) in Exp. I . Among the best estimates of Φ_p^* there exists one estimate which seems exceptional low although the associated cost function value does not differ significantly from the other best estimates. Depicting all model trajectories of these best estimates it becomes evident that the parameter set with the low growth estimate yields a different model result. This particular solution is due to a remarkably good fit to zooplankton observations which, on the other hand, coincides with larger misfits in dissolved nitrogen and primary production.

The parameter projections of all three experiments disclose relatively low sensitivities if one consideres the full range of possible cost function values. For these low sensitivities several reasons can be taken into consideration, such as an improper weighting of each cost function term or insufficient observational data. However, the perhaps most compelling reason is related with the existence of systematic model deficiencies in primary production. This systematic model error is evident for either of the two model configurations, see Figure(2.18). Depending on the weights such systematic errors produce an offset to the cost function. As a consequence, the effect of small parameter variations on cost function changes remain almost unnoticed due to a dominant offset. Presumably the sensitivity in the vicinity of the minimum would be clearly increased when the offset was absent. In case of an identical twin experiment the model is fully consistent with the synthetic observations. Therefore systematic errors are impossible. In an identical twin experiment with the same NPZ-model and an idealized daily sampling rate we could recover all parameters by the adjoint method, as it is additionally shown in Figure(2.11). This seems natural when nonlinearities are weak. The success of an identical twin experiment is ultimately linked to the increased sensitivity of the cost function. The sound theory of

data-assimilation already provides the mathematical background on parameter estimation errors and the sensitivity (e.g. Bard 1974, Thacker 1987, Navon 1997, Gunson and Malanotte-Rizzoli, 1996).

Best indication for an offset of the cost function is given in Exp. II . The "no grazing solution" lacks zooplankton biomass and therefore its misfit contributions to the cost function are the same, no matter what parameter combination is taken. Unless the quadratic phytoplankton mortality becomes smaller than 0.4 $m^3 mmol\ N^1 d^{-1}$, the zooplankton parameters remain redundant. There is no sensitivty of the cost function to variations of the zooplankton parameters. The quadratic mortality (Φ_p^*) plays a key role, suggesting that its initial guess decides over the parameter subspace within which the optimal values are estimated. Indeed, the stochastic evolutionary algorithm could cope with this particular problem. In Exp. III the minimum found is lower than those determined by the adjoint method. Actually, the number of model runs is competitive to the multiple adjoint method approach.

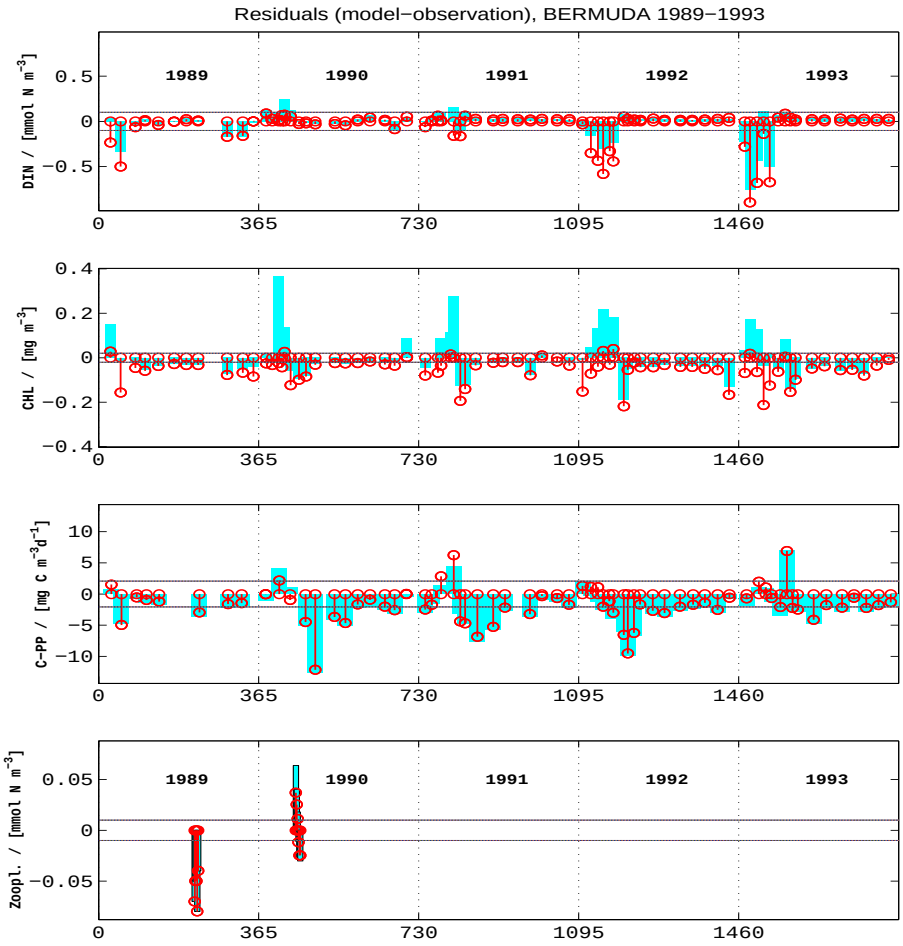

Figure 2.18: Residuals of the NPZ-model and BATS data. Bold bars show the residuals of the best model fit in Exp. I . Solid lines with circled markers (red/black) belong to the best fit in Exp. III . Note that the model configuration of Exp. I differed from Exp. III .

An intensive utilization of the adjoint method for assimilating real observational, interannual data into an ecosystem model has not been conducted before. According to the experiments performed here it is clear that optimisations with gradient methods, such as the adjoint method, need to be critically assessed. Reliable optimisations with a gradient search algorithm should include several trials starting from different initial parameter guesses. The investigation of the *a priori* and *a posteriori* statistics, such as the presented PDF-analysis, may then reveal useful information on the robustness of the optimisation process. With respect to the accuracy of the parameter estimation it is advisable to proceed with stochastic search algorithms, as utilized by Matear (1995), Hurtt and Armstrong (1996 and 1999) and as proposed by Vallino (2000). As long as computational costs remain low for zero- and one-dimensional ecosystem models the apparent superiority of the adjoint method is contestable.

2.4.2 Parameters and model deficiencies

Parameters

Table 2.4 lists the best parameter sets found in all three experiments. The residuals in Figure(2.18 clearly illustrate the general deficiencies of the NPZ-model. The optimal parameter values are estimated by assimilating data into an ecosystem model which is not completely adequate for the BATS site. Hence, the parameter estimates obtained here need not be ultimate. Nevertheless, some optimal estimates will be discussed briefly. The optimally determined maximum growth rates range between μ_m=1.7-3.8d^{-1}, which match typical growth rates determined from the formula of (Eppley 1972). Maximal growth rate estimates are also comparable to the values assumed by Fasham et al. (1990). Hurtt and Armstrong (1996) determined smaller growth rates of μ_m=0.48-1.2d^{-1}. But a direct comparision is difficult because they included an allometric relationship which resulted in nutrient limited growth rates for their smallest phytoplankton of μ_m=1.26 d^{-1} as well as to values of μ_m=4.86 d^{-1} for growth under light-limitation. Their optimal estimates of the photosynthetic efficiency α were relatively high. Comparable estimates are received in this study, mostly $\alpha > 0.2$ m^{2}W^{-1}d^{-1}, although these high values deviate from the value derived by Fasham et al. (1990), who assumed an initial slope of α=0.025 m^{2}W^{-1}d^{-1}.

The resulting grazing parameters (g and ϵ) are close to their upper penalty limits, presumably as a consequence of high productivity combined with low chlorophyll concentrations in all experiments. Nevertheless, these two parameters are hardly constrained. The parameter projections support this impression. Similar results were retrieved in **?**) from their identical twin experiments. They found a simple explanation for these low sensitivities. Due to the low phytoplankton biomass their grazing rates could only be evaluated within the lower linear branch of the grazing response function and hence the influence of g and ϵ on the modelled zooplankton was low. Sensitivity of the modelled zooplankton to variations in the assimilation efficiency β is greater than those of the grazing parameters g and ϵ. From variations it

Parameters			Penalty limits		Best estimate of parameter set ($\widehat{\mathbf{p}}$)		
					Exp. I	Exp. II	Exp. III
ν	SYMBOL	UNIT	p_ν^l	p_ν^u	$J_0 = 22.01$	$J_0 = 20.24$	$J_0 = 18.92$
1	μ_m	d^{-1}	0.100	3.000	**2.362**	**1.679**	**3.775**
2	α	$m^2W^{-1}d^{-1}$	0.025	0.700	**0.314**	**0.352**	**0.283**
3	Φ_p	d^{-1}	0.010	0.100	**0.016**	**0.033**	**0.017**
4	k	$mmolNm^{-3}$	0.100	0.700	**0.350**	**0.636**	**0.560**
5	g	d^{-1}	0.100	1.000	**0.743**	**0.982**	**1.560**
6	ϵ	$m^6mmolN^{-2}d^{-1}$	0.100	3.000	**3.088**	**3.473**	**3.740**
7	Φ_z	d^{-1}	0.010	0.100	**0.067**	**0.010**	**0.011**
8	β	1	0.100	1.000	**0.852**	**1.003**	**1.045**
9	m_r	md^{-1}	0.010	1.5/3.0*	**0.643**	**0.107**	**1.270**
10	Ω	1	0.010	1.000	**0.348**	**0.990****	**1.006**
11	γ	1	0.010	1.000	**0.937**	**0.990****	**0.870**
12	Φ_p^*	$m^3mmolN^{-1}d^{-1}$	0.010	1.000	–	**0.168**	**0.122**
13	Φ_z^*	$m^3mmolN^{-1}d^{-1}$	0.010	1.000	–	**0.257**	**0.098**

Table 2.4: Best parameter values of all three experiments. * the upper penalty limit of the maximal mixing rate was lowered to 1.5 md^{-1} in Exp. II and 1.37 md^{-1} in Exp. III in order to decrease the dilution of phyto- and zooplankton during the summer periods. ** in Exp. II the remineralization parameters remained constant.

can be seen how the modelled zooplankton abundances can be damped when the assimlation efficiency is decreased. As a consequence the observations suffice to constrain the assimilation efficiency.

The estimation of optimal remineralization parameters Ω and γ is a problem because primary production data and chlorophyll concentrations can not constrain these parameters very well. The modelled process of phytoplankton remineralization is a product of the phytoplankton loss parameter Φ_p and the remineralization parameter γ. If Φ_p remains uncertain then it is impossible to restrict γ. Hurtt and Armstrong (1996) obtained better results for remineralization by adding an extra recycling pool. Their recycling compartment is a sink for phytoplankton biomass and a potential source for ammonium which is then available for phytoplankton growth (primary production due to recycled nutrients). To limit the abundance of phytoplankton within their size classes they recovered high phytoplankton mortalities, ranging from 0.43-1.13d^{-1}. Optimal phytoplankton mortalities obtained in our study are one order of magnitude smaller. As long as there are moderate constraints on

zooplankton biomass the optimised model favours a solution with losses due to grazing rather than to other processes. But if the "no grazing solution" of Exp. II is equally considered then we would account for a solution where the zooplankton plays a neglegible role for the nitrogen fluxes. At this point, it is suggested to introduce a detritus compartment which should be constrained with observations of particulate organic nitrogen (PON). Modelled phyto– and zooplankton biomass as well as detritus should be combined in order to reproduce a counterpart to the observed PON.

Model deficiencies

In the first instance the observations are relatively well reproduced by the optimised model counterparts of all experiments. Exp. III provided the lowest final cost function value compared to the two other experiments with real data. All our experiments, however, clearly demonstrate that relatively high zooplankton abundances result when the BATS measurements are assimilated into the three compartment model . Optimal model solutions, with zooplankton biomass exceeding that of phytoplankton, do not confirm the knowledge about the general functioning of the ecosystem near Bermuda. The model fits coincide with zooplankton biomass up to 0.6 mmol Nm^{-3} in late winter and early spring that exceed observed concentrations $Z\approx$ 0.05 mmol Nm^{-3} by roughly a factor of 10.

The consideration of nitrite+nitrate, primary production together with chlorophyll data for the cost function still requires better constraints on zooplankton. Otherwise, zooplankton grazing and biomass will dominate the system while chlorophyll and primary production data seem to be surprisingly well reproduced by their model counterparts.

Primary production — The integrated and averaged primary production rates of the optimised NPZ-model are close to 0.6 mmol N $m^{-2}yr^{-1}$ which is equivalent to 48 mg C $m^{-2}yr^{-1}$, when constant molar C:N ratio of 6.625 is assumed. The flux of nitrate into the mixed layer is approximately 0.4 mmol N $m^{-2}yr^{-1}$ which proposes new production rates in the same magnitude, if everything is utilized within one year. Such a model approximation of new production is slightly lower than those estimated for Bermuda (e.g. Michaels et al., 1994 and Jenkins, 1985). However, the assimilated BATS data exhibit a distinct time lag between the maximum of ^{14}C-production and the maximum of chlorophyll concentration. Since the modelled primary production is derived from nitrogen based productivity, our experiments are not able to adopt these observed features. These model discrepancies in productivity are already described by Doney et al. (1996), who utilized a one-dimensional coupled physical-biological model for simulations at the BATS station. In their paper they mentioned several reasons for this model error, such as shifts in the community structure, nitrogen fixation or the decoupling of nitrogen and carbon.

Hood et al. (2001) modelled the effect of nitrogen fixation at the BATS site. Two model solutions were obtained of which one reproduced the trap flux data whereas

the other could better simulate observed dissolved inorganic carbon (DIC) concentrations in the mixed layer. Although the latter solution could possibly explain the observed DIC draw down, it is apparent that the associated trichodesmium biomass of the model then exceeded 1.0 mmol N m^{-3}. Measurements of total particulate organic nitrogen (PON) generally show concentrations which are lower by a factor of 2. Thus, if trichodesmium is measurable as PON then the biomass alone was already too high in the model. Furthermore, their solution with high nitrogen fixation rates would yield carbon-based productivities of approximately 0.2 mg C m^{-3} d^{-1}, when assuming a C:N ratio of 6.625 (which is actually rather close to 5 for nitrogen fixers). This would account for only 2% of the discrepancies that are apparent here.

Another hypothesis is that models lack mesoscale variability, which could be necessary to transport nitrate and nitrite to the euphotic layers by eddy pumping and horizontal advection (McGillicuddy et al., 1999 and Mahadevan and Archer, 2000). Three-dimensional model studies showed that additional eddies and fronts may lead to an increased productivity. Mesoscale features certainly contribute significantly to the total yearly productivity, but how could horizontal variability explain a systematic deficiency at the end of phytoplankton bloom within the upper oceans mixed layer? The formation of an eddy at a distinct time of the year is very unlikely and can therefore be excluded to explain the mismatch in primary production.

Malone et al. (1993) observed variations in phytoplankton productivity that were independent of the measurable chlorophyll concentrations in the euphotic zone. They attributed this phenomenon to the shift from a production which is limited by the total availability of entrained deep “new” nutrients to a production that is limited by the rate of nutrient regeneration.

Recent studies support the idea of a decoupling of the nitrogen and carbon based production when nitrate is depleted (Banse 1994, Sambrotto et al., 1993 and Antia et al., 1963). Possible explanation for high carbon assimilation ratios despite low biomass production might be due to exudation of carbohydrates and the formation of polymer carbohydrate particles (Wells 1998) in the ocean, e.g. TEP (Alldredge, Passow, and Logan 1993). An overestimation of the particulate production rates by up to 30% was reported by Karl et al. (1998). They found an evidence that ^{14}C-labeled dissolved organic carbon adsorped onto glass fiber filters. In addition, observations of dissolved organic matter (DOM) in the North Atlantic were presented by Kaehler and Koeve (2001). The authors emphasize the implicit role of carbon-rich DOM on the stoichiometry. In their study it was reported that in regimes of nitrate depletion the C:N ratios of DOM clearly increased above the Redfield ratio. Most compelling evidence for increased carbon assimilation ratios of phytoplankton can be derived from mesocosm studies made by Engel et al.(2001, personal communication) and Antia et al. (1963). In Engel et al. the exudation and formation of TEP could be shown when nutrient availability became the growth limiting factor in their mesocosm experiment. Furthermore, particulate organic carbon was still increasing while PON remained unchanged during nitrate limitation. This POC increase was concomitant with the TEP production.

As discussed here, the direct comparision of measured ^{14}C-production data with modelled phytoplankton production rates is apparently inadequate when a constant C:N ratio is assumed. The consideration of carbon exudation, producing variable C:N ratios for productivity, should improve the assimilation of ^{14}C-production data into the ecosystem model. A simple conversion of nitrogen to carbon with a constant C:N ratio is a severe model error.

Phytoplankton export — Nitrogen fixation was not considered in the model but has been suggested to have caused an increase in chlorophyll concentrations during summer. The modelled chlorophyll concentrations already remain too high if the herbivorous grazing pressure was reduced. In this case we must introduce a term which enhances the export of phytoplankton biomass. As a rudimentary first step, a quadratic phytoplankton loss can be added to the linear loss term, as introduced by Doney et al. (1996). This enhances phytoplankton losses. Furthermore, the quadratic mortality can be the prefered sink for phytoplankton rather than herbivorous grazing, as it is obvious from Exp. II . It is not possible to really evaluate whether the "no grazing solution" is reliable or not. According to the cost function, additional information on the zooplankton biomass would be helpful. Phytoplankton losses out of the mixed layer could be possible and the "no grazing solution" may be taken into consideration as well. Gardner (1997) points out that the combination of settling particle aggregates and diurnal changes in mixed layer depths can be a very effective mechanism to remove organic material from the upper ocean. This would be appropriate to an increased export during the months March and April when stratification commences and diurnal changes in mixed layer depths are maximal. Particle aggregates can be formed from phytoplankton cells, preferentially diatoms (Alldredge and Gotschalk 1989). But the relatively low chlorophyll concentrations near Bermuda suggest that the formation of aggregates is unlikely. Together with additional particles, such as polymer carbohydrates, the aggregation process might be far more effective due to increased collision rate and adherence (Engel 2000).

With respect to assimilation experiments of surface chlorophyll data we may need to better account for additional processes of phytoplankton export from the upper ocean layers. From the mentioned coincidence of highest productivity and a rapid chlorophyll decrease it is advisable to introduce sinking of detritus which could be constrained by adding PON data to the assimilation scheme as proposed before.

Deep nutrient availability — In all experiments the availability of the deep nutrient concentration N_D is parameterised. The parameterisation produces $N_D \approx 0.1$ mmol N m^{-3} during nutrient depletion in the summer periods (a similar value was determined by Hurtt and Armstrong), whereas it becomes $N_D > 4$ mmol N m^{-3} when deep mixing commences. Experiments with the constant gradient approach, as assumed by Hurtt and Armstrong (1996), did not produce model results as close to the observations as for the experiments presented here. Previous optimisations with a constant gradient parameterisation resulted in high estimates of the mixing rate

m_r which increased the entrained dissolved N and the $CHLa$ concentrations during summer. The parameterisation chosen for this study considered the remineralization process below the mixed layer, which could not be resolved by the model. Such an approach can be interpreted as a source of new nutrients to deeper layers. Thus, when deep mixing starts in late autumn the turbulent flux of nitrogen into the mixed layer is increased.

The formulation of the lower boundary conditions for an ecosystem model is a difficult task and requires further investigations. But, if the chosen ecosystem model configuration should be applicable to various places in the ocean it would be better to extend the resolution of the model. For example, the parameterisation of the deep nutrient availability can already be avoided if a model with vertical resolution is constructed, e.g. such as the physical-biological model of Doney et al. (1996), see next chapter.

The final value of the cost function alone is not sufficient to validate how well the NPZ-model performes at the BATS site. The residuals that remain between the data and the optimal model solution, must also be investigated. If the model was consistent with the statistical assumptions about the observational error variances σ_k^2, the residuals would have had a white noise character. Figure(2.18) clearly showed that this was not the case. The non-random distribution of the residuals indicated systematic deficiencies of the model, such as the underestimation of primary production after the decrease of the chlorophyll concentrations and the missing of phytoplankton export mechanisms. Our ultimate goal will be to determine the necessary model complexity that is required to achieve a model trajectory and residuals consistent with our assumptions about observational errors.

3

Data-assimilation into 1D-ecosystem models

3.1 Introduction

General circulation models (GCMs) coupled with ecosystem models are an important tool for determing basin-wide or even global biological productivity and the vertical export of organic matter in the ocean. Large-scale simulations of coupled models are helpful to investigate the ocean's biogeochemistry and its linkage to climate changes. The three dimensional (3D) physical ocean models have been continuously improved during the last decades. Major model modifications include the increase in resolution or the implementation of sophisticated numerical schemes for turbulent mixing and advection of water masses. Unfortunately, large uncertainties remain for biogeochemical simulations due to fundamental problems in the biological component. Most difficulties are related with the number of processes and their interactions within the ecosystem model.

A variety of marine ecosystem models have been developed (e.g. Evans and Parslow 1985, Fasham et al., 1990, Steele and Henderson 1992, Hurtt and Armstrong 1996, Doney et al., 1996 , Anderson and Williams 1999 and Bissett et al., 1999). These models differ significantly in complexity, from simplest models containing three biological state variables up to most complex ones with fourteen compartments. Nevertheless, in the case of large-scale biogeochemical simulations the complexity of the coupled ecosystem model is limited because of computational requirements. It has not yet been explored to what extend an ecosystem can be simplified while possesing reliable predictive skills. On the other hand, very complex models contain a large number of parameterisations and hence it becomes difficult to justify the associated parameter values. As the number of parameterisations increases with complexity the appropriate choice of parameter values tends to become subjective.

One general task for biogeochemical modelling is to represent ecological processes such that they can be utilized for local studies as well as for the entire ocean. The model suggested by Fasham et al. (1990) (hereafter named FDM-model) has become a standard ecosystem model which is still anticipated to cope with that particular challenge. The FDM-model is based on nitrogen and contains seven biological

compartments: Phytplankton, zooplankton, bacteria, detritus, dissolved organic nitrogen, ammonium and nitrate. Regarding coupled three-dimensional simulations of the North Atlantic Ocean, this FDM-model is the most complex model being implemented, as presented by Sarmiento et al. (1993) and Fasham et al. (1993). In their study they utilized biological parameter values of which some were directly adopted from literature whereas others were approximated from typical observed rates, thereby matching the typical order of magnitude at least. In the following years it was stressed to retrieve optimal parameter estimates for the FDM-model from data-assimilative investigations Fasham et al. (1993).

Parameter optimisations of the FDM-model were performed locally at the US-JGOFS station of the Bermuda Atlantic Time-series Study (BATS) near 32^{o}N 64^{o}W and at 47^{o}N 20^{o}W (site of the North Atlantic Bloom Experiment, NABE) by Spitz et al. (1998) and Fasham and Evans (1995) respectively, see Figure (3.1). In both studies a zero-dimensional model was applied, modelling the ecosystem within the upper ocean's mixed layer. Fasham and Evans (1995) were successful in simulating the observed nitrate and chlorophyll concentrations as well as the primary production of NABE with an optimised set of parameter values. Unfortunately, at the BATS site data-assimilation experiments seemed more problematic with the FDM-model, as shown by Spitz et al. (1998). Not all parameters could be constrained with the observed data, although BATS already provides an extraordinary data collection. When the ecosystem model contains large uncertainties with respect to its parameters,

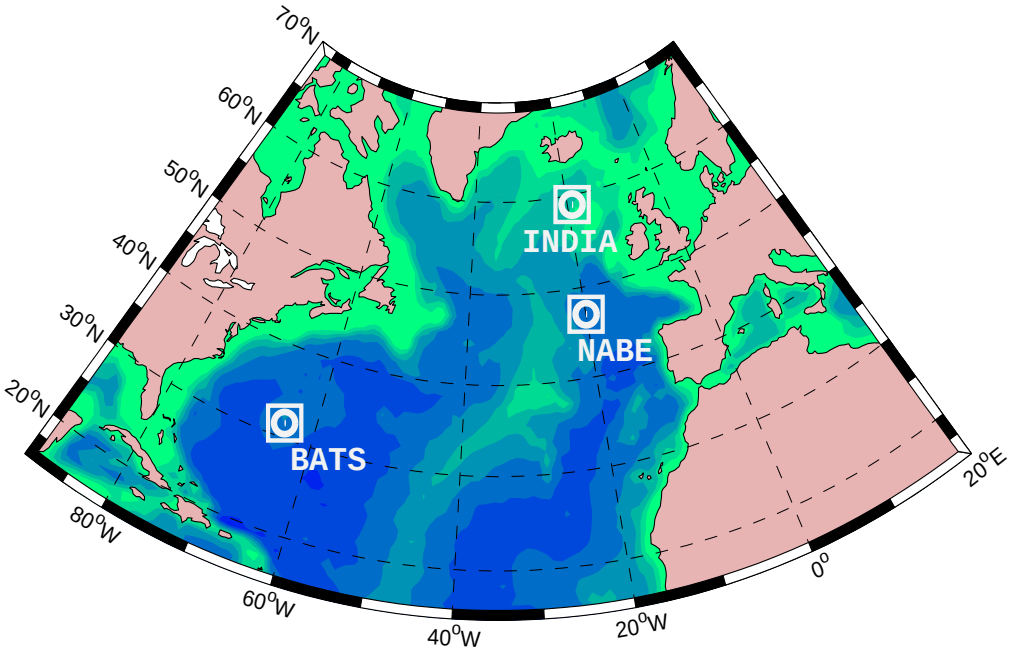

Figure 3.1: North Atlantic Ocean. The three locations of BATS (31^{o}N64^{o}W), of NABE (47^{o}N20^{o}W) and of OWS-INDIA (59^{o}N19^{o}W) used in our data-assimilative investigations are marked.

then the optimisation problem may become ill-conditioned. In this context two interpretations are possible: Either type and sampling rates of the observational data are deemed to be insufficient, or the model is considered to be too complex in order to be validated.

To develop an elaborate and simplified FDM-model with a reduced number of parameters, which could be sufficiently constrained, was the motivation of Hurtt and Armstrong (1996). They proposed a zero-dimensional model which accounts for allometric relationships for the mass exchange rates between the compartments. A modified version (hereafter named HA-model) was then optimised to data from two locations in the North Atlantic simultaneously, (Hurtt and Armstrong 1999). This was the first presentation of one single set of optimal parameters for the BATS site and the location of the Ocean Weather Ship India (OWS-INDIA).

More recent studies with a basin-wide, coupled physical-biological model of the North Atlantic included a reduced FDM-model, (Oschlies and Garçon 1999, Oschlies et al., 2000). Their ecosystem model combined nitrate and ammonium to dissolved inorganic nitrogen (N), phytoplankton (P), zooplankton(Z) and detritus(D) remained in the model whereas bacteria and dissolved organic nitrogen were neglected. Accounting for these particular compartments only, it is referred to as NPZD-model. For the coupled simulations they referred to parameter values similar to those published by Sarmiento et al. (1993) and Fasham et al. (1993). Eventually, it now appears highly desirable to determine an optimal set of parameters for such a relatively simple NPZD-model.

In this chapter it is attempted to estimate a best set of parameter values for a one-dimensional NPZD-ecosystem model at three sites in the North Atlantic simultaneously, see Figure (3.1). At these locations provide time-series observations are available whcih can be utilized for data-assimilation in order to constrain the model's parameters. These sites belong to three different biogeochemical provinces, according to Longhurst (1998). This is of particular interest, since in large-scale coupled models it is usually presumed that the physical environment controls the biological processes. Hence, one single set of biological parameters must suffice to simulate the different characteristics of the biogeochemical provinces, as long as the physical variables are trustworthy. Here, the physical components are extracted at the respective locations from three-dimensional ocean simulations (Oschlies personal communication). The data-assimilative investigations should provide optimised parameters which are aimed to be adoptable for basin-scale predictions of coupled three-dimensional models in the North Atlantic.

The NPZD-model is similar to the biological component of the basin-wide model of Oschlies and Garçon (1999) and Oschlies et al. (2000). Few modifications to the model have been conducted in order to allow for an enhanced recycling of nutri-

ents[1] and to better resolve deep chlorophyll maxima in oligotrophic regions [2], such as the BATS site. Besides the goal of estimating optimal parameter values we desire to identify model inaccuracies from remaining model misfits to observations. Either discrepancies with regard to the physical environment or due to inadequate formulations of the biological model should be revealed. The seasonal cycle is of major interest and therefore the focus is on monthly averaged variables. The monthly averages derived from observations are regarded as the best representatives of any particular month at the corresponding location.

3.2 Method

3.2.1 Model description

In general, the model simulates the biogeochemical cycle of nitrogen within a marine ecosystem. The model is a strongly simplified representation of every biological variable is subject to advective and mixing processes. In order to evaluate the correct vertical distribution with time of each biological state variable (C_i) an advective-diffusive equation is solved numerically. In the one-dimensional case an appropriate equation can be formulated as follows:

$$\begin{aligned}\frac{\partial C_i}{\partial t} &= -w\frac{\partial C_i}{\partial z} + \frac{\partial}{\partial z}\left(K_\rho \frac{\partial C_i}{\partial z}\right) + SMS(C_i) \\ &= -\frac{\partial (wC_i)}{\partial z} - \underbrace{(\nabla_h \cdot u)}_{-\frac{\partial w}{\partial z}} C_i + \frac{\partial}{\partial z}\left(K_\rho \frac{\partial C_i}{\partial z}\right) + SMS(C_i)\end{aligned} \tag{3.1}$$

where t denotes time, z depth (upward positive). K_ρ is the turbulent eddy coefficient while u and w are the horizontal and vertical velocities. The terms on the right hand side represent vertical advection, turbulent mixing and source minus sinks regarding the inherent biological processes (SMS). If vertical velocity varies with depth and water mass is to be conserved, any convergence in the vertical advective flow has to be compensated by a horizontal divergent flux and vice versa (underbraced brackets in equation 3.1). In the following, the term $-C_i \nabla_h \cdot u$ will be referred to as horizontal divergence. Because the model is only of vertical resolution some assumptions are necessary with respect to the horizontal tracer distribution[3]. The model layers are considered to have horizontally homogeneous tracer fields which means that horizontal gradients of the tracer are omitted. Vertical gradients in the vertical velocities should be accompanied by horizontal divergence or convergence of water mass at

[1] In three-dimensional simulations the productivities in oligotrophic regions remained too low by one order of magnitude. This is attributed to inefficiencies in the recycling of nutrients which results in a decreased regenerated production.

[2] Preliminary model optimisations (which will not be discussed here) at the BATS and NABE sites have shown significant improvements with respect to observations as soon as variable chlorophyll to nitrogen ratios were applied.

[3] Note that solely biological tracer are modelled.

the location where the model is applied. Figure (3.2) illustrates the relation between vertical and horizontal divergence.

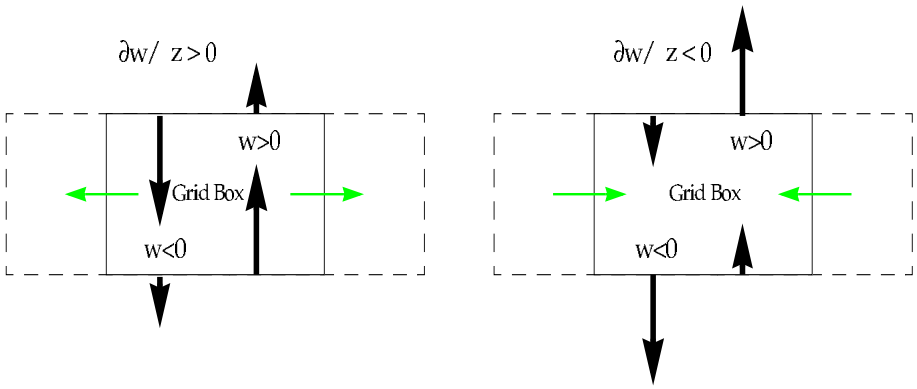

Figure 3.2: Model grid box at one depth and sketch of vertical velocities. Vertical velocities are retreived at the bottoms of the grid boxes. For conservation of water mass (under the assumption of incompressibility) the divergencies in the vertical flow field are compensated by horizontal flow.

Physical forcing

For reliable simulations of the biogeochemical fluxes the ecosystem model is embedded in a physical environment which is obtained from a primitive-equation ocean circulation model, similar to Oschlies, Garçon, and Koeve (2000). The model originates from the Geophysical Fluid Dynamics Laboratory (GFDL) Modular Ocean Model (MOM) version 1.1 (Pacanowski et al. 1991). The vertical mixing has been improved by implementing a more elaborate turbulence closure scheme to the model. A model of turbulent kinetic energy (TKE) by Blanke and Delecluse (1993) was used, which is a modified version to the originally described model of Gaspar et al. (1990). Furthermore, a multidimensional positive definite centered differences (MPDCD) advection scheme was utilized, as introduced by Lafore et al. (1998). Appropriate flux corrections with the MPDCD-scheme assure that the outgoing fluxes from a single grid cell do not exceed the corresponding tracer concentration of the previous timestep.

The resolution was chosen to allow for mesoscale variability (“eddy permitting”) with a meridional grid of $1/3^o$ and a zonal grid spacing of $2/5^o$. According to the OG-model, the water column is partitioned into 37 levels with the first 10 levels resoving the upper 126 meter, see Table (A.1) in the Appendix. A more detailed description of the model’s configuration is given in Oschlies and Garçon (1999). The model was forced with daily mean reanalysed data of the European Center of Medium Range Weather Forecast (ECMWF), covering the period 1989 through 1993 (Ferry and Oschlies, personal communication). Regarding the one-dimensional simulations here,

the same surface shortwave radiation data from ECMWF is used as it was chosen for the basin-scale simulations, see Figure (3.3). Besides the shortwave radiation,

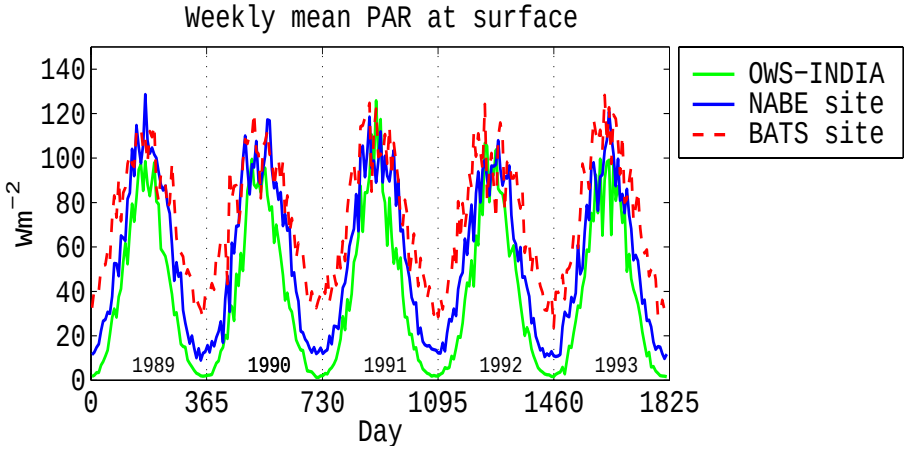

Figure 3.3: Photosynthetic available radiation (PAR) on the ocean's surface at the three locations of interest. The plot shows weekly mean values whereas the model is forced with daily data.

physical components are extracted from three-dimensional (3D) simulations at three locations of interest (BATS, NABE and OWS-INDIA sites). For this study, the physical model data is utilized in order to solve the advective-diffusive equation (3.1) for our local one-dimensional ecosystem simulations.

Vertical velocities (w) and turbulent mixing coefficients (K_ρ) are obtained from the three-dimensional model runs. The vertical velocities from the 3D-model comprise fluctuations with a dominant period ranging between five to six days at all locations. These fluctuations can be attributed to variablities on a synoptical scale. For example, fluctuations are evoked by storm tracks which are resolved by the ECMWF forcing fields. For the evaluation of mean annual biogeochemical fluxes the net advective transports are of particular interest. Vertical profiles with five year averages of the vertical velocity are shown in Figure (3.4) for the respective locations. At the BATS location the mean vertical velocities yield a net downwelling within the upper 160 meters of depth. This modelled vertical flow is generated by convergence of the flow field within the surface boundary layers. The BATS region is mainly influenced by westerly winds having a slight northward component. Towards the north of Bermuda the westerly mean wind stress becomes stronger which induces a convergence in the Ekman transport (Ekman 1927) leading to the expulsion of water mass and hence to downwelling motions ("Ekman pumping"). Similar conditions exist for the NABE site, except that variations in the wind stress are much larger. It is particularly true for the winter months when westerly winds are strengthened, (e.g. Wright 1988 in Tomczak and Godfrey 1994). However, according to the maximal mean vertical velocity at the BATS and NABE sites (at approximately 50 meters) an annual pumping of 27 m yr^{-1} can be depicted. Similar Ekman velocities are obtained by Marshall et al. (1993)

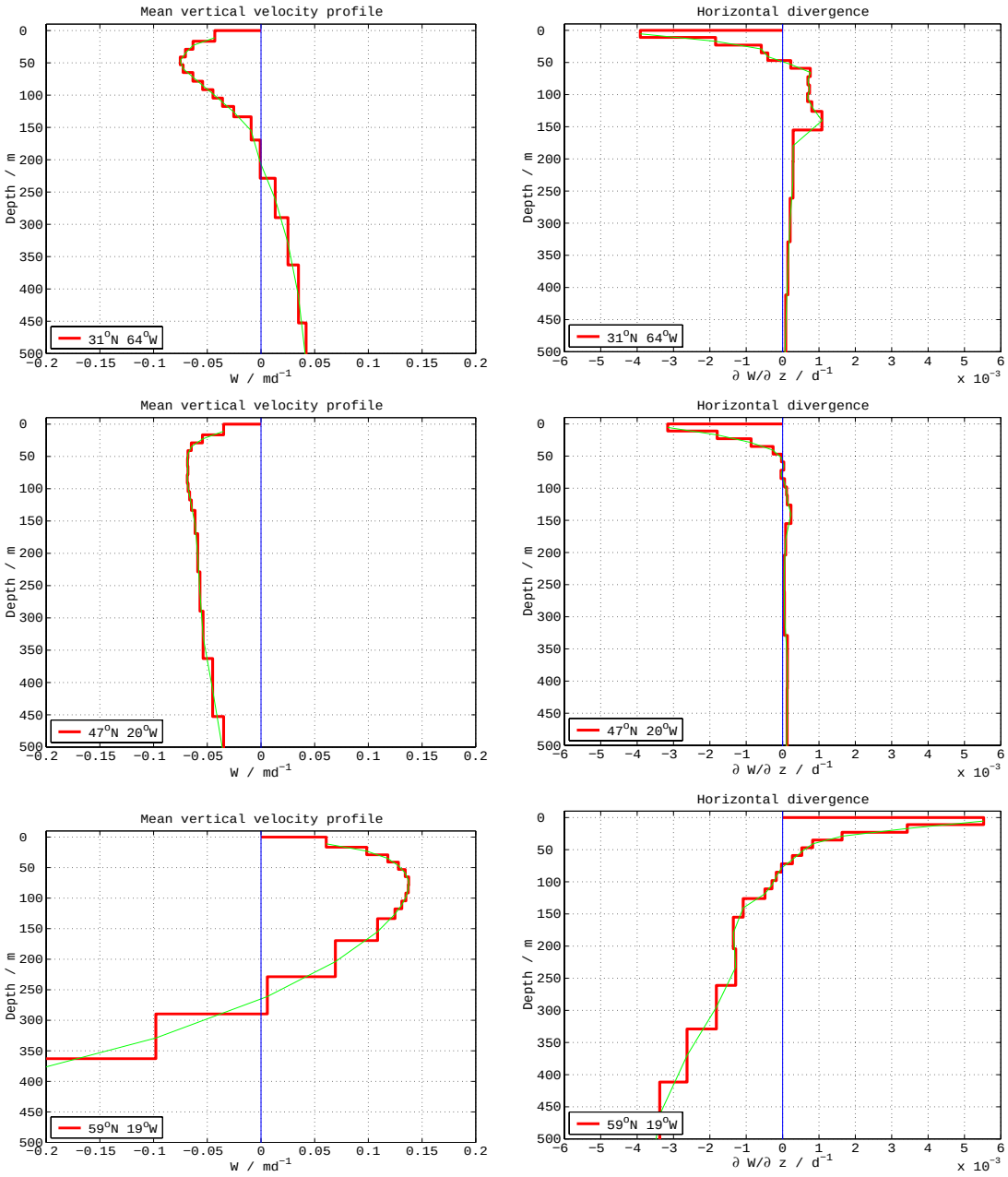

Figure 3.4: Five year averages of the vertical velocity within the upper 500 meters. Left side: Vertical velocities (w); Right side: Vertical gradients of the vertical velicities ($\frac{\partial w}{\partial z}$). The units are md^{-1} and d^{-1}, for w and its gradient respectively. From the vertical gradients informations with respect to the horizontal divergence can be retrieved, compare with Figure (3.2).

when referring to Isemer and Hasse (1987) climatological data. At the most northern location (OWS-INDIA) the wind field induces divergencies in the Ekman transports. Such transports are accomplished with upwelling. The maximal annual velocity is at approximately 70 meters, yielding 51 m yr^{-1}.

Modelled temperatures are additionally considered for the evaluation of maxi-

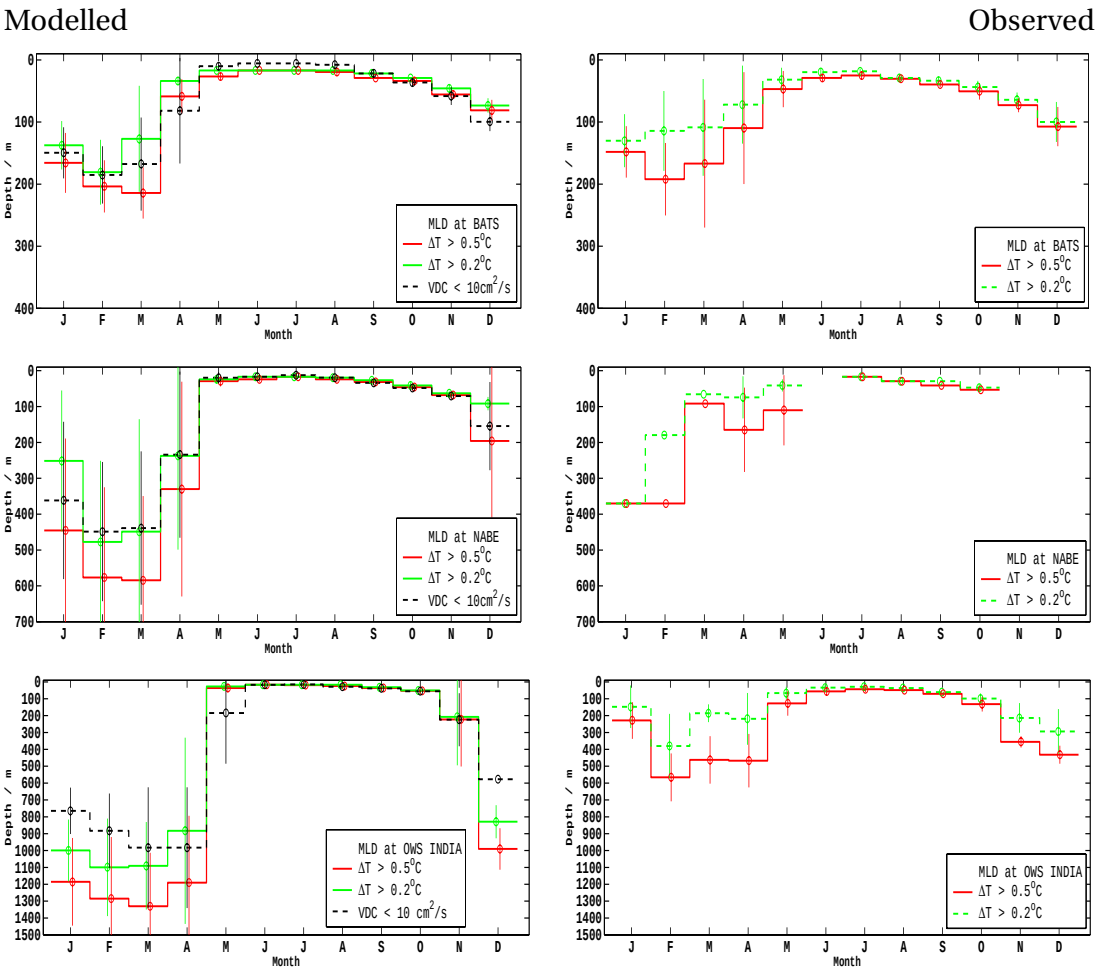

Figure 3.5: Mixed layer depths at the BATS (top), NABE (middle) and OWS-INDIA (bottom) sites. The shown mixed layer depths result when a 0.2^{o}C (green/gray solid lines) and a 0.5^{o}C (red/black solid lines) temperature criterion is applied. For the model, those depths at which the vertical turbulent mixing coefficient becomes less than 10cm^{2}s^{-1} are additionally shown (dashed lines). Vertical bars indicate the satndard deviations due to interannual variabilities.

mal phytoplankton growth rates (Eppley 1972) and variable chlorophyll to nitrogen ratios. Mixed layer depths can be approximated from modelled and observed temperatures. A simple criterion is applied that determines the depth at which the temperature deviations from its surface value exceed a given increment (here $\triangle$T=0.2^{o}C and $\triangle$T=0.5^{o}C). Mixed layer depths show differences between model results and observations, Figure (3.5). In addition to the utilization of a temperature criteria, those depths at which the vertical turbulent mixing coefficient becomes less than 10 cm^{2}s^{-1} has been evaluated for the model as well.

The mean seasonal cycle of modelled and observed temperatures are shown in Figure (3.6) for the three sites of interest. The model's monthly averaged temperatures at the BATS site are in very good agreement with the observed counterparts

from spring through autumn. Only in December and January the simulated temperatures tend to be lower than observed within the upper 100 meters. In particular, the depth of the 19^{o}Celsius isotherm is well reproduced by the model throughout all months. Beneath 200 meters the model is colder which results in a 1^{o}Celsius offset at approximately 400 meters. Nevertheless, the temperature deviations mentioned here are small. As a consequence the mixed layer depths derived from the model are appropriate with regard to the observed depths, as it can be seen in Figure (3.5).

At 47^{o}N20^{o}W the model shows a slightly poorer performance, if compared with the results near Bermuda. Observations yield highest mean temperatures in August, close to 18.5^{o}Celsius. The model predicts temperatures that are above 18^{o}Celsius during the whole summer within the upper 23 meters. While the model shows a tendency towards increased temperatures during summer it underestimates temperatures in the winter period. Figure (3.5) shows the corresponding mixed layer depths which seem slightly deeper in the model. However, according to those mixed layer depths that are determined from the vertical turbulent mixing coefficient (the depth at which K_ρ becomes smaller than 10 cm^{2}s^{-1}) the discrepancies between observation and model are small.

The overestimation of summer temperatures by the model is stronger for the site of OWS-INDIA at 59^{o}N19^{o}W. Although predicting higher temperatures in summer the model is cooler during winter time, as it is emphasized by the outcrop of the 7^{o}C isotherm. As a result the model winter-mixing is deeper than observed. It is noteworthy that the observed temperatures cover the period of 1970 through 1974, recalling that the model was forced with ECMWF reanalysis data from 1989 through 1993. The location of the OSW-INDIA falls into an ocean region where anomalies in heat fluxes are induced by interdecadal variabilities such as the North Atlantic Oscillation (NAO). For instance, the index for the NAO remained in a low phase within the period of observations (1970 to 1974) while the NAO index was higher during the period of simulation. A weakening of westerly winds is associated with a low NAO-index around the OWS-INDIA site which means that the corresponding observed mixed-layer depths are expected to be shallower than for the years 1989-1993. Recent simulations of Oschlies (2001) with low-NAO forcing are in agreement with these expectations. Nevertheless, It is not clear wether this can fully explain the mentioned differences between modelled and observed temperatures.

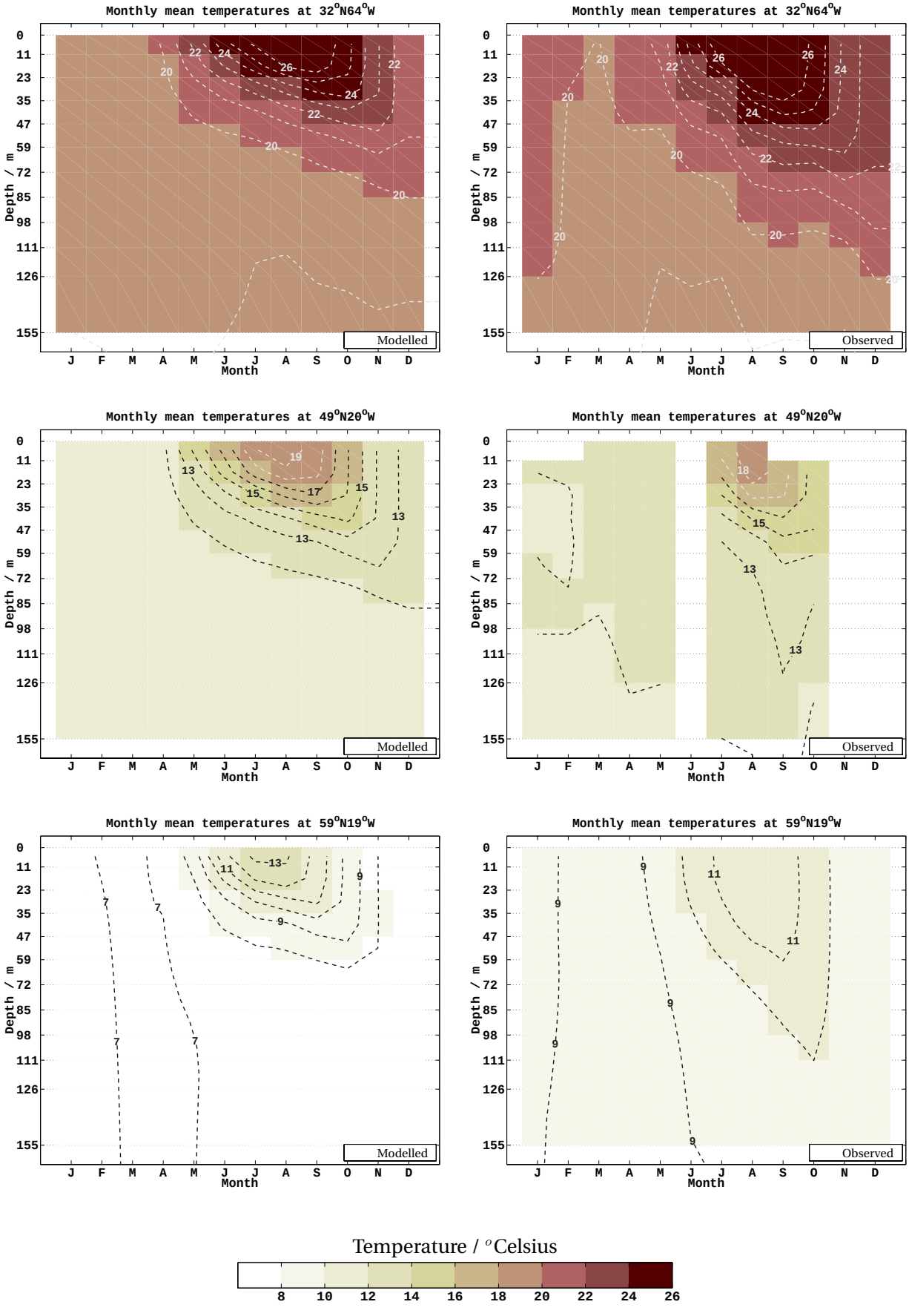

Figure 3.6: Monthly averaged temperatures within the upper 15 model grids: Modelled temperatures (left side) and the observational counterparts on the same grid (right side). Locations: BATS site (top), NABE site (middle) and OWS-INDIA site (bottom).

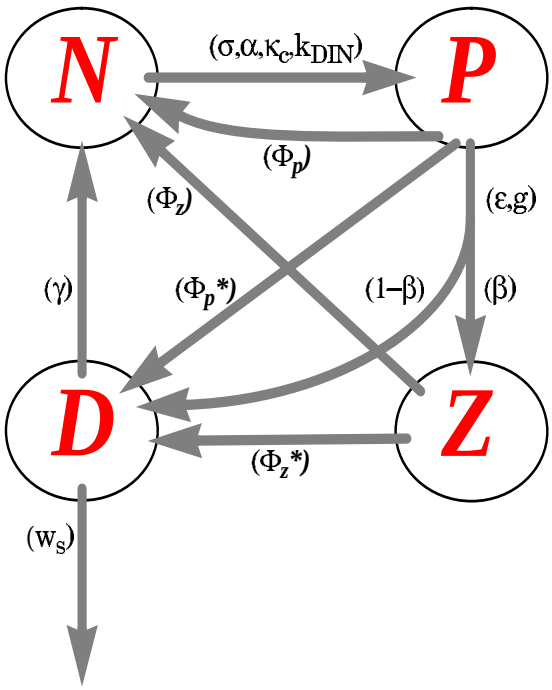

Figure 3.7: Structure of the ecosystem model. The compartments (state variables) are dissolved inorganic nitrogen (N), phytoplankton biomass (P), herbivoreous zooplankton (Z) and detritus (D). The arrows indicate the direction of mass flux while the attached brackets list the parameters that control the corresponding mass flux rate. The parameter symbols are explained in Table (3.1).

Biological processes

The ecosystem is split up into four state variables: Dissolved inorganic nitrogen (N), phytoplankton (P), herbivorous zooplankton (Z) and detritus (D). The interactions of the four compartments in the NPZD-model are sketched in Figure (3.7). The arrows in Figure (3.7) indicate the nitrogen fluxes, with symbols indicating those parameters that are associated with the rates for each particular flux. All model parameters are listed in Table (3.1). The daily light-limited growth rates are determined according to Evans and Parslow (1985) while zooplankton grazing is calculated with a Holling Type III function. The full model equations are listed in the Appendix (A.2). With respect to the previously used NPZ-model, see Chapter 2, the basic structure has been extended. Such a model modification can be justified since phytoplankton export and remineralization turned out to be processes which are needed to be better resolved, as it was discussed in Chapter 2. The ecosystem model in this study resembles that of Oschlies and Garçon (1999) and Oschlies et al. (2000) (hereafter referred to as OG-model).

The parameterisations of phytoplankton losses have been reconsidered. Formulations for the phytoplankton mortality rates are adopted from Doney et al. (1996), see also Oschlies (2001). Hence, a quadratic mortality (Φ_p^*) is introduced that should

approximate the loss of phytoplankton due to the formation of aggregates. As a consequence, this quadratic loss term must enter the detritus compartment which sinks through the water-column, see Figure (3.7). The phytoplankton's linear nitrogen loss now enters the dissolved nitrogen compartment directly. This is different to the previous approach where it entered the detritus compartment. In that case, the prevailing idea is to enhance the model's regenerated production without including bacteria and dissolved organic nitrogen (DON) as additional state variables to the model. Proceeding like this simply implies that a fraction of the phytoplankton's nitrogen is lost via exudation, leakage or cell lysis. This phytoplankton nitrogen loss is presumably (DON) which is immidiately remineralized and becomes then available as regenerated nutrient.

The implementation of a variable chlorophyll to nitrogen (CHL:N) ratio is the fi-

p_ν	Symbol	**Parameters for variation**	Unit
p_1	μ_m	Maximum growth rate	d^{-1}
p_2	α	Slope of photosynthesis versus light intensity	$m^2 W^{-1} d^{-1}$
p_3	Φ_P	Phytoplankton loss	d^{-1}
p_4	Φ_P^*	Phytoplankton quadratic loss	$m^3 mmol N^{-1} d^{-1}$
p_5	k_{DIN}	Half saturation constant of N uptake rate	$mmol N m^{-3}$
p_6	κ_c	Attenuation coefficient due to chlorophyll	$m^2 mg CHL a^{-1}$
p_7	g	Maximum grazing rate	d^{-1}
p_8	ϵ	Prey capture rate	$m^6 mmol N^{-2} d^{-1}$
p_9	Φ_Z	Herbivore mortality	d^{-1}
p_{10}	Φ_Z^*	Herbivore quadratic mortality	$m^3 mmol N^{-1} d^{-1}$
p_{11}	β	Assimilation efficiency of herbivores	dimensionless
p_{12}	γ	Remineralization rate of detritus	dimensionless
p_{13}	w_s	Detrital sinking velocity	$m d^{-1}$
		fixed Parameters	Value and unit
	k_w	Light attenuation due to water	0.04 m^{-1}
	R	molar carbon to nitrogen ratio	6.625
	f_{PAR}	shortwave fraction of PAR	0.43
	q_{10}	growth coefficient (EPPLEY 1972)	1.066
	c	growth coefficient (EPPLEY 1972)	1.000 $(^o C)^{-1}$

Table 3.1: Parameters of the ecosystem model. The first thirteen parameters of the list will enter the optimisation process.

nal modification to the original OG-model. As for the NPZ-model in Chapter 2, an empirical relationship is used as originally proposed by Cloern et al. (1995). At this point it should be noticed that the light attenuation includes the self shading effect of phytoplankton due to its chlorophyll adsorption. As a consequence variable CHL:N ratios have an influence on the light distribution with depth.

The biological model is initialized with vertical nitrate profiles from Conkright et al. (1994). The timesteps of integration are 15 minutes for the biological state variables whereas they are 1 hour for the advective-diffusive equation. The spin up time equals two identical years with the same physical componenents as derived for the year 1989.

3.2.2 Observational data

Monthly mean observational sets are collected from repeated investigations at each of the three locations of interest, generally covering a certain time period with intense measurements. At all three locations five types of observations are selected in order to be assimilated into the NPZD-model: Nitrate+nitrite (NO_3+NO_2), chlorophyll a (CHL), ^{14}C-primary production (C-PP), particulate organic nitrogen (PON) and zooplankton biomass (ZOO). If no nitrite measurements exist then nitrate is solely considered. All observations are interpolated onto a 1 meter vertical grid and averaged over those depths which are resolved by the model's grid boxes. Monthly averages are calculated for each data type within the upper 411 meters.

Locations:

31^{o}N 64^{o}W — Near Bermuda data is available from the BATS, as a part of the U.S. JGOFS project (Michaels and Knap 1996). The BATS data is provided by the Bermuda Station for Research (BBSR)[4], see also Chapter 2. Except for zooplankton biomass, all monthly mean values are obtained from biweekly to monthly data, covering the years 1989-1983. Zooplankton biomass is taken from literature (Caron et al. 1995), referring to their measurements of heterotrophic nano- and microzooplankton.

47^{o}N 20^{o}W — Here, most measurements occured during NABE (Ducklow and Harris 1993) in the year 1989. Therefore, the derived monthly mean observational values are dominated by measurements retrieved from that year. A collection of observations has been received from the British Oceanographic Data Centre (BODC, Roy Lowry personal comunication). This data set is extented by German JGOFS investigations until 1996 which have been kindly collected by W. Koeve (personal communication) and can now be attained from the German JGOFS data management[5]. All data entering the calculations are selected from an area with 5^o latitudinal and 5^o longitudinal extension (17.5 ^{o}W–22.5 ^{o}W, 44.5^{o}N–49.5^{o}N). Microzooplankton biomass data, used here, is identical to those observed values utilized in Fasham and

[4]BATS extraction site http://www.bbsr.edu/users/ctd/

[5]Web site of German JGOFS data management http://www.ifm.uni-kiel.de/jgofs/dm/parametr.htm

Evans (2000) for data-assimilation, referring to measurements of Verity et al. (1993) and two additional observations made in late summer of 1989.

59°N 19°W — Frequent observations from this northern Atlantic site were maintained during the years 1971-1974 Williams (1988), already yielding a good time-series of observations. Additional observations fell into the years 1989 and 1996. Data from this area is part of the Plankton Reactivity In the Marine Environment (PRIME) project data set, available at the BODC (supplied by Roy Lowry and Polly Hadziabdic). As for the NABE site, data within a 5^o latitudinal and 5^o longitudinal area is solely considered (16.5°W–21.5°W, 56.5°N–61.5°N).

3.2.3 Definition of the cost function

Cost function terms

The cost function is defined as a weighted least square misfit between model results and observations, see also Chapter 2. The basic least square term of the cost function is derived on the assumption of a normal error distribution, regardless whether this distribution is in fact normal or not. Weights are attributed to the locations, to the different variables and to the data availability.

The total misfit combines the individual cost function contributions at all three locations of interest ($\mathcal{J}_l$) and is calculated as follows:

$$\mathcal{J}_{total} = \frac{1}{2} \sum_{l=1}^{L} \frac{\mathcal{J}_l}{\mathcal{J}_l^{(0)}} \tag{3.2}$$

with L being the number of locations (here, L=3) and a scaling (or weighting) factor according to the different locations $\mathcal{J}_l^{(0)}$. The individual cost functions are defined as:

$$\mathcal{J}_l = \sum_{j=1}^{J} \frac{1}{\mathcal{N}_{jl}} \sum_{t=1}^{\mathcal{N}_{jl}} \sum_{k=1}^{Kmax} \frac{1}{\sigma_j^2} \left(f_j - y_j^{obs} \right)_{tk}^2 \tag{3.3}$$

with the monthly mean observation y_j^{obs} in month j and its modelled counterpart f_j. The total number of observational types is J=5 (since NO_2+NO_3, CHL, C-PP, PON and ZOO are utitlized). $\mathcal{N}_{jl}$ is the number of months for which observations of type j at location l are available. The maximal depth for data to be assimilated into the model is 411 meters which is equivalent to the K_{max}=15 (grid box) $\equiv$ 411 meters.

Assumptions for covariances are neglected. That is, correlations among the variables are not accounted for. Further, deviding by the number of available observational months gives higher weights to observations which are scarce if compared with those yielding a full seasonal cycle. This is particularly true for zooplankton observations which are very important for the parameter optimisation process, Schartau et al. (2001).

The assigned weights for NO_2+NO_3 are adopted from Chapter 2, yielding σ_N= $8.25 \cdot 10^{-2}$ mmol N m^{-3}. For chlorophyll and PON concentrations standard devia-

tions of $\sigma_{CHL} = 0.1\,\mathrm{mg\,m^{-3}}$ and $\sigma_{PON} = 1.0\,\mathrm{mg\,m^{-3}}$ are assumed, respectively. Note that any relative error which can be attributed to spatial heterogenities is omitted, for comparision see section (2.2.2) in Chapter 2. For primary production different weights are given with regard to the locations. These are 15 % of the annual mean primary production at the respective sites, yielding σ_{PP}=1.2 mg C $\mathrm{m^{-3}d^{-1}}$ for the OWS-INDIA site, 1.8 mg C $\mathrm{m^{-3}d^{-1}}$ for the NABE site and 0.5 mg C $\mathrm{m^{-3}d^{-1}}$ for the BATS site. The weights for zooplankton biomass remain identical for all locations and are classed with σ_{ZOO}=0.01 mmol N $\mathrm{m^{-3}}$.

Scaling

The simplest idea for an overall cost function is to add together all least square misfits of the three locations. Unfortunately, this results in any sort of preference for one particular location. For instance, as soon as some sort of observation (e.g. chlorophyll concentrations) differ between two locations by one order of magnitude, it is likely that the smaller concentrations at one location produce misfits which become apparently neglible. Furthermore, at the location with small concentrations, the differences between zero and the observed value could become less than differences at another location. The latter problem would be a worst case scenario, but is obviously very realistic, as it appeared during our first optimisation attempts. Without any additional scaling of the locations, the optimisation resulted in parameter values which produced a model solution where the biology became extinct only at Bermuda location, while the misfits at NABE and INDIA still produced the largest contributions to the cost function (not shown here).

Due to this difficulty it becomes necessary to think of a scaling. The scaling should assure that at each location sum of the respective least square misfits contributes to the cost in the same order of magnitude. Therefore, a scaling is introduced that considers averaged observational values at the individual locations:

$$\mathcal{J}_l^{(0)} = \frac{1}{2}\sum_{j=1}^{J} \frac{\left(\overline{\mathbf{y^{obs}}}\right)_j^2}{\sigma_j^2} \tag{3.4}$$

with the subscript i being the different sorts of observation, as they were previously declared, see equations (3.2.3) and (3.2.3) . At every location a $\mathcal{J}_0$ is determined, which is the square of the mean observation (e.g. vertically and time averaged primary production) devided by the variances of observations.

The value $\mathcal{J}_l^{(0)}$ is dimensionless and its calculation does not provide any useful information other than the typical order of magnitude of observations at the corresponding location. Finally, the new cost function is determined with additional factors for each location and the scaling then enters the cost function as follows:

$$\mathcal{J}_{total} = \frac{\mathcal{J}^{BATS}}{\mathcal{J}^{(0)}_{BATS}} + \frac{\mathcal{J}^{NABE}}{\mathcal{J}^{(0)}_{NABE}} + \frac{\mathcal{J}^{INDIA}}{\mathcal{J}^{(0)}_{INDIA}} \tag{3.5}$$

$$= 0.0055 \cdot \mathcal{J}^{BATS} + 0.00026 \cdot \mathcal{J}^{NABE} + 0.00011 \cdot \mathcal{J}^{INDIA} \tag{3.6}$$

At the oligotrophic location near Bermuda the observational values are much smaller than at the rather eutrophic regions at NABE and the OWS-INDIA. Due to this fact the misfit contributions of NABE and INDIA to the combined cost function are reduced. The proposed weighting ratios (BATS:NABE:INDIA) are equivalent to 50:2:1.

Value of expectation
According to our weights and the scaling in the cost function the value of expectation becomes $< J >$=0.22, having least square data-model misfits within the prescribed variances. Because most observational errors are unknown for the different variables, or they remain undocumented in the literature, their is a certain arbitrariness in the choice of the weights (in particular for the zooplankton biomass). Due to these uncertainties in the assignment of weights and possible systematic errors this value of expectation is not seriously attempted to be achieved.

3.2.4 Errors of parameter estimates: Monte Carlo bootstrap method

Knowledge about the reliability and robustness of the optimisation process is required when an optimal set of parameters is found. In this chapter, the uncertainties of the best parameter estimates are retrieved from a Monte Carlo bootstrap method.

The overall idea of the bootstrap approach is to replace the original data by a simulated data set. The statistics of the bootstrap method is described by Efron (1994). Originally, it is proposed to construct a new synthetic data set from real observations by adding noise whose error distribution should be derived from the residuals that remain between the best model fit to observations. When systematic errors exist one has to account for the error distribution of the residuals individually. An alternative approach is considered by adding Gaussian noise to the observations, referring to the same probability distribution of the oberved data as it is assumed for the cost function. Evans (1999) successfully utilized this alternative technique. Optimisations are then repeated with the synthetically generated data starting from a different random distribution of initial parameter guesses. A simulated data set $\mathcal{D}^s$ is obtained by adding Gaussian noise ($\boldsymbol{\eta}$) to the original data ($\mathbf{y}$):

$$\mathcal{D}^s \equiv \mathbf{y}(z,t) + \boldsymbol{\eta}(\boldsymbol{\sigma_{obs}}, 0), \quad \forall \; t \,\epsilon\, \{1, \ldots, 12\}, z \,\epsilon\, \{1, \ldots, 15\} \tag{3.7}$$

with t and z being the months and grid depths of the observational counterpart to the model.

The optimisation with the original data set $\mathcal{D}_0$ produces a best estimate of the parameter vector $\hat{\mathbf{p}}_0$. Let $\hat{\mathbf{p}}_i^s$ be any additional estimated set of parameters that has been recovered by the i'th optimisation with the corresponding simulated data set $\mathcal{D}_i^s$. Due to computational costs, only three synthetic data sets are generated here. Hence, three additional parameter estimates can be determined from the optimisation procedure. Together with the original best estimate, four independent optimisations results (realizations) are available. The standard deviations of the parameter estimates were determined from two errors. For each parameter vector component

ν, the approximated standard deviation becomes:

$$(\widehat{\sigma})_\nu = \sqrt{(\widehat{\sigma_{sd}})_\nu^2 + (\widehat{\epsilon})_\nu^2} \tag{3.8}$$

with $(\widehat{\sigma_{sd}})_\nu$ being the standard deviation with respect to the mean value retrieved from all four realizations with. Hence, the first error is calculated according to:

$$(\widehat{\sigma_{sd}})_\nu = \left[\frac{1}{3}\sum_{i=0}^{3}(\hat{p}_i - \langle\hat{p}\rangle)_\nu^2\right]^{1/2} \tag{3.9}$$

referring to the mean parameters $\langle\hat{p}_\nu\rangle$. The second error $(\widehat{\epsilon})_\nu$ accounts for the deviation of the best parameter estimate to the mean value:

$$(\widehat{\epsilon})_\nu = (\hat{p}_0 - \langle\hat{p}\rangle)_\nu \tag{3.10}$$

3.2.5 Optimisation procedure

A total of four optimisations are performed in order to retrieve additional approximations of variances on the parameter estimates and to dislose the robustness of the parameter estimations. Figure (3.8) illustrates the process of optimisation. The ab-

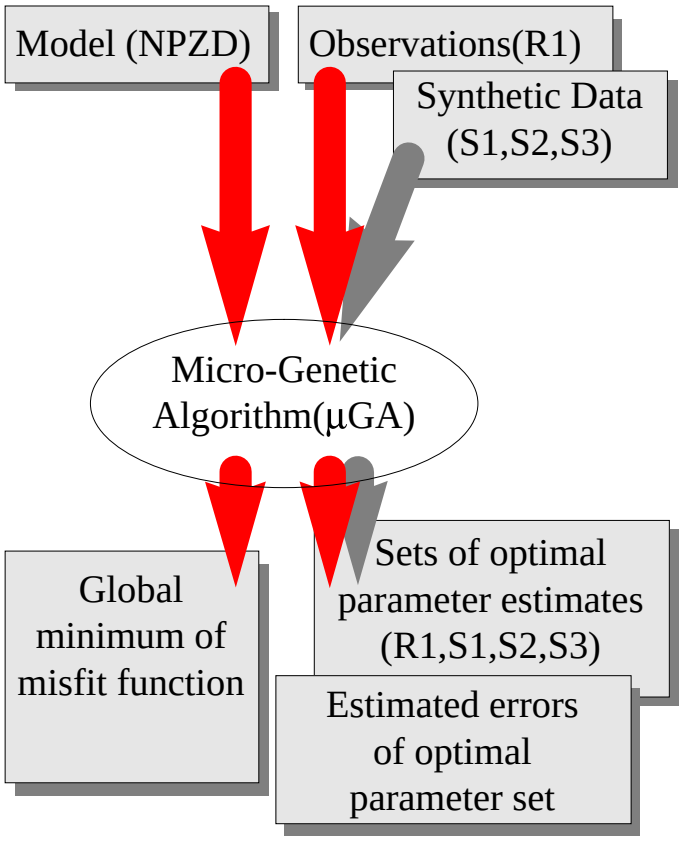

Figure 3.8: Sketch of the optimisation procedure.

breviation R1 denotes the optimisation with the original observations. S1 to S3 stand for optimisations performed with the three resampled data sets. For each of the four

optimisations the μGA is utilized but starting from different initial parameter values.

Table (3.2) lists the different parameters for optimisation and their precisions, given by the increments (see Appendix, A.3.1). That is because the μGA contains "chromosomes" which are binary coded with a single bit string representing one parameter. The length of a single bit string (or number of binary digits) describes the number of possible values for the parameter within its range for variation. For example, for a bit length of 7 there are 2^7=128 possibilities to resolve the maximal growth rate μ_m within its lower and upper bounds (0.02 d^{-1} and 1.47 d^{-1}), yielding an increment of 0.01 d^{-1}. Therefore upper and lower bounds for the parameter's values are prescribed and listed as well.

The population yields 13 individuals and a total number of 2000 generations is prescribed, yielding 2000*13=26000 iterations. Additional control variables of the μGA are described and given in the Appendix (A.3.1).

PARAMETER CONFIGURATION FOR MICRO-GENETIC ALGORITHM				
PARAMETER	**Lower bound**	**Upper bound**	**Increment**	**# of possibilities**
μ_m	0.020	1.470	0.010	128
α	0.001	0.256	0.001	256
Φ_p	0.000	0.635	0.005	128
Φ_p^*	0.010	0.955	0.015	64
k	0.100	0.730	0.010	64
κ_c	0.010	0.073	0.001	64
g	0.025	1.600	0.025	64
e	0.025	1.600	0.025	64
Φ_z	0.000	0.635	0.005	128
Φ_z^*	0.010	0.955	0.015	64
β	0.300	0.935	0.005	128
γ	0.020	0.146	0.002	64
w_s	1.000	128.0	1.000	128

Table 3.2: Parameter setup for optimisation with micro-genetic algorithm. The increments yield the highest precisions that can be achieved with the μGA.

3.3 Experiments and results

The experimental setup is such that optimal parameter estimates should be retrieved for an NPZD-model. This is achieved by assimilating observational data into the model. The cost function, as defined in equation (3.2.3), enters the optimisation process and is minimised while varying the model's parameter values. Hence, the cost function's minimum yields the best parameter estimates. Two model configurations are subject to the optimisation process in order to reveal differences in the parameter estimates that are associated with the consideration of vertical advective velocities. One model regards vertical advection of all the model's state variables by the vertical velocity fields extracted from the 3D simulations, hereafter referred to as NPZD-wW model. The other configuration (NPZD-nW) neglects these vertical advective transports, with the sinking of detritus being the only exception.

The cost function minimization of the micro-genetic algorithm (μGA) is satisfactory. Figure (3.9) demonstrates its ability to minimise the cost function. A total of 26000 iterations have been conducted for each optimisation, which is equivalent to 77 hours of computational time[6]. A significant decrease of the cost function values (hereafter called 'costs') is accomplished with respect to those initially obtained. The initial costs typically range between J=17 and J=30, whereas the minima yield much

[6] on a DEC/ALPHA with 677 MHz

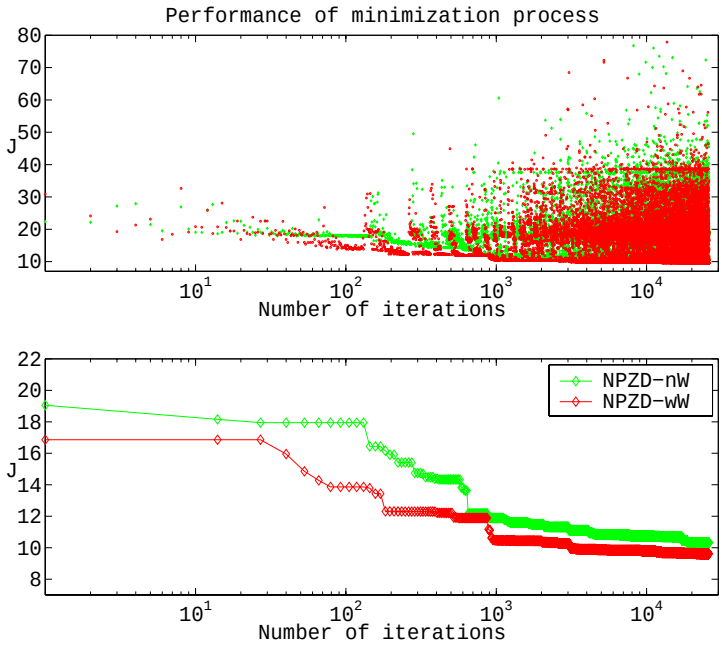

Figure 3.9: Cost function values during the minimization process: The top graphic shows the costs of all iterations during search for both model configurations (red/black=NPZD-wW) and (green/gray=NPZD-nW). The bottom plot shows the minimal costs within each generation that are being retained (one generation has 13 individuals = 13 iterations). The ideal value of expectation for the cost function is $< J >$=0.22.

COST FUNCTION VALUES				
MODEL CONFIGURATION	J_{total}	J_{BATS}	J_{NABE}	J_{INDIA}
A priori (NPZD-wW)	15.87	6.40	5.42	4.05
With advection (NPZD-wW)	**9.62**	3.94	2.88	2.80
No advection (NPZD-nW)	10.32	4.19	2.93	3.20

Table 3.3: Cost function values that are associated with 1) the NPZD-model when the *a priori* parameter set is utilized, 2) with the optimal estimate for the model which fully considers vertical advection and 3) with the optimal parameters for the model with sinking of detritus only. The theoretically "ideal" value of expectation for the cost function is $< J >$=0.22.

lower costs, J=9.62 and J=10.32 for the model configurations with and without vertical advection respectively. Although the lowest achieved costs are retained during the search process, the entire parameter space is exploited until the end. This produces fluctuations of the costs, as they can be seen in Figure (3.9,top), which is a characteristic feature of the μGA.

In Table (3.3) the cost function's minima are shown for the two model configurations, resolving the misfit contributions at all three locations. For comparision, the costs of the *a priori* configuration are additionally listed. The *a priori* model includes vertical advection and contains parameter values which are identical to the previously applied values in Oschlies and Garçon (1999) and Oschlies et al. (2000). Due to the mentioned model modifications, the *a priori* values for the linear and quadratic phytoplanklankton losses (Φ_p and Φ_p^*) are taken from Doney et al. (1996). First of all, the success of the optimisation becomes apparent when comparing the individual misfit contributions with the costs of the *a priori* model. According to the total costs of the NPZD-wW model, the misfits have been reduced by approximately 40%. The best optimisation is achieved for the NABE-site (47% to the *a priori* costs).

3.3.1 Parameters

The identified minima of the cost function suggest that the differences between the two model configurations are not large. Nevertheless, the optimised parameter values need not be similar when producing comparably low costs. Table (3.4) lists the best parameter estimates together with their errors for both configurations. Note thet the error also accounts for the deviation of the best estimate to the mean value. The optimal parameter estimates for the different configurations are remarkably close to each other. Furthermore, for some parameters (e.g. the maximum growth rate σ_m and the zooplankton loss parameters Φ_z and Φ_z^*) the best estimates are near the *a priori* values. This is noteworthy since these *a priori* values do not have any influence on the optimisation process. At this point, it must be recalled that the two optimisa-

Parameters				Optimised NPZD-wW	Optimised NPZD-nW
ν	SYMBOL p_ν	UNIT	***A priori***	$\widehat{\mathbf{p}_0} \pm \widehat{\boldsymbol{\sigma}}$	$\widehat{\mathbf{p}_0} \pm \widehat{\boldsymbol{\sigma}}$
1	μ_m	d^{-1}	**0.600**	**0.530**$\pm$0.186	**0.500**$\pm$0.266
2	α	$m^2W^{-1}d^{-1}$	**0.025**	**0.112**$\pm$0.037	**0.087**$\pm$0.042
3	Φ_P	d^{-1}	**0.075**	**0.230**$\pm$0.087	**0.195**$\pm$0.110
4	Φ_P^*	$m^3mmolN^{-1}d^{-1}$	**0.100**	**0.010**$\pm$0.010	**0.010**$\pm$ ($< 10^{-3}$)
5	k_{DIN}	$mmolNm^{-3}$	**0.500**	**0.200**$\pm$0.063	**0.260**$\pm$0.086
6	κ_c	$m^2mgCHLa^{-1}$	**0.030**	**0.064**$\pm$0.011	**0.062**$\pm$0.010
7	g	d^{-1}	**2.000**	**1.600**$\pm$ ($< 10^{-3}$)	**1.575**$\pm$0.043
8	ϵ	$m^6mmolN^{-2}d^{-1}$	**1.000**	**0.725**$\pm$0.291	**0.600**$\pm$0.329
9	Φ_Z	d^{-1}	**0.030**	**0.025**$\pm$0.034	**0.025**$\pm$0.021
10	Φ_Z^*	$m^3mmolN^{-1}d^{-1}$	**0.200**	**0.220**$\pm$0.112	**0.235**$\pm$0.119
11	β	1	**0.750**	**0.935**$\pm$0.081	**0.935**$\pm$0.003
12	γ	d^{-1}	**0.050**	**0.020**$\pm$ ($< 10^{-3}$)	**0.020**$\pm$0.005
13	w_s	md^{-1}	**5.00**	**24.00**$\pm$1.285	**44.00**$\pm$6.855

Table 3.4: The model's parameter values. *A priori* values refer to those typically applied in ecosystem models, see text. The best parameter estimates $\widehat{\mathbf{p}_0}$ are given together with their approximated errors $\widehat{\boldsymbol{\sigma}}$ for the model that includes vertical advection (NPZD-wW) and the one without (NPZD-nW).

tions have been conducted independently, starting from different initial parameter guesses. Otherwise it could be postulated to obtain very similar results when identical selection criteria apply during the minimization course. Such a scenario can be excluded here. In fact, the robustness of the optimisation process is expressed in terms of the bootstrapped approximations which are additionally listed in Table (3.4).

Differences of the optimal estimates to the *a priori* values are clearly noticable for most of the phytoplankton parameters. The maximum growth rate (μ_m) turns out to be the only exception. For the NPZD-wW configuration the best estimate of μ_m=0.53 d^{-1} is retrieved. The estimate for the NPZD-nW model is similar (μ_m=0.50 d^{-1}). The estimation of the initial slope parameter of the P-I relation (α) is very robust and optimal values of α=0.112 $m^2W^{-1}d^{-1}$ and α=0.087 $m^2W^{-1}d^{-1}$ are determined for the

NPZD-wW and NPZD-nW models respectively. Referring to the phytoplankton loss parameters (Φ_p and Φ_p^*), it is evident that both optimal values are contrary to the *a priori* guesses of Doney et al. (1996). Moreover, the quadratic loss term appears almost negligible according to the small estimates of Φ_p^*. Relatively low half saturation constants for the nutrient uptake are obtained, k_{DIN}=0.2 mmol N m^{-3} and (k_{DIN}=0.26 mmol N m^{-3}. This is not of a great surprise because the NPZD-model does not resolve ammonium explicitely. The half saturation constant must be viewed as a representative parameter for a combined rate of nitrate and ammonium uptake.

Focusing on the zooplankton parameters, only small deviations of the best estimates to the *a priori* values exist and are less emphasized than for the phytoplankton parameters. The two grazing parameters (g and ϵ) together with the assimilation efficiency (β) are closest to their imposed upper bounds. Differences of the loss parameters to the previously used *a priori* values are even less than their approximated standard deviations.

The loss terms of the detritus compartment are controlled by the remineralization rate (γ) and sinking velocity (w_s). The only apparent difference in parameter estimates between the two model configurations can be restricted to the detrital sinking velocities. Nevertheless, in both cases the optimisation proposes relatively high sinking rates. The highest velocity of 44 md^{-1} is retrieved for the model without vertical advection of water masses, whereas 24 md^{-1} is obtained for the NPZD-wW configuration. The small errors for the sinking rates give confidence in the goodness of these estimates. This suggests that the discrepancy cannot be attributed to uncertainties of the optimisation procedure.

Cost function sensitivity to parameter variations

Figure (3.10) shows parameter guesses in the course of the optimisation and their associated costs (projected on orthonormal axes). These figures provide very useful informations on sensitivities of the cost function to parameter variations and hence on the relative importance of different parameters. A detailed description of such figures can be found in the method section (2.6) of Chapter 2. Note that the sensitivities, shown here, do not necessarily contain the same information as for the errors of the optimisation. Small errors may be depictable despite low sensitivities of the cost function to variations of the parameters. Here, short hints are recalled for their interpretations. The figure should be read as follows:

- Each subplot represents one parameter which is indicated by its symbol. The horizontal axes resolve the parameter's values within their prescribed ranges for variation. The vertical axis shows the corresponding cost function values (J). Every combination of parameter values (set) that occured during the optimzation is shown unless the costs exceed J=13. The best parameter combination correspond to the lowest cost (the minimum found).
- As the parameter values deviate from the best estimates the costs naturally increase. The larger the increase of the costs with distance from the best value, the larger the sensitivity.
- High sensitivities impose a great importance of the parameter. That is, small variations of the parameter produce large changes to those model results which enter the cost function. The subplots cover the full range of parameter values as given by the upper and lower bounds.

In Figure (3.10) the projections of the two optimisations (NPZD-wW and NPZD-nW) are combined in order to see differences in their sensitivties. On the first sight, most projections of both configurations coincide, with the half saturation constant and the sinking velocities being the only exceptions. Highest sensitivity can be appointed to the quadratic loss parameter of phytoplankton Φ_p. During optimisation it converged towards its lower bound. Assigning slightly larger values than its best estimate already induces a huge increase of the costs. It appears to be very unlikely to find a parameter combination which includes values of Φ_p beyond 0.1 $m^3 mmol\ N^{-1} d^{-1}$ and, on the other hand, produces costs lower than J=12. The detrital sinking velocity exhibits lowest sensitivities, particularly when the optimal estimates are exceeded. Around the best sinking speeds small bumps can be recognized which suffice to be allocated by the minimization algorithm. It is noteworthy that low *a posteriori* variances are determined from the Monte Carlo bootstrap approach despite low sensitivities. This will be recalled in the discussion section. Similar conclusions can be made for the estimates of the remineralization rate (γ). The last subplot resolves the projections of a control parameter (ζ) which does not alter the cost function since it has no effect on the model results. This redundant parameter entered the optimisation process as an indicator for premature convergence. It should give information

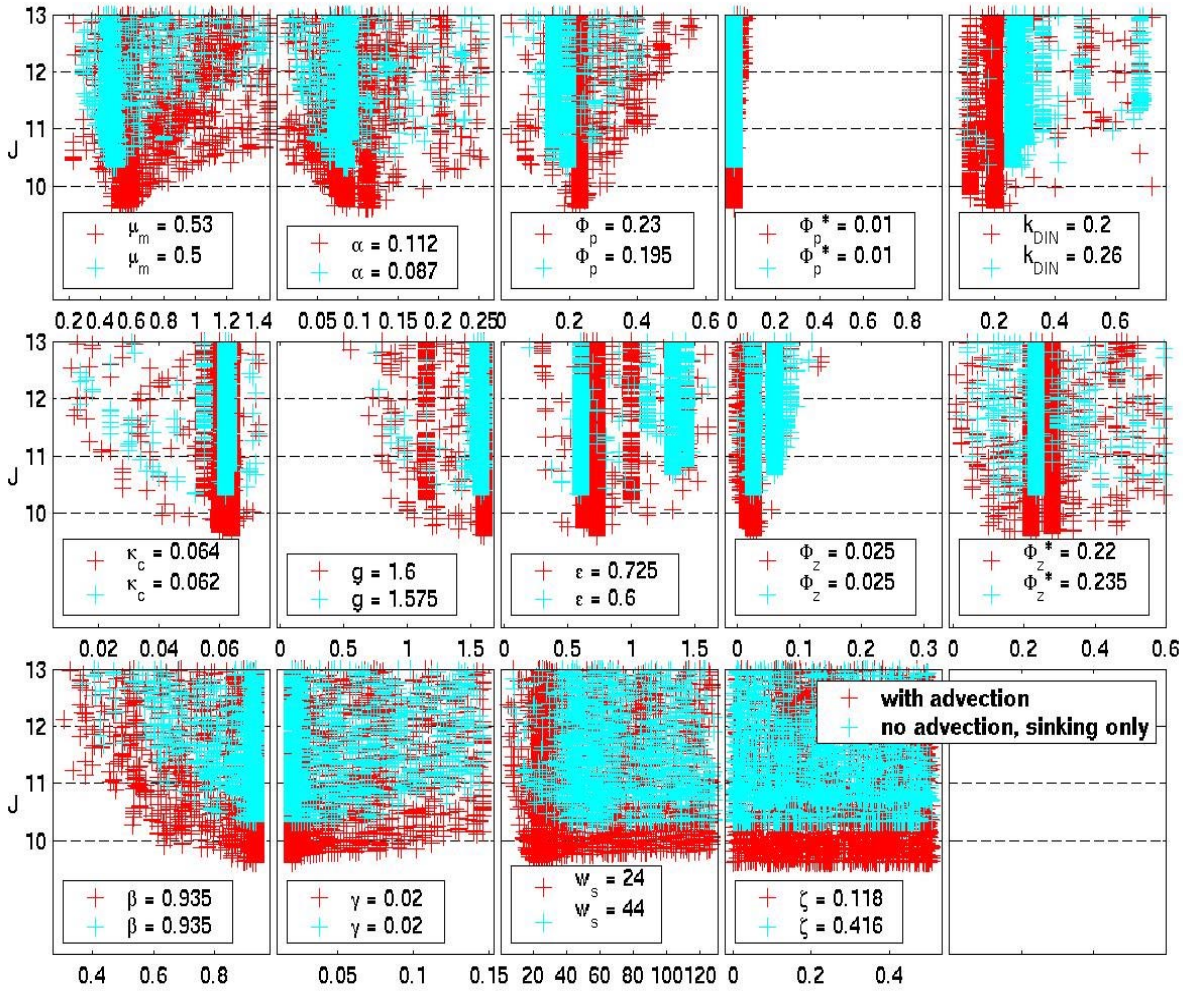

Figure 3.10: Parameter sets and their corresponding cost function values that occured during the seach process. One single cost function value is associated with a combination (set) of fourteen parameters which are explicitely resolved. The fourteenth parameter (ζ) is a control variable and has no effect on the model results.

wether the algorithm artificially converges towards a certain value although the costs remain uneffected. The subplot does not reveal any prefered value of the algorithm, yielding estimates within the prescribed lower and upper bounds until the minimum has been found.

3.3.2 Nitrogen fluxes

The biogeochemical conditions of the models can be expressed in terms of their averaged annual fluxes. According to Figure (3.11) these fluxes will be evaluated for three model configurations at the three locations . First, the fluxes of the NPZD-wW model with the *a priori* parameter set are derived, see Table (3.4). Referring to the *a priori* parameters allows to interpret flux changes with respect to the data-assimilation. *A priori* fluxes are followed by those of the NPZD-wW configuration with the best parameter estimates. Finally, the optimised fluxes of the NPZD-nW model are given. In case of the NPZD-nW configuration, the advective fluxes reduce to sinking of detritus only. The fluxes are calculated for three depth ranges (I:0m-126m, II:126m-411m, III:411m-1000m), see Figure (3.11). The internal fluxes of the ecosystem are only resolved for the upper depth range I.

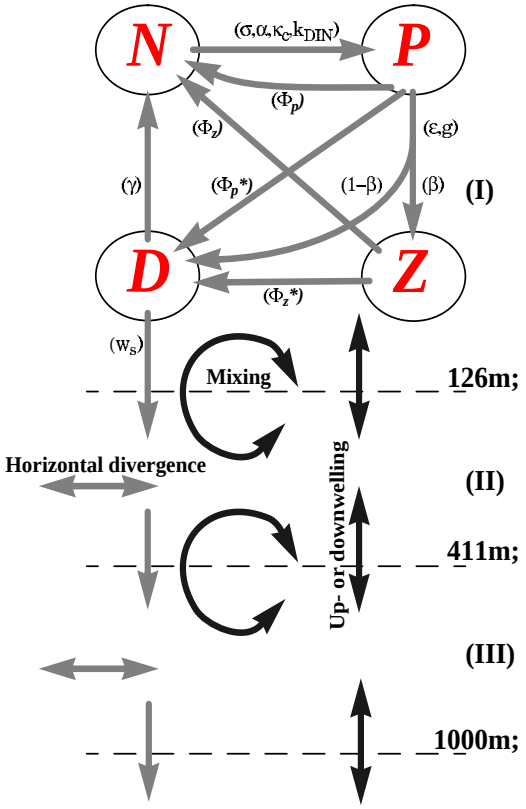

Figure 3.11: Annual net fluxes of nitrogen as they are evaluated at all three locations. The upper 1000 meters are resolved into three depth ranges (I-III). Horizontal arrows represent advective fluxes according to horizontal divergence in order to conserve water volume, see model describtion in main text. Vertical arrows show advective fluxes unless in the model vertical velocities are neglected (as in NPZD-nW). Open circles refer to turbulent and convective fluxes. Upward as well as incoming horizontal fluxes are indicated with positive signs. Diapycnal mixing at 1000 meters is not shown since it has no effect on the biology within the upper 400 meters. The internal biological exchange rates of nitrogen are given within the upper 126 meters (gray arrows between compartments).

Drastical changes of the fluxes can be inferred from data-assimilation for the model that includes vertical advection (NPZD-wW), if compared with the *a priori* fluxes, see Figure (3.12). Focusing on the advective fluxes of inorganic nitrogen, phytoplankton and zooplankton, flux differences are small.

The most compelling change is associated with the flux from phytoplankton to dissolved inorganic nitrogen, which represents the rapid transformation of organic nitrogen to ammonium, via bacteria. A significant increase in primary production, from 606 mmol N $m^{-2}yr^{-1}$ to 2082 mmol N $m^{-2}yr^{-1}$ is concomitant with this process of fast recycling. Surprisingly, the sinking flux of detritus has become less although the total production has increased. However, comparing the nutrient recycling pathways of the *a priori* model with the optimised fluxes, then one can see how formation and remineralization of detritus turned out to play a minor role in the optimised solution near Bermuda. For the optimised models, a large fraction of particulate organic nitrogen PON (which is detritus, phytoplankton together with zooplankton) is actually exported via mixing at 126 meter depth, -100 mmol N $m^{-2}yr^{-1}$ and -104 mmol N $m^{-2}yr^{-1}$, for NPZD-wW and NPZD-nW respectively. Regarding zooplankton, we can see that the phytoplankton losses due to grazing are enhanced for both optimised model runs.

The only remarkable diffence between NPZD-wW and NPZD-nW can be derived from the inventories of total annual nitrogen (particulate and inorganic). An annual net gain of 0.23 mmol N $m^{-3}yr^{-1}$ is obtained for NPZD-wW whereas a net loss of 0.12 mmol N $m^{-3}yr^{-1}$ leads to a decline of the total available nitrogen during the simulated five year period. Both models are not in steady state because of interannual variations of the forcing fields. The net gain for the NPZD-wW can obviously be attributed to the averaged upwelling rate of 92 mmol N $m^{-2}yr^{-1}$ for nitrate at 411 meters. This vertical advective transport of nutrients does not exist for NPZD-nW configuration. At 126 meter the NPZD-wW model maintains a net downwelling which pushes a small fraction (-2 mmol N $m^{-2}yr^{-1}$) of phytoplankton and zooplankton out of the upper layers. The dissolved nitrogen concentrations above 100 meters are relatively low so that there is no evidence for net downwelling of nutrients.

The NABE site produces a picture completely different picture to the location of BATS. Generally, the optimised annual primary production is slightly lower for 47^{o}N 20^{o}W than for Bermuda, but the grazing pressure on phytoplankton is strengthened. The largest fraction that enters the detritus compartment now comes from the zooplankton. The role of zooplankton is accentuated in the model at the NABE site. When we consider the changes according to the optimisation it must be stated that the magnification of total production within the upper 126 meters with respect to the *a priori* run is not as high as for the BATS site. The pathway for nutrient recycling via detritus has significantly decreased for the optimised fluxes, from 442 to 36 mmol N $m^{-2}yr^{-1}$. At 47^{o}N 20^{o}W the optimised fluxes maintain an enhanced vertical export of detritus at 126 meters, 427 and 478 mmol N $m^{-2}yr^{-1}$ for NPZD-wW and NPZD-nW respectively. Despite the augmented flux of detritus there is no enlargement of ni-

trate mixing into to upper layers in the same magnitude. This leads to an imbalance of the total nitrogen content. A net loss of total nitrogen as much as -360 mmol N $m^{-2}yr^{-1}$ is then retrieved within the upper 411 meters for the NPZD-wW configuration and -312 mmol N $m^{-2}yr^{-1}$ for NPZD-nW.

At the location of OWS-INDIA the total productivities of NPZD-wW and NPZD-nW are comparable, yielding 1016 and 1061 mmol N $m^{-2}yr^{-1}$ respectively. For both configurations the total primary production is slightly lower than for the a priori model run. As for the NABE and BATS sites, the optimised nutrient recycling is dominated by phytoplankton and zooplankton exudation or leackage of nitrogen rather than detrital remineralization. The detrital export happens too fast in order to allow rapid recycling within the upper 126 meters. The export of detritus out of 411 meter depth is largest at the INDIA site. Relatively high grazing fluxes can be depicted from Figure (3.14). These induce large fluxes of zooplankton nitrogen to the detrital compartments, which could be viewed as sinking of fecal pellets. The annual nitrogen fluxes at OWS-INDIA include large net advective transports for the NPZD-wW models. For instance, the advective net loss of inorganic nitrogen due to horizontal divergence is -517 mmol N $m^{-2}yr^{-1}$ for the optimised model. As a consequence, the optimised model with vertical velocities looses 26 mmol N m^{-3} of total nitrogen within the upper 411 meters over a five year period whereas without vertical advection only 6 mmol N m^{-3} are lost. Unfortunately, errors in the inorganic nitrogen distribution with depth are apparent for the NPZD-wW model, see Figure (3.15). Until approximately 400 meters of depth both model configurations remain actually comparable. Nevertheless, the total nitrogen inventory of the entire upper 1000 meters is problematic because the amplitudes of vertical velocities increase with depth by a factor of ten. In addition, the nitrate concentrations below 400 meters are usually above 20 mmol N m^{-3}. Hence, large uncertainties arise below 400 meters with respect to the net advective transports.

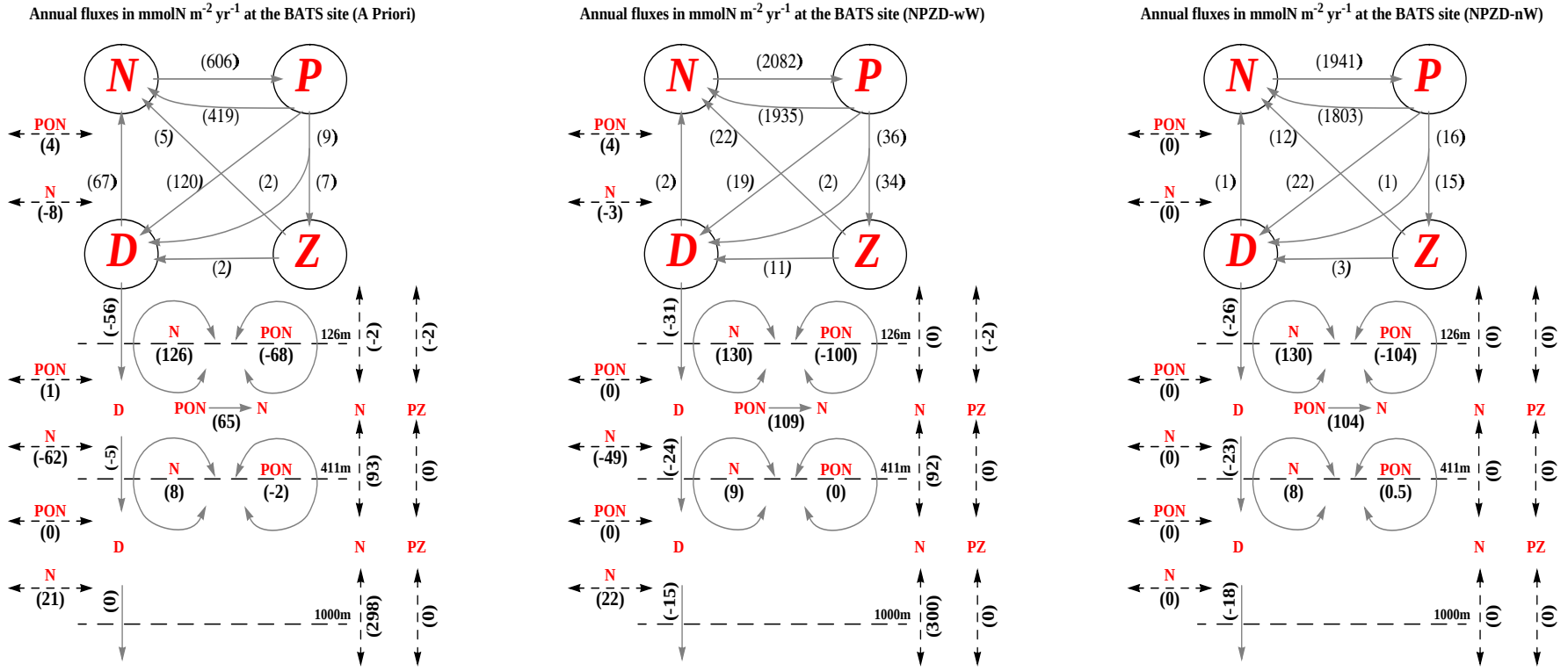

Figure 3.12: Simulated annual fluxes of nitrogen at 31°N 64°W (BATS site). The units are mmol N m^{-2} yr^{-1}. Vertical arrows illustrate vertical advective fluxes, with positive values meaning upward flux. Due to the divergence of the obtained vertical velocity field we must also solve for horizontal advective fluxes. This simply accounts for the continuity equation, conserving the water mass. LEFT: Resulting fluxes when *a priori* parameter values are used. MIDDLE: Fluxes of model with vertical velocities (NPZD-wW) when optimal parameter set is considered. RIGHT: Optimised model fluxes when neglecting vertical velocities. Only advection due the sinking of detritus (NPZD-nW) is allowed.

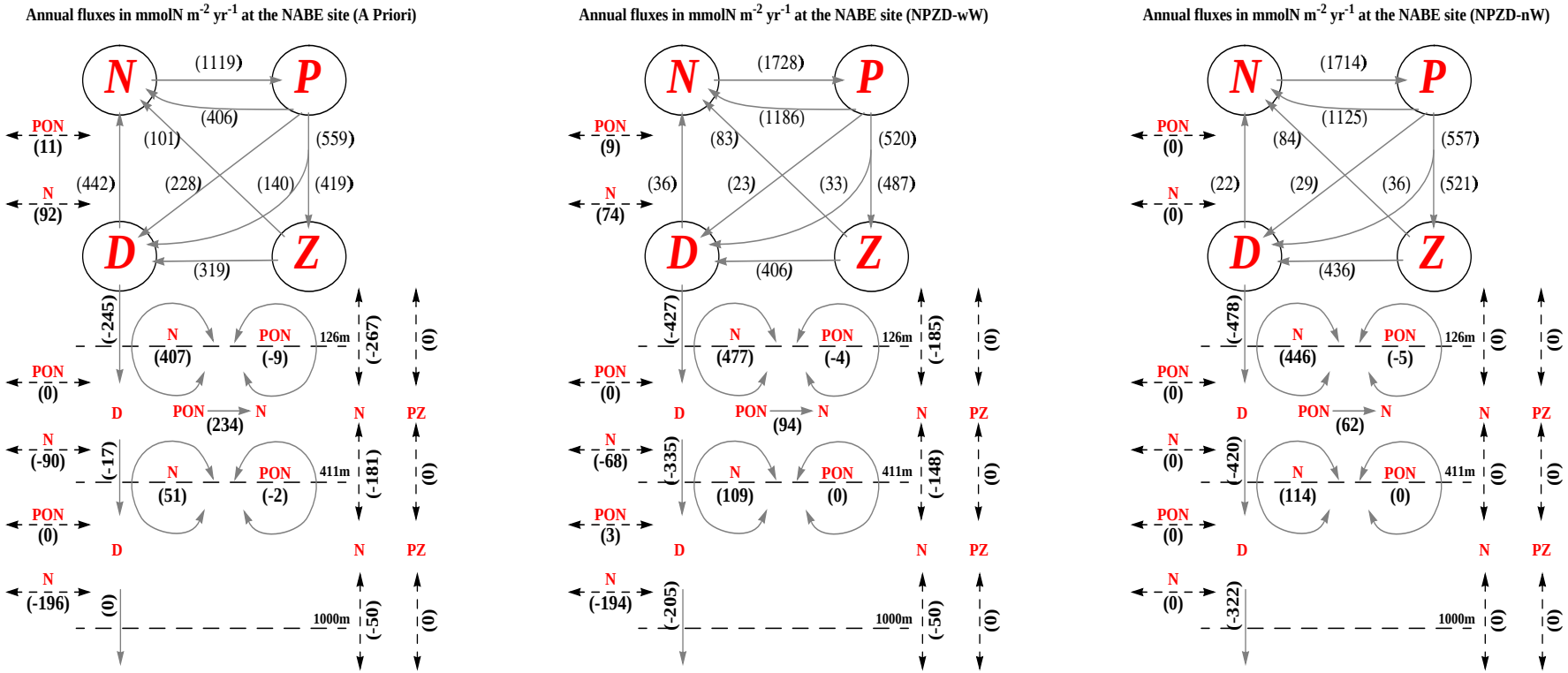

Figure 3.13: Simulated annual fluxes of nitrogen at 47^{o}N20^{o}W (NABE site). The units are mmol N m^{-2} yr^{-1}. LEFT: Resulting fluxes when *a priori* parameter values are used. MIDDLE: Fluxes of model with vertical velocities (NPZD-wW) when optimal parameter set is considered. RIGHT: Optimised model fluxes when neglecting vertical velocities. Only advection due the sinking of detritus (NPZD-nW) is allowed.

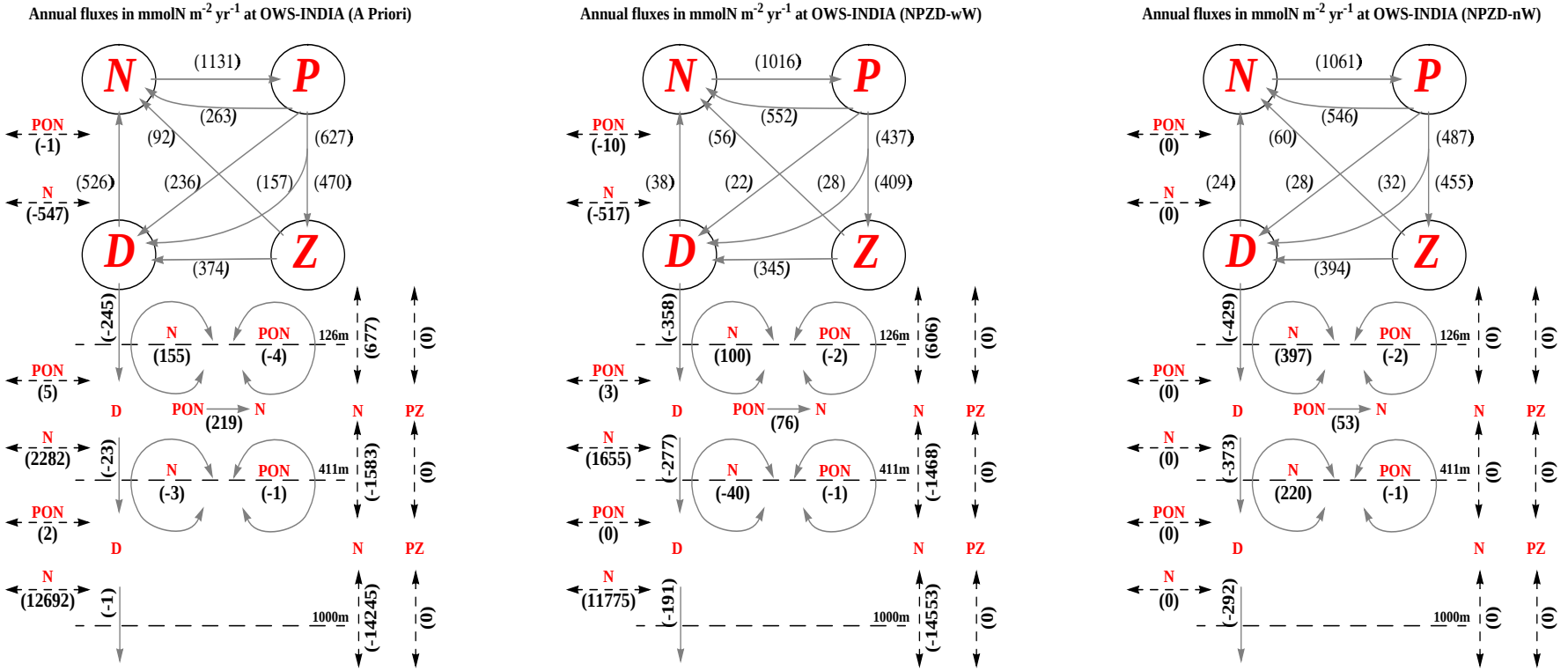

Figure 3.14: Simulated annual fluxes of nitrogen at 59^{o}N19^{o}W (OWS-INDIA). The units are mmol N m^{-2} yr^{-1}. LEFT: Resulting fluxes when *a priori* parameter values are used. MIDDLE: Fluxes of model with vertical velocities (wW) when optimal parameter set is considered. RIGHT: Optimised model fluxes when neglecting vertical velocities. Only advection due the sinking of detritus (nW) is allowed.

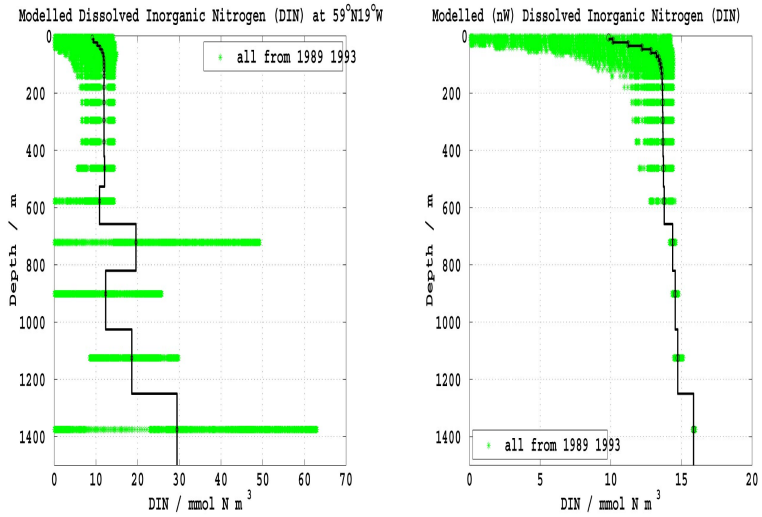

Figure 3.15: Modelled concentrations of dissolved inorganic nitrogen at the INDIA location for the model configurations NPZD-wW (LEFT) and NPZD-nW (RIGHT). Gray bars indicate modelled nitrate concentrations during the five year period of simulation. The black solid stairs represent mean concentrations at respective depths.

3.3.3 Seasonal cycles

In the following section the seasonal cycles of chlorophyll, primary production, dissolved inorganic nitrogen (in terms of nitrate) and particulate organic nitrogen (PON) will be presented for the optimised NPZD-wW model configuration. Observational counterparts to the model results will be additionally shown. The observational data is gridded and monthly averaged [7]. Eventually, they are plotted in the same way as they enter the cost function in the upper 155 meters.

BATS site

Near Bermuda the predicted monthly averages of model chlorophyll are in relatively good agreement with observations, Figure (3.16, top). The maximal monthly average of chlorophyll concentration is 0.29 mg m^{-3}, whereas 0.26 mg m^{-3} is derived from the time series. In general, the observed concentrations show their deep maxima extending throughout a greater depth range than the model results. The modelled deep chlorophyll maxima rather emerge from one single grid cell, with the early spring bloom being the only exception. The timing of the spring bloom is, however, accordant with observations. In February the maximal model concentrations are spread over 25 meters, ranging from 47 to 72 meters. Observed maxima in chlorophyll tend to be shallower, ranging from 23 to 72 meters. At the first sight, this

[7] Constructing observational counterparts to the model is easier. Mostly, the observational data is better resolved with depth than the model results. This means that integrating and averaging over observational depths provides better data than extrapolating model results to observational depths.

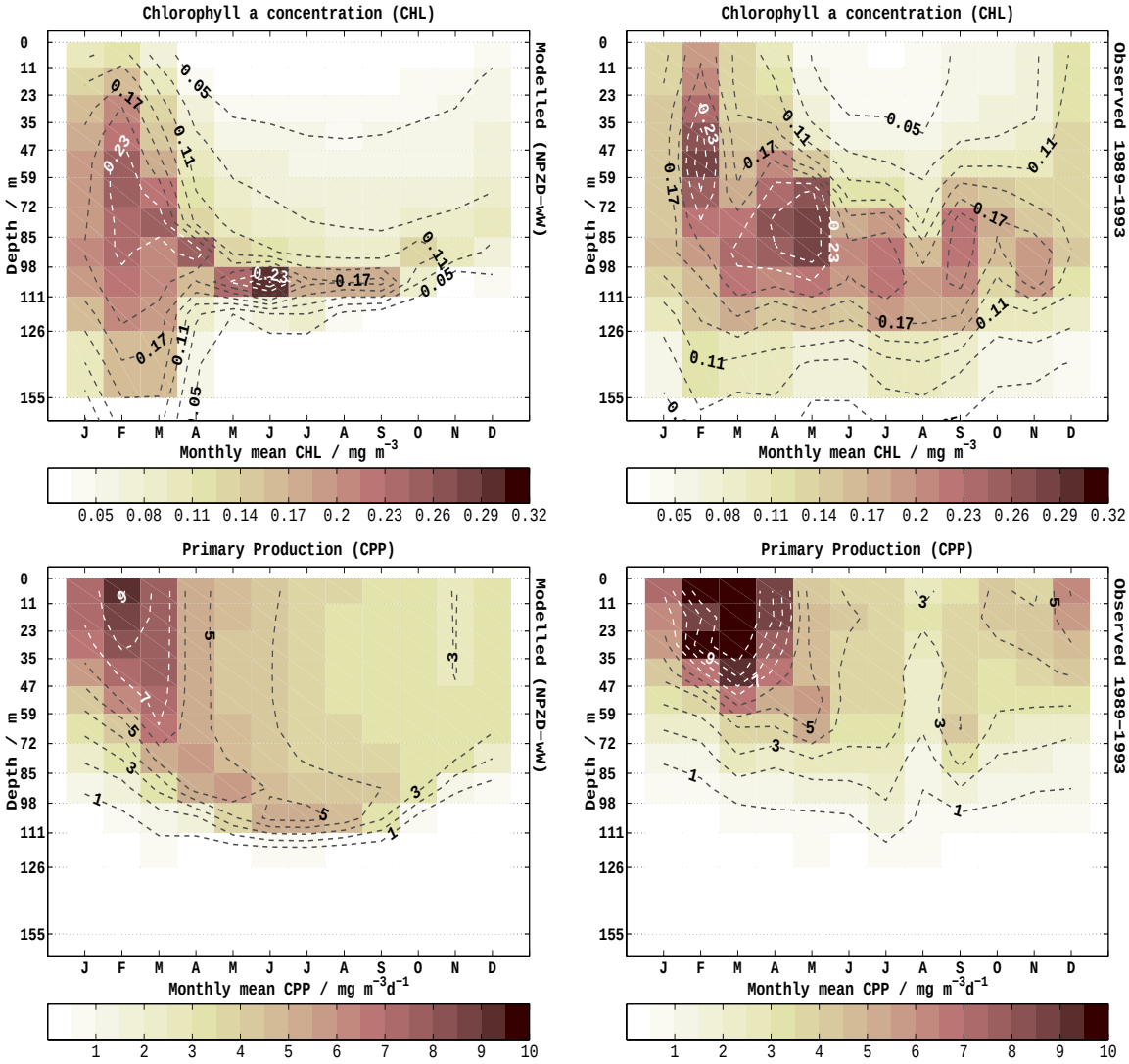

Figure 3.16: Monthly averaged chlorophyll concentration (contour interval=0.03 mg CHL m^{-3}) and primary production (contour interval=1 mg C $m^{-3}d^{-1}$) within the upper 11 model grid cells: Modelled variabels (left side) and the observational counterparts on the same grid (right side). Location: BATS site.

discrepancy between model and observation seems quite negligible but the overall depth distribution of the modelled chlorophyll concentrations become actually too high at greater depths in February and March. Although being less pronounced here, such data-model discrepancies are known from other models and were already noticed by Fasham et al. (1993) and Doney et al. (1996). Comparing modelled chlorophyll concentrations of the upper two boxes (0m-23m) with observations, shows an early increase during late autumn in the observations while the model concentrations remain low within that period. Furthermore, the model could not maintain sufficiently high chlorophyll concentrations during the summer periods. Typical ob-

served concentrations range between 0.02 to 0.05 mg CHL m^{-3} from June through August within the upper 30 meters.

The measured ^{14}C-production rates suggest highest productivities in March, Figure (3.16, bottom). In some years the productivity becomes larger than 20 mg C $m^{-3}d^{-1}$ in the upper 30 meters. The modelled maximal rates did not exceed 12 mg C $m^{-3}d^{-1}$. This results in a highest monthly average of 9 to 10 mg C $m^{-3}d^{-1}$ for the month February. Regarding the maximal rates of primary production, the model results do not seem too bad but they preceed the observed peak in production rates by approximately one month. In Chapter 2, we already discussed this systematic deficiency for the zero-dimensional NPZ-model. Best agreement between modelled and observed productivities is achieved for the depth distribution of the deepest isoline representing 1 mg C $m^{-3}d^{-1}$. A seasonal cycle is hardly noticable at approximately 100 meters. For the modelled rates as well as for observations the net primary production extends down to approximately 100 to 110 meters, matching the typical depth at which PAR has decreased to 1% of its surface value (1% PAR isolume), (Sorensen and Siegel 2001). The signal of maximal production spreads down to 111 meters in the model with a instantaneous drop down below. As a consequence, primary production of the model must be regarded as too high above these 111 meters, particularly from April to September. Last but not least, it can be seen how the observational data yields a break down in primary production during August which is not captured by the model. Eventually, the decoupling of primary production from chlorophyll concentrations is less accentuated in the model than observed.

At the BATS site the observed nitrate concentrations range from maximal 2 mmol N m^{-3} around 150 meters down to the lower detection limit near the surface, Figure (3.17). The overall distribution of modelled inorganic nitrogen reveals a lower inventory of total inorganic nitrogen than observed. Although the modelled nitrate counterpart decreases similarly to the observed, there remains less inorganic nitrogen within the upper 155 meters of the water column. This is noteworthy because for the optimised model dissolved nitrogen is obtained via remineralization between 126 and 411 meters and upwelling, according to Figure (3.12). Either nutrient supply of the model into the upper 126 meters is insufficient or the modelled dissolved nitrogen is utilized too fast by the phytoplankton. The observations show an outcrop of the 0.1 mmol N m^{-3} nitrate isoline in February which is not resolved by the model results. During summer the modelled vertical gradient between 111 and 85 meters matches that of the observations but becomes obviously underestimated below. Referring to the drawdown of nitrate, the signal that is obtained from the observations penetrates down to approximately 100 meters in August. One month later in September an increase of the nitrate concentration is observed. Apparently, this signal is concomitant with an increase in primary production, in chlorophyll, as well as in PON concentrations and is associated with the year 1992. Deviations in September and October of 1992 can be attributed to a high saline water parcel that did not form locally (Siegel et al. 1995) and will be recalled in the discussion section.

The modelled PON becomes maximal in May between 85 and 98 meters, predict-

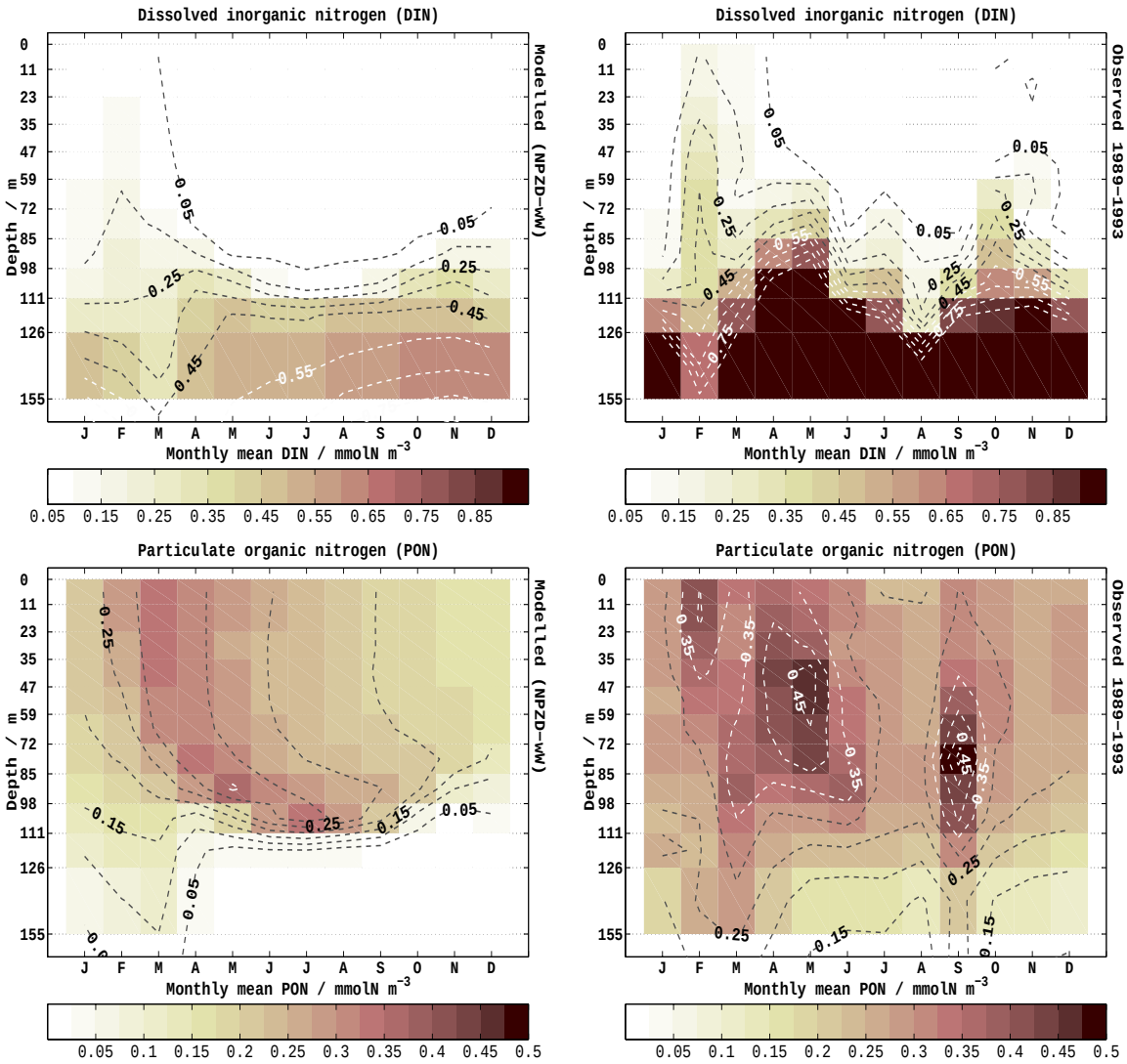

Figure 3.17: Monthly averaged concentrations of dissolved inorganic (contour interval=0.1 mmol N m^{-3}) and particulate organic nitrogen (contour interval=0.05 mmol N m^{-3}) within the upper 11 model grid cells: Modelled variabels (left side) and the observational counterparts on the same grid (right side). Location: BATS site.

ing 0.45 mmol N m^{-3}. The same concentrations are observed at lower depths, typically ranging from 30 to 80 meters. The model mostly underestimates the observed PON measurements but the mismatch becomes relatively large below 111 meters in the summer periods. These PON distributions at depth seem almost impossible to be reproduced by the model. If we focus on the distinct increase of PON in the September observations it seems that an advected water parcel signal enters the calculation of the monthly average, as mentioned before.

NABE

The study region of NABE shows physical features different from those of the oligotrophic site near Bermuda and therefore the biological responses differ as well. Chlorophyll concentrations always exceed 1 mg m^{-3} during phytoplankton blooms. Observational data indicate a bloom in May with a maximal chlorophyll concentration of approximately 1.5 mg m^{-3} near the surface, Figure (3.18). From the model simulations a bloom can be depicted for the same month, yielding a monthly average of approximately 1.3 mg m^{-3}. According to the observations the bloom extends down to almost 100 meters which is not recovered by the model. Below 60 meters

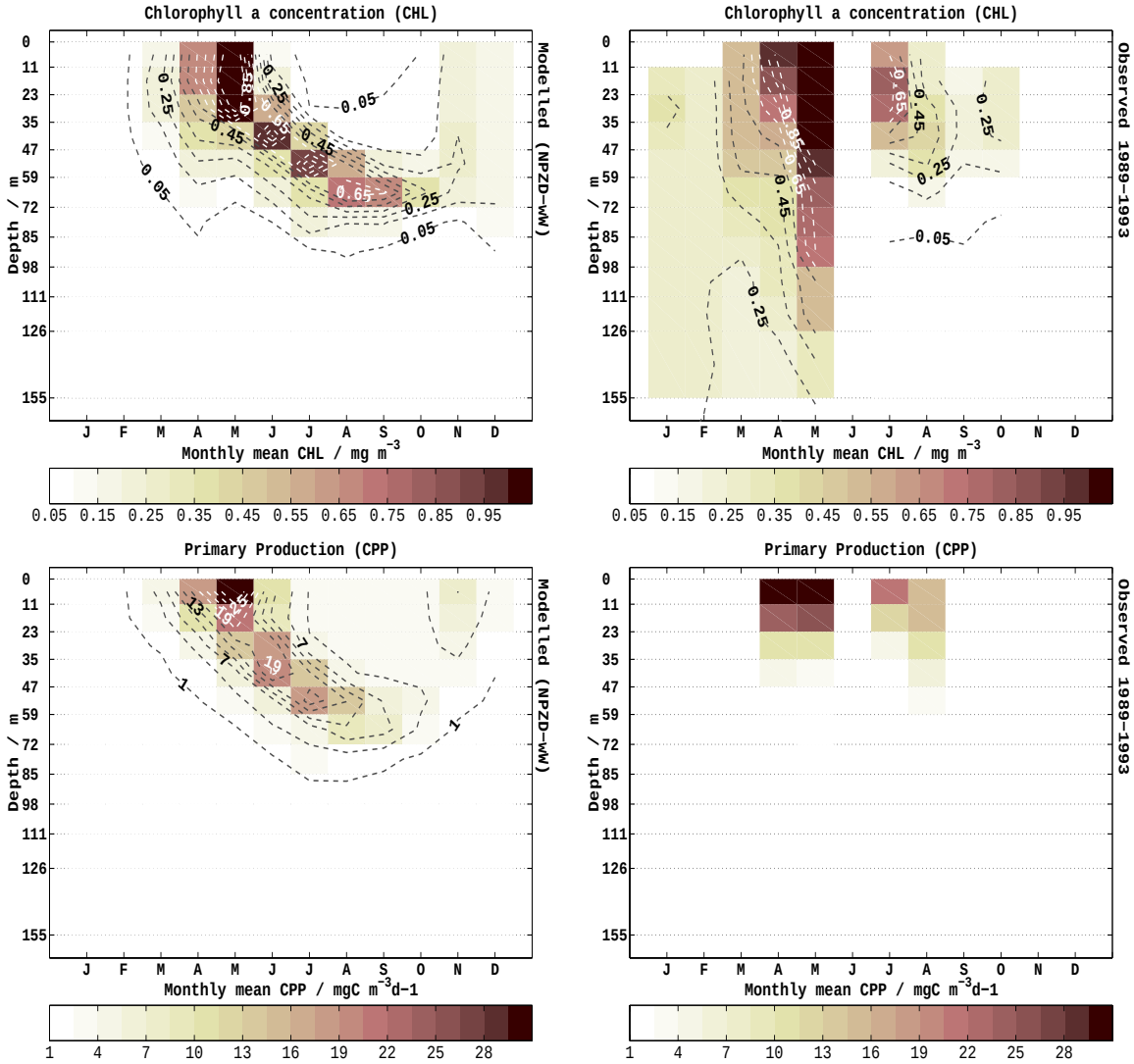

Figure 3.18: Monthly averaged chlorophyll concentration (contour interval=0.1 mg CHL m^{-3}) and primary production (contour interval=3 mg C $m^{-3}d^{-1}$) within the upper 11 model grid cells: Modelled variabels (left side) and the observational counterparts on the same grid (right side). Location: NABE site.

the model is not able to maintain sufficient chlorophyll for April and March. Actually, from the observational data only a small deep chlorophyll maximum could be depicted for July and August with concentrations close to 0.3 mg m^{-3}. The model clearly predicts an intensified deep maximum throughout the whole summer. Unfortunately no chlorophyll measurements are available for June, the month when the model starts to evolve its deep chlorophyll maximum. This model signal deepens down to 72 meters until October with a remaining chlorophyll concentration of 0.35 mg m^{-3}. During the early spring period observations exceed modelled concentrations. This can be attributed to interannual variabilities and will be discussed in the following section.

The depth-time distribution of the simulated primary production rates harmonize with that of the chlorophyll signal. Obviously, productivity and chlorophyll appear to be less decoupled at the NABE site than for Bermuda. The observations show a similar picture. Nevertheless, the model's predicted primary production rates underestimate the near surface observations in June and August. In May, during the bloom phase, model and observations match surprisingly well; primary productivition rates of 38 mg C $m^{-3}d^{-1}$ are derived from observations whereas the model produces 34 mg C $m^{-3}d^{-1}$. Apparently, as long as primary production is maintained by an input of fresh nutrients to the upper layers the misfits between model and observation almost vanish.

The top of Figure (3.19) shows the seasonal cycle of modelled dissolved inorganic nitrogen and nitrate observations. During the spring periods the observational data exhibit large variations but their monthly averages from March through May maintain almost the same surface concentrations (around 3 mmol N m^{-3}). However, highest surface concentrations of nitrate that could be measured were close to 6 mmol N m^{-3} for April. When comparing the model results with observations a maximal mismatch of approximately 4 mmol N m^{-3} exists for March. The depletion of nitrate in the summer time leads to minimal concentrations close to 0.03 mmol N m^{-3} in the model. Lowest nitrate concentrations were observed in September with 0.1 mmol N m^{-3}. The nutrient decrease in summer seems little emphasized in the model, according to the depths of the 1 mmol N m^{-3}-isoline.

Only few observations could be procured for PON, which provided reasonable averages for April, May and July. During May the model could not catch up with the relatively high PON concentrations at the surface. The observations yield 3.7 mmol N m^{-3} while the model produces 1.35 mmol N m^{-3} for that particular month. It is noteworthy that a corresponding error of 100% in PON is not evident in chlorophyll. The deepening of the 0.2 mmol N m^{-3} isoline in the model results can be attributed to the formation and sinking of detritus. To derive a similar picture from observations seems impossible.

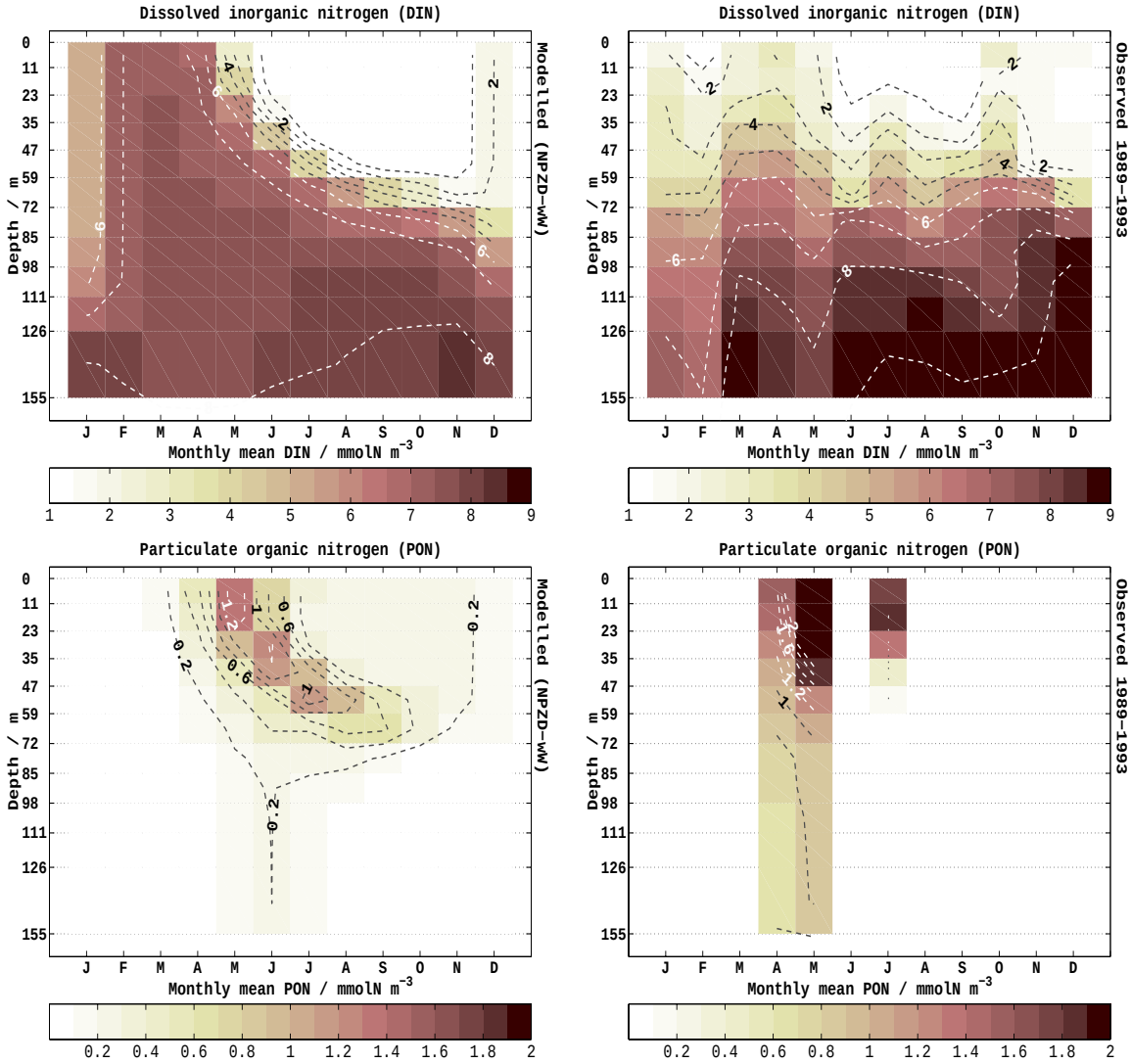

Figure 3.19: Monthly averaged concentrations of dissolved inorganic (contour interval=1 mmol N m^{-3}) and particulate organic nitrogen (contour interval=0.2 mmol N m^{-3}) within the upper 11 model grid cells: Modelled variabels (left side) and the observational counterparts on the same vertical grid (right side). Location: NABE site.

INDIA

At the location of 59^{o}N 19^{o}W the model's seasonal cycle of chlorophyll reveals a short but intense bloom in June near the surface. Among all three locations the biological response at the INDIA site exhibits the largest sensitivity to the timing of stratification. From the chlorophyll observations it can be seen that phytoplankton already starts to grow in March and April. In these two months the model is not able to build up any biomass at all. This can be clearly attributed to the deep mixing which is followed by a delayed stratification. As already discussed in section (3.2.1), differences with regard to mixing and temperature distribution may be related to inter-

decadal variablities, recalling that the observation period (1971-1974) fell into a low NAO phase with weakened westerly winds.

According to the model's timing of stratification there are more nutrients present in the euphotic zone in June and July to be utilized by phytoplankton under increased PAR levels. It seems quite natural that these two factors lead to an amplified raise in chlorophyll concentrations up to 2.4 mg m^{-3}. The measurements suggest averaged concentrations close to 1 mg m^{-3}, with its maximum in May. At this point it must be reminded that the measurements comprise large fluctuations within the "bloom" months, presumably because of patchiness and interannual variations.

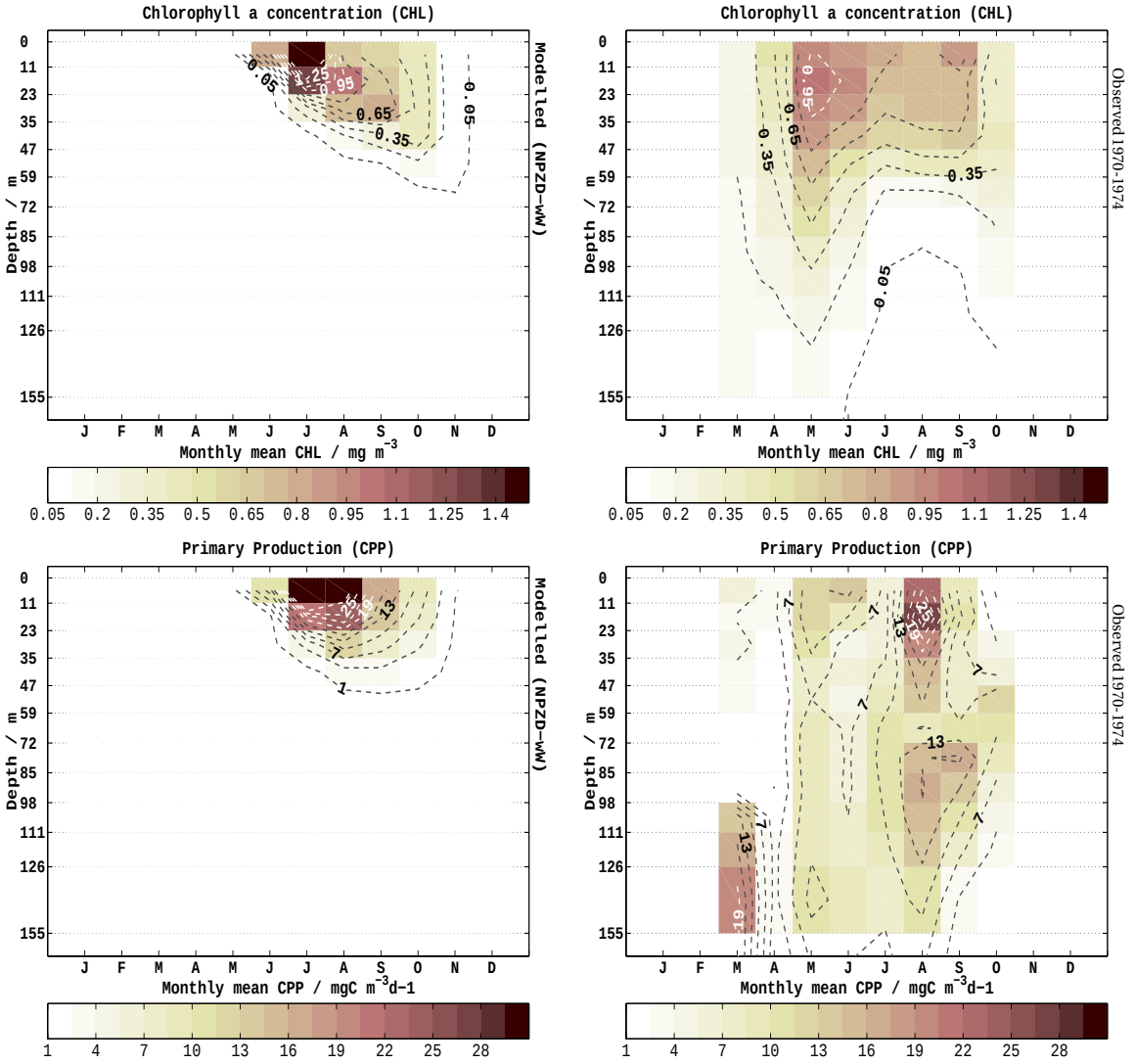

Figure 3.20: Monthly averaged chlorophyll concentration (contour interval=0.1 mg CHL m^{-3}) and primary production (contour interval=3 mg C $m^{-3}d^{-1}$) within the upper 11 model grid cells: Modelled variabels (left side) and the observational counterparts on the same vertical grid (right side). Location: OWS-INDIA site.

Hence, chlorophyll concentrations above 2.5 mg m^{-3} could be observed and entered the calculation of monthly averages. Besides the mismatch of the blooming time the model's physical environment maintains a greater stratification during the summer periods than observed which, in addition, keeps all the chlorophyll within upper 35 meters. Late summer and autumn concentrations are in much better agreement with observations, at times when convection and mixing commences.

The acquired primary production rates of the model reveal a similar picture as the evolution of modelled chlorophyll. From the observations relatively high primary productivities can be depicted from depths close to 100 meters for August and

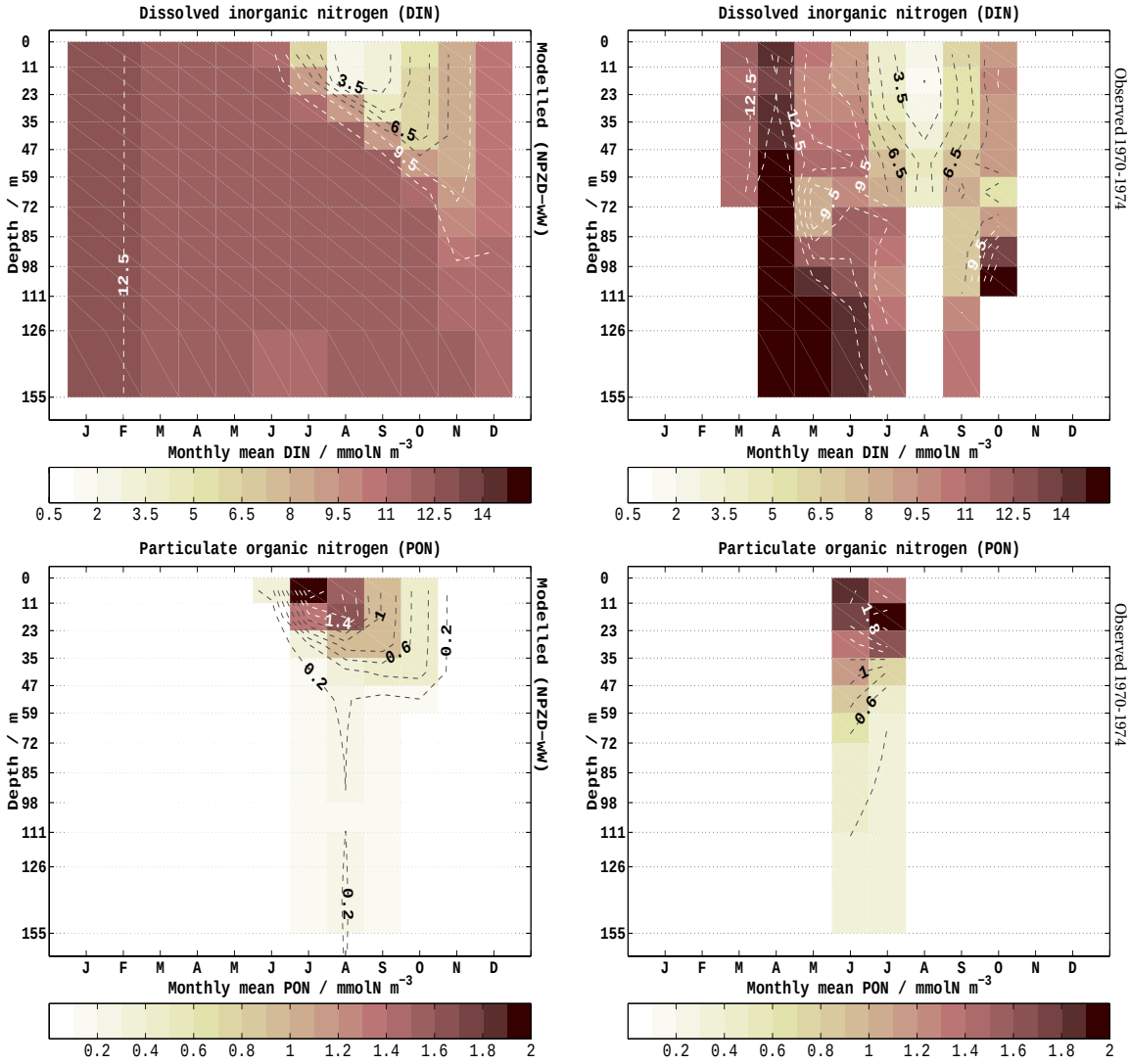

Figure 3.21: Monthly averaged concentrations of dissolved inorganic (contour interval=1.5 mmol N m^{-3}) and particulate organic nitrogen (contour interval=0.2 mmol N m^{-3}) within the upper 11 model grid cells: Modelled variabels (left side) and the observational counterparts on the same grid (right side). Location: OWS-INDIA site.

September. During these months the model completely fails to build up any biomass. Surprisingly, the model predicts monthly mean production rates which are higher than observed during the summer period, yielding rates up to 50 mg C $m^{-3}d^{-1}$ for July. The observed maxima in primary productions can be found in August with a monthly mean rate of 28 mg C $m^{-3}d^{-1}$. A comparision of depth integrated primary production rates would suggest a much better agreement between observations and model results.

With regard to nitrate concentrations, it is frequently documented that nitrate does not become depleted in summer. The observed monthly means do not fall below 1 mmol N m^{-3} near surface even in August at depths with maximal primary productivity. It is interesting to see that the model results show a similar picture, approximately 2 mmol N m^{-3} remain unutilized despite the high production rates.

PON observational data could be obtained from two summer months, June and July respectively. Maximal PON concentrations were observed in July, rendering 1.9 mmol N m^{-3} as a monthly average. The model's PON is similarly high in the same month. In general, the model results cannot adopt the high concentrations at depth, although enhanced PON concentrations (0.2 mmol N m^{-3}) are predicted at depth in August which can clearly be attributed to the model's detritus. Hence, in the model this is a matter of export from the surface layers rather than the formation of new organic matter with depth.

3.4 Concluding discussion

3.4.1 Parameter optimisation

Optimal estimates of parameter have been retrieved for two model configurations which only differ with regard to vertical advection. For both model configurations the optimal parameter estimates are quite similar, with the detrital sinking velocities being the only noteworthy exception.

Parameter estimates

The optimal estimate of the maximum growth rate of 0.53 d^{-1} is remarkably close to the *a priori* value. It is quite clear that this growth parameter plays an important role, in particular for the new production in the model (e.g. Evans 1999). Because the *a priori* and optimal estimate agree well, this gives supporting confidence in large scale model approximations of new production such as in Sarmiento et al. (1993) and Oschlies and Garçon (1999). In Evans (1999) the same growth function was utilized and he retrieved an optimal estimate of 0.95 d^{-1} when assimilating only NABE-data into a FDM-model. The estimates of Fasham and Evans (2000) ranged between 2 d^{-1} for the FDM-model and 2 d^{-1} for a modified version with an additional diatom compartment. Simultaneous optimisations of Hurtt and Armstrong (1999) produced optimal values which are significantly higher for light limited growth but cell growth was inhibited by iron in their function which makes a direct comparision difficult. Referring to these recent estimates the maximal growth rate of 0.53 d^{-1} for the NPZD-model can be regarded as lower limit.

The initial slope parameter of the P-$\mathcal{I}$ relationship turns out to be close to 0.1 $m^2W^{-1}d^{-1}$ which is a factor of four larger than the *a priori* values. Similarly high values have been estimated for the NPZ-model, see Chapter 2. The tendency towards higher initial slope values can be inferred from other data-assimilation experiments as well (e.g. 0.164 $m^2W^{-1}d^{-1}$ in Fasham and Evans (2000) or 0.93 $m^2W^{-1}d^{-1}$ in Hurtt and Armstrong (1999)). The very high estimates of Hurtt and Armstrong (1999) were attributed to the circumstance that the initial time of the bloom at OWS-INDIA had to be fitted by their model correctly, getting a rapid bloom under low light conditions. Estimates close to the present *a priori* value were obtained by Fennel et al. (2001) with BATS data and Evans (1999) at the NABE site, 0.0245 $m^2W^{-1}d^{-1}$ and 0.035 $m^2W^{-1}d^{-1}$ respectively. These two studies comprised *a priori* parameter information in their cost function, which was 0.025 $m^2W^{-1}d^{-1}$ for the intial slope parameter.

Another important parameter for phytoplankton growth is the half saturation constant of nitrogen uptake by phytoplankton. For model simulations this constant is often chosen to be 0.5 mmol N m^{-3} for nitrate uptake. The dissolved inorganic nitrogen pool in the NPZD-model combines nitrite, nitrite and ammonium. Therefore the estimates of 0.2 mmol N m^{-3} are lower, mostly to assure rapid nutrient utilization under oligotrophic conditions.

The simultaneous optimisation of the grazing parameters yields high rates for

the NPZD-model (g=1.6 d^{-1} and ϵ=0.725m^6mmol $N^{-2}d^{-1}$). As a consequence the modelled zooplankton induces a high and rapid grazing pressure on phytoplankton as soon as the zooplankton biomass evolves. This is in general aggreement with other data-assimilation studies, e.g. maximum ingestion rates of 1.27 d^{-1} were estimated by Fasham and Evans (2000).

For the detritus compartment only two parameters are of particular interest, the remineralization rate and sinking velocity. Both parameters cannot be independently estimated. Similar amounts of nutrients can be remineralized when sinking and remineralization rate increase in the same proportions. Therefore the estimated sinking velocities of 24 md^{-1} and 44 md^{-1} should be considered only in combination with the remineralization rates of 0.02 d^{-1}. It is noteworthy that the optimal parameter estimates, which could be determined in this study are the first estimates for a one-dimensional ecosystem model in the North Atlantic. The optimal estimates of the remineralization rate and detrital sinking velocity, which are obtained here, are better constrained than those recovered for an ecosystem model of the upper mixed layer.

Robustness and associated errors

For a better interpretation of the optimal parameter sets information on their precisions and reliabilities are needed. Toward this end, the Monte Carlo bootstrap approach has been applied here. The standard deviations of the optimal estimates are derived from optimisations performed with resampled data sets. This clearly differs from error analyses that rely on the cost function's sensitivities only. It is generally stated that for high cost function sensitivities the parameter is well-determined whereas for low or no sensitivities they are viewed as bad- or even ill-determined. From the parameter projections, such as Figure (3.10), one can already depict the overall sensitivities of the cost function to variations of the parameters. In this context the sensitivity is expressed mathematically by the curvature of the cost function. Hence, there appears to be a linkage between the errors in the parameter estimation and the particular curvatures.

A commonly applied method to determine error variances of the parameter estimates is to compute the inverse of the Hessian matrix. The Hessian is the matrix of the second derivatives with respect to the parameters, yielding the curvature of the cost function. From a full hessian matrix, containing off-diagonal elements, even correlations among the different paramters can be identified. Unfortunately, as soon as strong nonlinearities exist in the vicinity of the cost function's minimum, the inverse of the computed Hessian may not be a good approximation to the error covariance, as stated by Gunson and Malanotte-Rizzoli (1996). In their study they investigated nonlinear effects on the error covariance matrix, adopting two methods of approximations. One method is based on the construction of the sensitivity matrix, which expresses the derivatives of the model's state variables with respect to the parameters of interest at every datum of observation (Thacker 1989). The other

method relied on finite differences and included the first derivatives of the cost function, which were available from an adjoint model. This yielded a discrete Hessian matrix which could be inverted, as long as it remained well conditioned.

So far, approximations of discrete Hessian in data-assimilation studies with ecosystem models were generated by Fennel et al. (2001) and Vallino (2000). One associated problem is to assign correct step sizes in order to avoid asymmetries in the Hessian, which could yield complex eigenvalues. Furthermore, it is presumed that the nonlinear optimisation problem resembles an ideal (linear) problem within a small parameter space that is sufficiently close to the minimum solution. This definitely holds for those parameters whose eigenvalues do not produce an infinite condition number or become too large (ill-conditioned). A similar assumption needs not be made for the bootstrap approach. To obtain proper statistics, one would actually need to perform several hundreds of optimisations with resampled data sets. For the present work, having only three additional optimisation results from resampled data, it should be remembered that the standard deviations are a crude approximation. Nevertheless, if all three parameter estimates, as retrieved from the additional optimisations, remain close to those originally obtained then the entire estimation process and its results must be considered as trustworthy. Fortunately, this is the case for the simultaneous optimisation performed.

How representative are the parameter projections, such as Figure (3.10), for the sensitivitiy of the cost function to parameter variations? — In Figure (3.22) the sensitivities of the cost function are emphasized for the NPZD-wW model. For every parameter the lowest achieved costs are plotted for the entire range of variation. To do so, the full parameter range is split up into 10 equidistant increments and the lowest cost that is obtained for any particular increment determines the lower limit indicated by the gray line. The projections of the three optimisations with resampled data are included. For better understanding the projections as well as their lower limits are shown in the first subplot of the maximum growth rate (μ_m). In the subsequent plots the projections are omitted while their lower limits remain. In addition, those cost function values are shown that can be retrieved from the one-dimensional parameter variations when all other parameters remain at their best values (bold black lines). Close to the minimum the cost function curvatures due to the one-dimensional variations are identical to those that would be obtained for the diagonal elements of the Hessian matrix. Figure (3.22) suggests that the sensitivities according to the one-dimensional variations are either larger or equal to sensitivities derived from the parameter projections.

Costs and residuals

The cost function expresses the misfit between observational data and model results. It is dimensionless and provides a single value which is the sum of weighted least square terms at every location. Two optimisations have been performed with

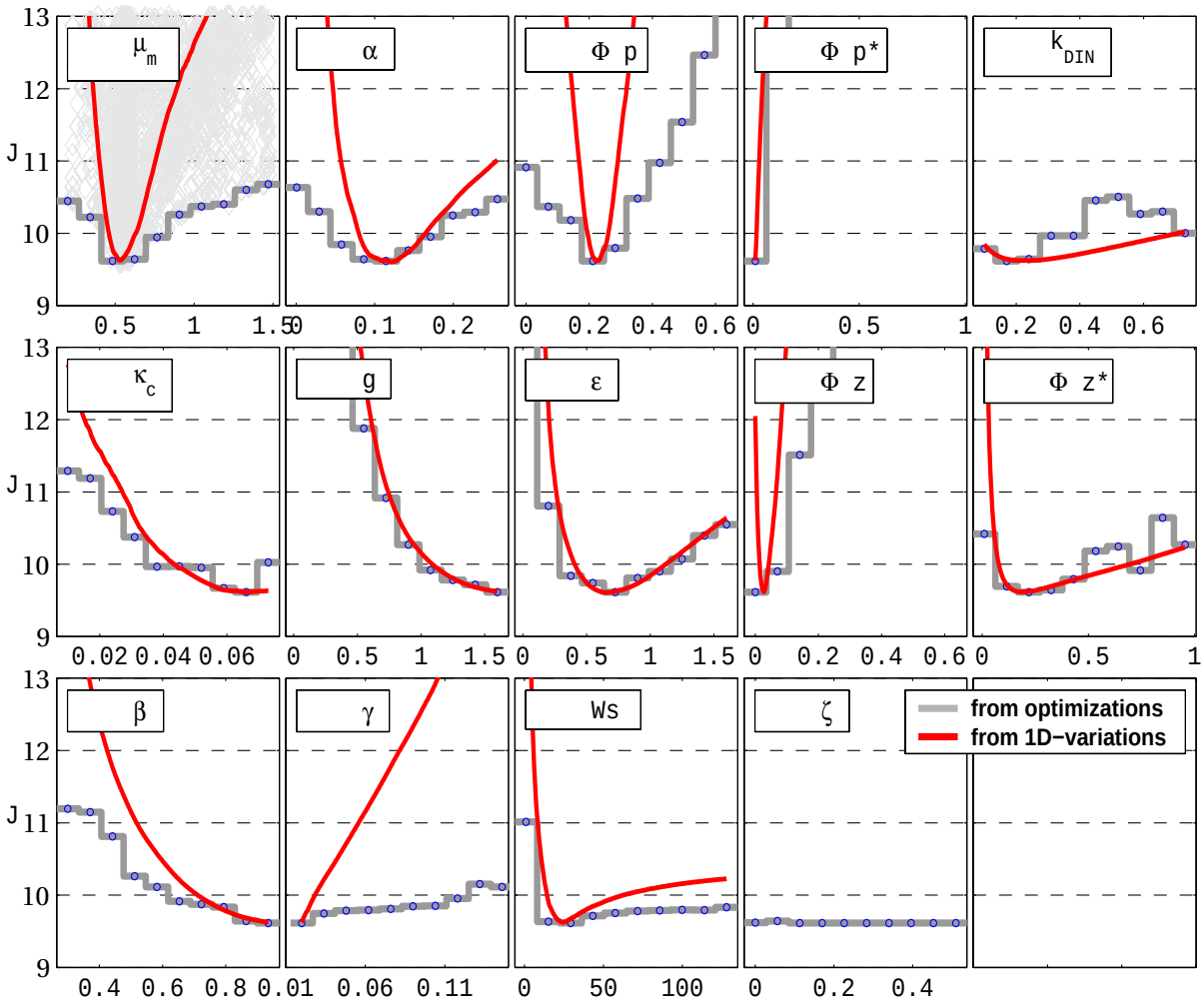

Figure 3.22: Parameter sets together with their lower limits in costs that occured during the seach process of all four optimisations (the three bootstrap optimisations are included). For a better understanding, the first subplot at the top includes all parameter projections as well as their lower limits. The red line represents the costs that belong to one-dimensional parameter variations when all other parameters remain at their best values, referring to the real data set. The fourteenth parameter (ζ) is a control variable and has no effect on the model results.

slightly different model configurations. For the model which includes vertical advection (NPZD-wW) the minimization process ended with lower costs than for the other configuration (NPZD-nW). However, if compared with the *a priori* costs the differences between the two minimal cost function values are small, approximately 10%. Information whether this difference is substantial or not can be retrieved from an analysis of the individual misfit contributions to the cost function. At all three locations the largest remaining least square contributions come from dissolved inorganic nitrogen (N) and chlorophyll concentrations (CHL). As a consequence it becomes expedient to look at the monthly costs of CHL and N. Figure (3.23) shows the monthly

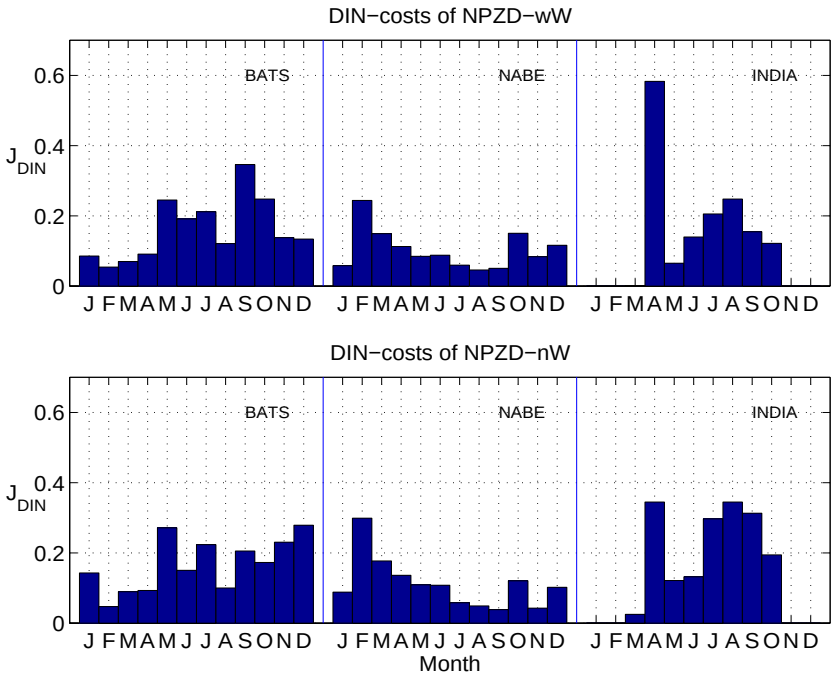

Figure 3.23: Cost function contributions of dissolved inorganic nitrogen (DIN) at the BATS, NABE and INDIA sites. The bars indicate the sum of the vertical contributions for each month.

cost function terms of N at the three locations for the model configuration NPZD-wW and NPZD-nW, respectively. Contrary to our expectations the monthly misfits yield similar distributions, in particular at the NABE site. At the INDIA site differences between the two models are apparent throughout the year. Near Bermuda, changes in the misfits are restricted to the winter months November through Janurary. Even less emphasized are the differences among the chlorophyll misfits, as presented in Figure (3.24). Misfit contributions of primary production, particulate organic nitrogen and zooplankton show a similar picture as for chlorophyll. Due to the similarities in the misfit contributions it seems rather difficult to elaborate the major implications of the slightly different optimisation results. To proceed, the question can be reformulated as follows.

What leads to higher estimates of the detrital sinking velocity in the NPZD-nW configuration? — Among the optimal parameter estimates the sinking velocities turn out to be the most destinctive between the two model configurations. For the NPZD-wW model the optimal sinking velocity is 24 md^{-1} while for the NPZD-nW model a velocity of 44 md^{-1} is retrieved. Hence, some increase of the cost function must be expected when the sinking velocity is decreased for the NPZD-nW model. This increase of the costs is resolved in Figure (3.25). The figure shows the cost function changes when the sinking velocity is reduced from 44 md^{-1} to 24 md^{-1} for the NPZD-nW configuration. Reducing the sinking speed leads to tiny improvements in primary production, PON and zooplankton. Nevertheless, the net raise in costs equals 0.123 which is approximately 1% of the total costs. The distribution of dissolved in-

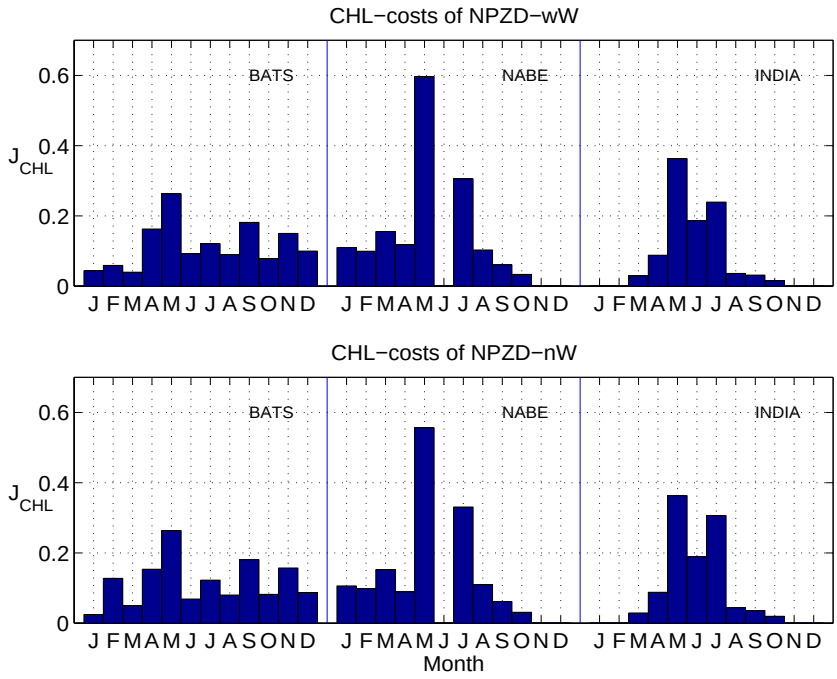

Figure 3.24: Cost function contributions of the chlorophyll term (CHL) at the BATS, NABE and INDIA sites. The bars indicate the sum of the vertical contributions for each month.

organic nitrogen can be considered as the responsable variable for constraining the sinking velocity towards lower values. Apparently, the increase in the cost function is associated with misfits mainly in summer (Figure, 3.25). During summer the concentrations are lowest. Thinking of the consequences which correspond to decreased sinking speeds the direct linkage to the remineralization of nutrients becomes quite obvious. As long as the remineralization parameter remains simlarly low for both configurations the ultimate model response to decreased sinking velocities is the increase in remineralization due to an prolonged residence time of detritus within the upper layers.

Referring to the overall monthly shares of the cost function both model configurations yield similar pictures. Although the NPZD-wW model yields slightly lower costs than the configuration without vertical advection there is no ultimate evidence for any preference in model configurations. The only extraordinary difference accounts for the increased estimate of the sinking velocity of the NPZD-nW model. Sinking speeds lower than the optimal estimate of the NPZD-nW model produce a net increase of the costs which is associated with enlarged misfits in dissolved inorganic nitrogen during the summer periods.

Is the basin-wide optimisation competative with with local optimisation results? — Assimilating data from the different locations simultaneously provides parameter estimates which minimise the combined misfits at the corresponding sites. Thus, the

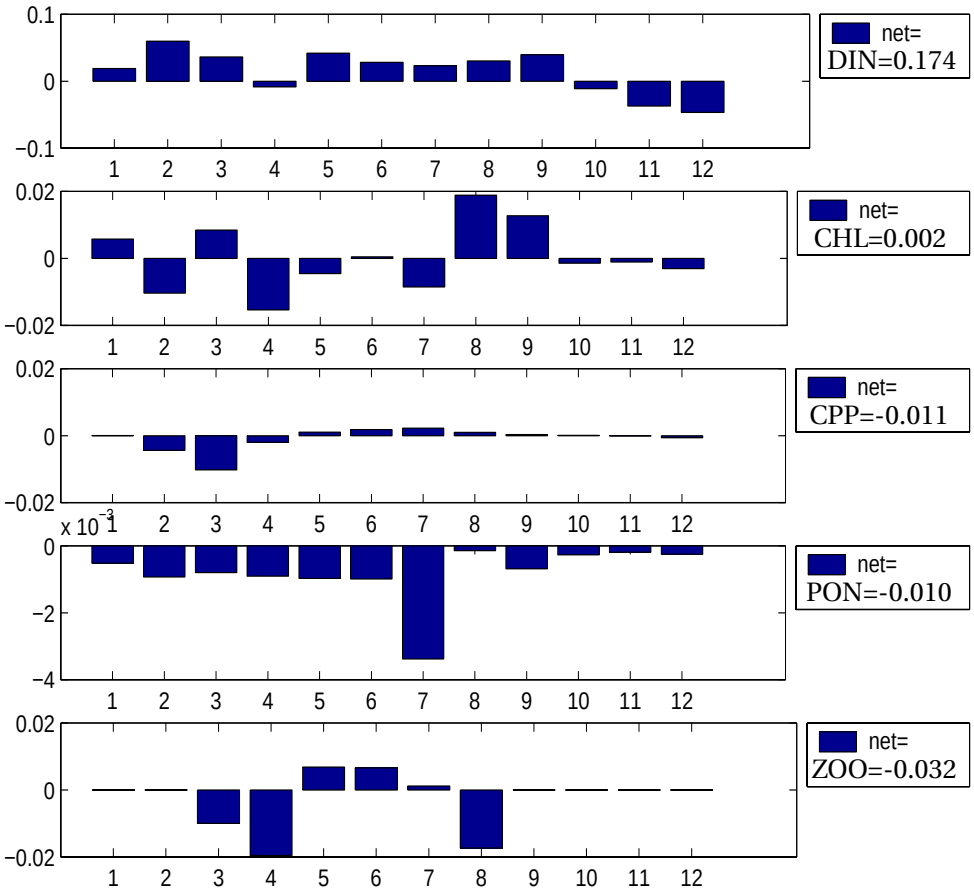

Figure 3.25: Changes in the monthly cost function that are associated with a decreased sinking velocity in the NPZD-nW model (when decreasing from 44 md^{-1} to 24 md^{-1}). From top to bottom: Dissolved inorganic nitrogen (DIN), chlorophyll a (CHL), carbon based primary production (CPP), particulate organic nitrogen (PON) and zooplankton biomass (ZOO).

parameter estimates can be regarded as best representatives on basin-scale. A compromise has to be made and eventually this particular parameter set might not be the best for each of the local site. Comparing the local best parameter estimates with those obtained from the simultaneous optimisation is desirable but goes beyond the scope of this chapter. However, some aspects can be taken into consideration.

The BATS data is deemed to be most informative and therefore some local optimisation results are taken, as an example, for comparision. First of all, according to Table (3.3) the lowest misfit contribution of the BATS site to the total (simultaneous) cost function is $\mathcal{J}_{\mathcal{BATS}}$=3.94 for the NPZD-wW configuration. While implementing the same type of data the local optimisation yields a minimal cost of $\mathcal{J}^{local}_{BATS}$=3.12, which is an improvement of over 50% with respect to the *a priori* costs. The local parameter estimates differ significantly from the simultaneous solutions. The most remarkable deviation can be seen from the sinking velocity whose local estimate is 4 md^{-1}. In addition, the half-saturation constant for nutrient uptake has risen to

k_{DIN}=0.73 mmol N m^{-3}. These two deviations alone should already have an effect on the model results. In Figure (3.26) the seasonal cycle of dissolved inorganic nitrogen and chlorophyll concentrations are shown for the local optimisation. The ni-

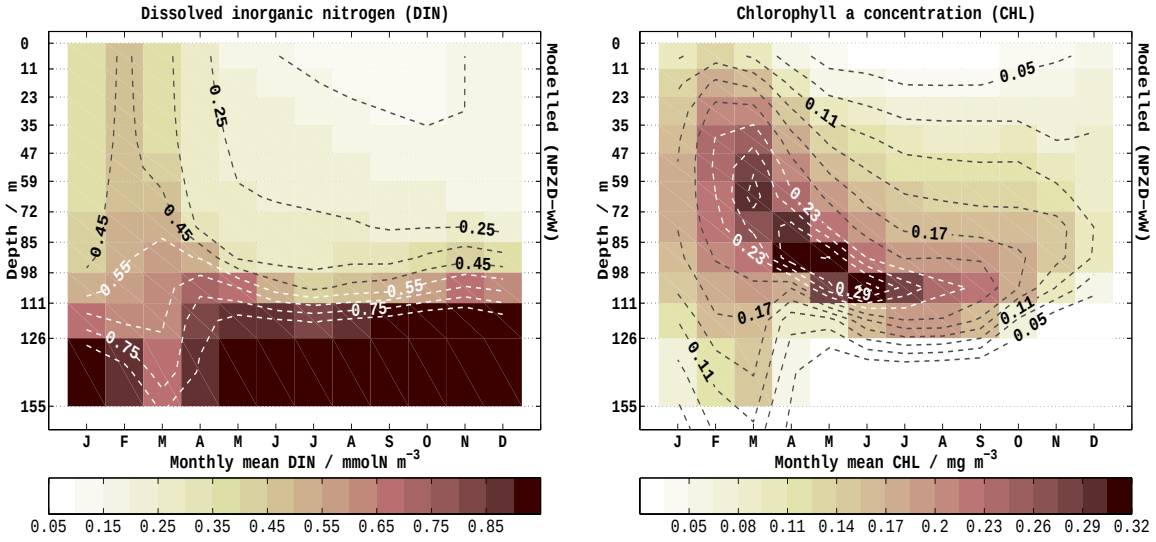

Figure 3.26: Optimal model results near Bermuda when assimilating BATS data only. LEFT: Dissolved inorganic nitrogen. RIGHT: Chlorophyll concentrations. Model configuration = NPZD-wW.

trate distribution, in particular, is different from the results of of the simultaneous optimisation. Furthermore, the deep chlorophyll maximum has a greater vertical expansion, in better agreement with observations. Since the nutrient utilization rate seems to be decreased and the residence time of detritus is extended there remains more inorganic nitrogen within the upper 150 meters. To emphasize the discrepancies between local and simultaneaous optimisation results near Bermuda, the residuals are plotted for dissolved inorganic nitrogen and chlorophyll, Figure (3.27). As mentioned before, the predicted nutrient distributions exhibit an opposite pattern, apart from values below 126 meters where both results underestimate the observed nitrate concentrations. When comparing the residuals in chlorophyll there are generally higher concentrations for the local result. It is noteworthy that both model results maintain chlorophyll concentrations which are too high at depth from January through March, indicating a systematic deficiency of the model formulation itself.

From the discrepancies between local and simultaneous optimisation results at the BATS site it can be concluded that their optimal parameter sets should be interpreted separately. Wherever the NPZD-model is utilized locally the parameter estimates retreived from the simultaneous optimisation are a compromise. Nevertheless, the estimates could be taken as a first approximation, knowing that these parameter values produce fitted model results at the three selected locations. With regard to the parameterisations it is possible to introduce more dynamical parameters, simi-

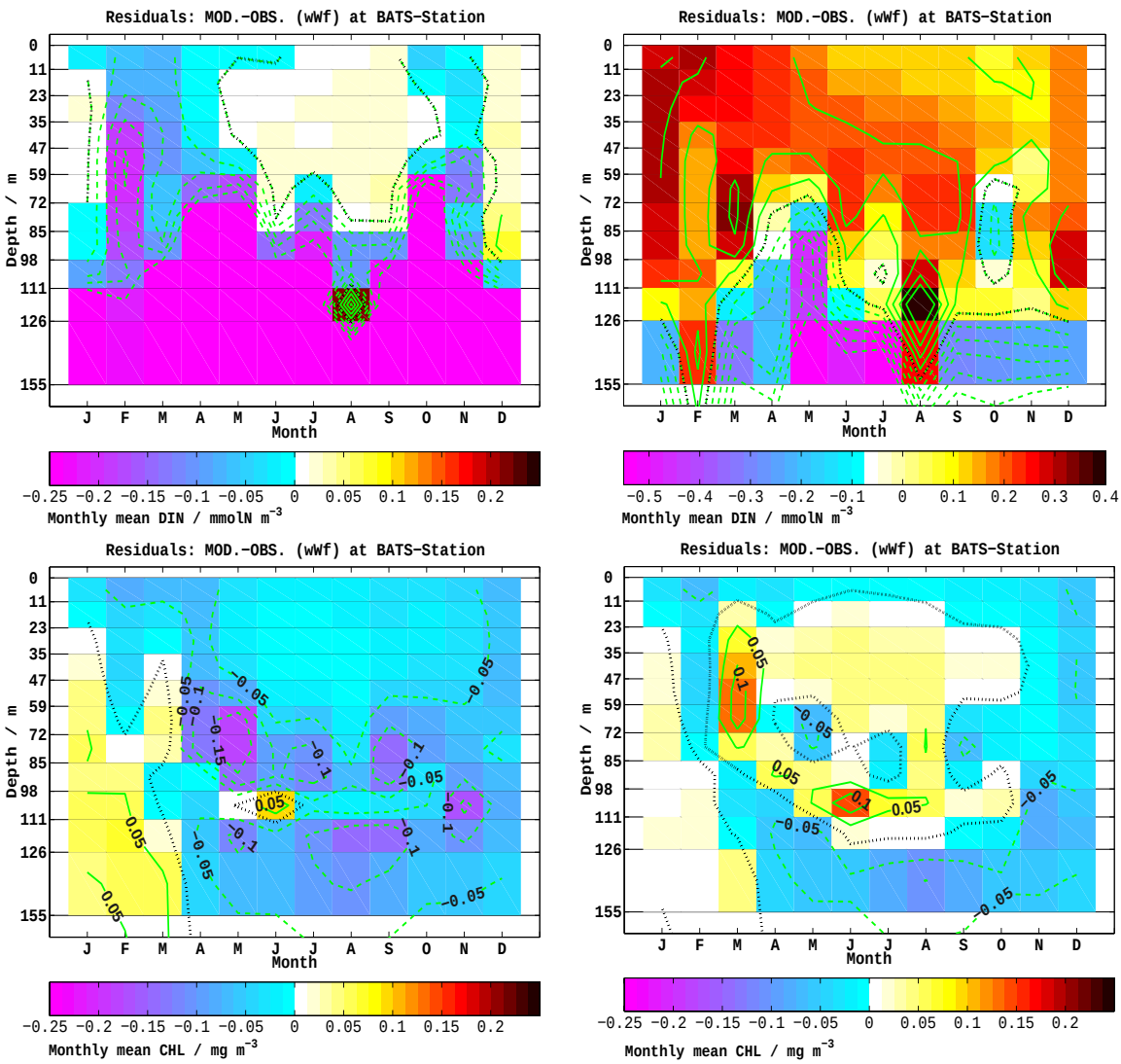

Figure 3.27: Residuals (model-observation) of dissolved inorganic nitrogen (top) and chlorophyll (bottom) after data-assimilation at the BATS site. LEFT: simultaneous optimisation, RIGHT: local optimisation

lar to the temperature dependend growth rate. For example, a variety of temperature dependent parameterisations were used for large-scale simulations with a coupled physical-biological model of the North Pacific by Kawamiya et al. (2000).

3.4.2 Model results

The following, model results will be discussed within the context of biogeochemical provinces and their characteristics following the specifications of Longhurst (1998). The central question is: How well can the optimised model results simulate the characteristics of the different biogeochemical provinces with a single set of parameter values?

BATS site (31^{o}N 64^{o}W)

The region around the Bermuda time series station belongs to the western part of the North Atlantic Subtropical Gyral Province (W-NAST). Typical oceanographic characteristics near Bermuda include Ekman pumping with a prevailing downward direction and mesoscale variability. Mesoscale features near Bermuda are subject to recent investigations because and have been proposed to increase new production in areas of the Sargasso Sea (Siegel et al., 1999 and McGillicuddy et al., 1999). As described by McGillicuddy Jr. et al. (1998), the concept of enhanced productivity due to mesoscale variations is based on the idea that eddy-induced upwelling events supply the euphotic zone with new nutrients to be utilized by the phytoplankton. The effect of this process is still debated since it is not yet clear how fast the elevated isopycnals are refilled with nutrients after utilization. However, the one-dimensional model could not capture eddy-induced upwelling events. Even if the 3D-model simulations could completely resolve eddies in the Bermuda area their effect on the vertical velocity and temperature field would have been averaged out. That is because the effect of mesoscale variations is intended to be minimised by the assimilation of monthly averaged observations.

According to the monthly data at the BATS site the documented mesoscale variability does not seem very troublesome for data-assimilation. Nevertheless, one mesoscale event in late August and September of 1992 becomes apparent and contributed to the cost function. From measured salinities and temperatures in August the passage of a warm water parcel was identified which probably induced a biological response, high enough to alter the monthly mean September values. A high salinity lense with a maximium of 36.85 psu between 60 and 80 meter depth is associated with that water parcel. These anomalous water mass is thought to have formed nonlocally and it is likely that it was advected into the BATS region (Siegel et al. 1995). The pycnocline is slightly deepened in August and hence the biota is expected to collapse. But in September the primary productivity rates, chlorophyll and PON concentrations increased to untypically high values for that month. Obviously, there is a link between this advective event and the biota but the ecosystem response is far from being clear. Several possible explanations for these observations exist. The increase in PON may be caused by horizontal advection. The mixing conditions were altered such that nutrients were able to reenter the euphotic layers and envoked phytoplankton growth. One could also interpret the ecosystem response as a matter of restratification after the disturbance with remineralized nutrients being available again for utilization. Eventually, all the above mentioned scenarios are speculative although it seems clear that the observed features are linked to the high salinity anomaly in 1992.

The effect of Ekman pumping on the biogeochemistry generally results in a net downwelling flux of organic matter out of the euphotic layer. In the coupled physical-biogeochemical model of Doney et al. (1996) a downwelling flux of 23 mmol N m^{-2}yr^{-1} is obtained which is about 10% of their upward turbulent flux into the upper 140 me-

ters. The downwelling is much less accentuated in the optimised NPZD-wW model. Only 2 mmol N $m^{-2}yr^{-1}$ of PON is vertically advected at 126 meters. A much larger downward flux of PON (100 mmol N $m^{-2}yr^{-1}$) is obtained by turbulent mixing in the model which, on the other hand, is quite similar to the 112 mmol N $m^{-2}yr^{-1}$ determined by Doney et al. (1996).

The supply of new dissolved nitrogen to the euphotic zone is 0.13 mol N $m^{-2}yr^{-1}$ in the optimised model. Assuming that this nitrogen is fully utilized by the phytoplankton, this flux describes the magnitude of new production (Dugdale and Goering 1967). The annual new production retrieved here is rather comparable with observational estimates by Altabet (1989) and Lohrenz et al. (1992) who obtained 0.19 and 0.10 mol N $m^{-2}yr^{-1}$ from the analysis of sediment trap fluxes. Previous model studies suggested annual mean new production rates ranging between 0.24 molN $m^{-2}yr^{-1}$ to approximately 0.57 molN $m^{-2}yr^{-1}$, in Doney et al. (1996) and Fasham (1995) respectively. A value of 0.5 mol N $m^{-2}yr^{-1}$ has been recently supported by Siegel et al. (1999). In their study they assigned a flux of approximately 0.24 molN $m^{-2}yr^{-1}$ to the above mentioned process of eddy pumping. Neglecting the eddy-pumping mechanism as a possible additional source of new nitrogen, they approximated a flux of 0.17 molN $m^{-2}yr^{-1}$ from wintertime convection. Actually, this would be the actual flux to be compared with our results since there exists no eddy-pumping in the NPZD-wW model.

Despite relatively high primary production rates the export of organic matter is low at the BATS site, which is typical for an oligotrophic province. BATS-sediment trap data yield an annual flux of approximately 0.10 mol N $m^{-2}yr^{-1}$ at 150 meters depth. In the model only 0.03 mol N $m^{-2}yr^{-1}$ are obtained at a similar depth, only one third of the observed flux estimates. The model's sedimentation rates are derived from the detritus that sinks through the water column. For shallow traps, however, it is likely that the sinking of detritus is not the adequate model counterpart to observations because the turbulent mixing flux of PON is significantly larger at low depths around 150 meters. As an example, Figure (3.28) shows the monthly sedimentation rates. Model results exhibit a destinct deviation from observations in February when winter mixing reaches depths down to 200 meters. It is not clear how the measured sediment trap fluxes are influenced by winter convection. Perhaps some fraction of the turbulent PON flux in the model must be added to the sinking of detritus in order to be comparable. Data from sediment traps at depths deeper than the deepest annual mixed layer would be better suited for a data-model intercomparision. Unfortunately, the flux rates become very low with increasing depths and therefore the uncertainties become larger as well.

Although little is known about remineralization near Bermuda, as well as in the rest of the W-NAST province, high rates are generally expected. This is associated witht the fact that high primary production is observed under nitrate depleted conditions. For the moment the fitted model results indicate an extraordinary high flux of nitrogen from the phytoplankton compartment back to its inorganic pool in the optimised model. Recent estimates of nitrogen remineralization rates are given by Ono

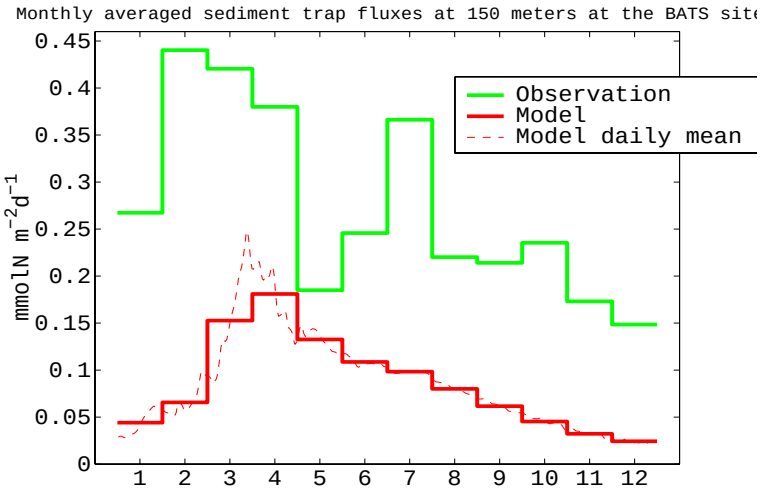

Figure 3.28: Seasonal cycle of sediment trap fluxes (mmol N $m^{-2}d^{-1}$) in 150 meter depth at the BATS site. The observed monthly averages are calulated from 9 years of observations (1989-1997).

et al. (2001) who developed a diagnostic model for determining the seasonal budget of remineralization from oxygen, dissolved inorganic carbon and nitrate measurements. From their model analysis they evaluated a nitrate remineralization of 80±46 mmol N m^{-2} within a 240 days period (from April 16 until December 12) integrated over 100 to 150 meters. The NPZD-wW model yield a mean remineralization of 135 mmol N m^{-2} for the same period (within all five years) over a similar depth range. In previous modelling studies, such as Fasham et al. (1993), Doney et al. (1996) and Schartau et al. (2001) (also Chapter 2), a significant fraction of remineralization occured via zooplankton, mostly attributed to the production of ammonium. Eventually, the zooplankton abundances were too high in all of the models mentioned.

The development of deep chlorophyll maxima (DCM) is a characteristic property of the NAST provinces. The DCM evolves at depths where nutrients are still available while the PAR remains sufficiently high. Variable chlorophyll to nitrogen ratios are suggested to better simulate the chlorophyll concentrations together with the PON distribution (Doney et al., 1996 and Hurtt and Armstrong 1999). The empirical function of Cloern et al. (1995), as referred to in the model, was based on variable chlorophyll to carbon ratios. Applying the constant nitrogen to carbon conversion factor of 6.625, as suggested by Redfield et al. (1963), this function produces chlorophyll to nitrogen ratios below 1.56 mg CHL mmol N^{-1} within the euphotic zone at the BATS site. Near surface the ratio can become even slightly lower than 0.1 mg CHL mmol N^{-1} during the summer, when the incoming radiation and temperatures are high. These near surface ratios are probably too low. There would exist a severe model error as soon as the carbon assimilation ratios of phytoplankton are not proportional to nitrogen uptake. This scenario does not seem unrealistic since carbon assimilation can continue under sufficient light while nutrients become depleted (e.g. Banse 1994). With regard to the nitrogen–carbon conversion factor for phytoplankton sim-

ilar problems arise for the representation of primary production in the model.

To track the observed depth distribution of primary production remains a difficult task for ecosystem models and is subject to recent model investigations in oligotrophic regions. The optimised NPZD-model results for the BATS region exhibit a similar data-model mismatch for primary production as described by Doney et al. (1996), who discussed discrepancies between modelled productivities and measured ^{14}C-primary production rates. Systematic deficiencies in production rates were also described in Schartau et al. (2001) for the NPZ-model of the upper mixed layer, see Chapter 2 as well. To recall, within the mixed layer the NPZ-model could not resolve the observed maximum in primary production which follows after the decline of chlorophyll concentrations. The one-dimensional model shows a similar picture near the surface. Many models simulate nitrogen based productivity and usually these rates are converted to primary production with the Redfield ratio. Regarding integrated primary production the model is actually in very good agreement with the observations, Figure (3.29). This may be misleading because in late spring and

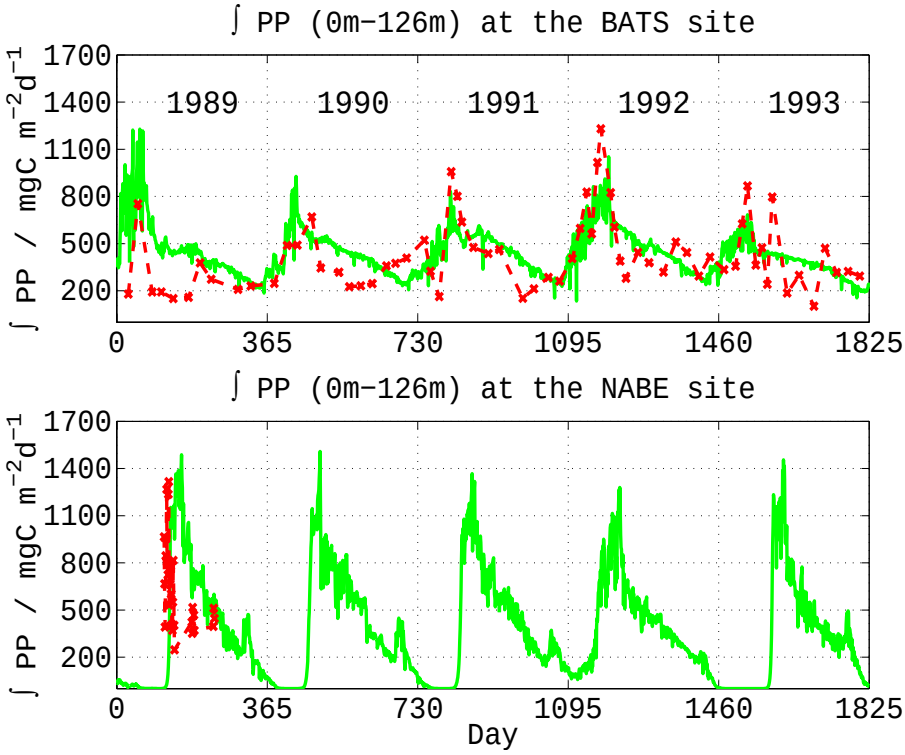

Figure 3.29: Integrated primary production rates (upper 126 meters): green/gray solid line=modelled, red/black dashed line=observed. The model counterparts to the ^{14}C-measurements are determined with a constant molar carbon to nitrogen factor of 6.625 (Redfield ratio). Top figure at 31^{o}N 64^{o}W (BATS site), Bottom figure at 47^{o}N 20^{o}W (NABE site).

summer the modelled productivity is maximal at depth (between 70 and 100 meters) whereas observed productivity remains maximal between surface and 60 meters. Integrated productivities of nitrogen based ecosystem models should therefore be crit-

ically assessed if compared with ^{14}C-measurements in oligotrophic regions.

The results of the NPZD-wW model at BATS maintain a high flux of organic nitrogen back to its inorganic form in order to allow for relatively high productivities despite low nutrient conditions. Zooplankton plays a minor role for regenerated productivity in the model. The models depth distribution of chlorophyll matches observed concentrations well but is believed to be too low near surface during the summer periods because of unrealistic chlorophyll to nitrogen values. A temporal and spatial decoupling of maximal chlorophyll concentrations and primary productivity is present in the model but remains less accentuated than apparent in observational data. The retrieved remineralization rates are only slightly higher than the most recent estimates from literature and therefore the increased recycling depticted from the optimzed model may be realistic.

NABE site (47^{o}N 20^{o}W)

The area chosen for the process study NABE is located within the North Atlantic Drift Province Region (NADR). The particular cite around 47^{o}N 20^{o}W belongs to the southern part of that province and is influenced by the North Atlantic Drift. According to the hydrographic field observed by Robinson et al. (1993) the drift region is interspersed with mesoscale features. During NABE spatial heterogenities are attributed to three cyclonic eddies (Robinson et al. 1993). Most of the observations used for data-assimilation are obtained from the NABE period and the mesoscale events are treated as spatial noise which are averaged out when combining all measurements around 47^{o}N 20^{o}W. As derived from the observational data, winter mixing usually extends down to approximately 350 meters in January and February. Initial stratified water patches become apparent during March and April and are associated with short periods of increased heat fluxes due to the elevated sun angle, likely in combination with mesoscale dynamics. In April a continuous stabilization of the water column occurs which entails a rapid biological response.

Simulated interannual variations of the marine biota are large for the NABE site. Therefore it must be stated that a direct comparision of monthly mean model results with the averaged observations at the NABE site is problematic. That is because most observations are associated with the year 1989 (Ducklow and Harris 1993) whereas the model counterparts are calculated from five years of simulation, starting in 1989. In order to evaluate the annual fluxes which are obtained from the optimised NPZD-wW model it is reasonable to depict those model results which cover the period of extensive measurements in 1989.

Referring to Lochte et al. (1993) the spring bloom in 1989 was devided into three phases. The first phase can be described as a period with initial phytoplankton growth and a build up of biomass. This phase is followed by a drawdown of biomass within approximately 10 to 15 days. The final bloom phase is characterized by a stabilization with minor changes in total biomass. In Figure (3.30) model results are shown for the

upper three grid boxes, resolving the spring bloom period in 1989. These depths were chosen in order to resolve the contributions to the model's mean flux results and to compare them with the mean nitrogen flux across 35 meteres, obtained by Martin et al. (1993).

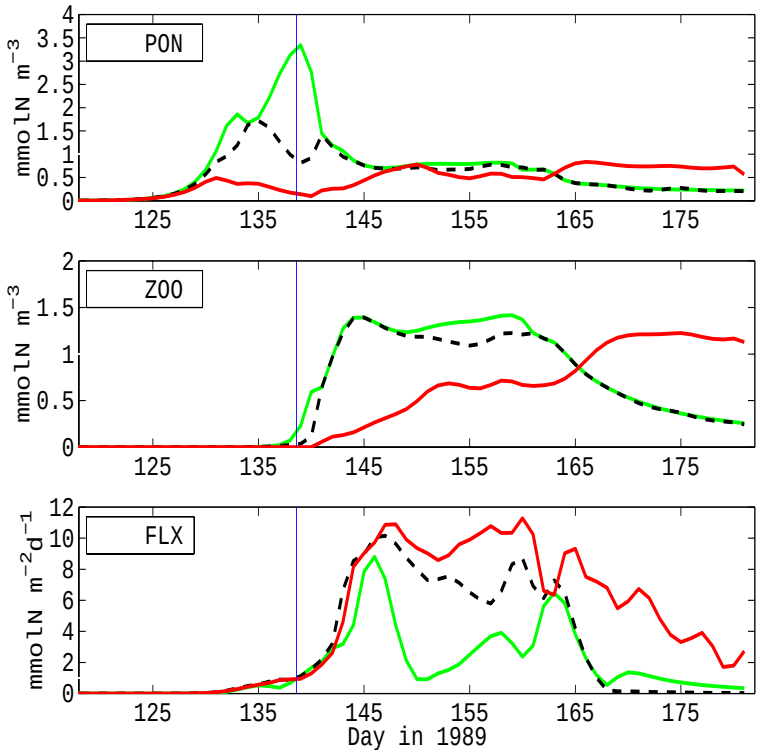

Figure 3.30: Model results at the NABE site during the period of extensive measurements in 1989. Upper grid box (0m-11m): green/gray solid lines; second grid box (11m-23m): dashed lines; third grid box (23m-35m): solid red/black lines. (PON) combines phytoplankton, zooplankton biomass and detritus, (ZOO) zooplankton biomass, (FLX) detrital sinking flux. The vertical line indicates the time when grazing becomes the dominant sink for phytoplankton.

The NPZD-wW model results capture the initiating of the phytoplankton bloom fairly well. As documented by Lochte et al. (1993), the initial bloom was dominated by diatoms. Abrupt changes in phytoplankton compositions followed as soon as silica became depleted. The modelled bloom starts at day 124 (May 4) and developes rapidly within 10 days until maximal chlorophyll concentrations of 3.7 mg m^{-3} are predicted in the middle of May. The chlorophyll concentrations are too high, having a chlorophyll to nitrogen ratio close to 1.9 mg CHL mmol N^{-1}. Naturally, the first raise in phytoplankton biomass coincides with an increase in PON. The model does not predict zooplankton before mid of May (day 138). Hence, the first drawdown of phytoplankton biomass and hence in PON concentrations is associated with a flux to the detritus compartment. This actually means that the phytoplankton's quadratic loss term, at this time, dominates over the zooplankton grazing term. This situation holds until day 138 when grazing becomes the dominant sink for the phytoplankton,

indicated by the vertical line in Figure (3.30) and explicitely resolved in Figure (3.31). Other model studies (Marra and Ho 1993 and Fasham and Evans 2000) simulated silicate concentrations explicitly in order to have a distinction in the bloom between diatom and the other phytoplankton groups like dinoflagellates and picoplankton.

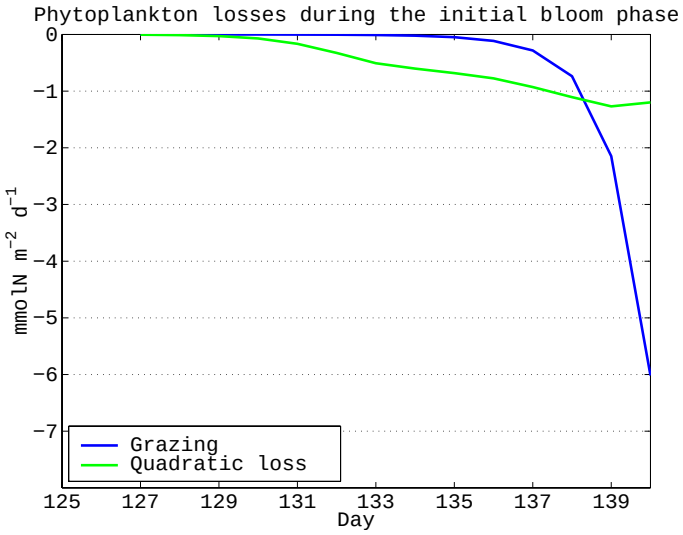

Figure 3.31: Modelled phytoplankton losses due to quadratic "mortality" and grazing in 1989, integrated over the upper 35 meters.

The observed carbon flux at 35 meters was 0.04 mol C $m^{-2}d^{-1}$, as determined by Martin et al. (1993). For the same period of time the modelled flux becomes 0.02 mol C $m^{-2}d^{-1}$, about half as much. There could be two possible explanations for the mismatch. One is related with the carbon to nitrogen ratio which could be higher for the detritus. To fit the observed carbon flux a carbon to nitrogen ratio of 13 would be necessary. Another possible source of error is the detrital sinking velocity since much higher sinking rates than 24 md^{-1} are possible when diatom aggregates are involved (e.g. Alldredge and Gotschalk 1989). If the estimated sinking velocities are wrong then the same model deficiency should be detectable from flux estimates at greater depths. Applying a fitted power function, which was proposed by Martin et al. (1993), a nitrogen flux of 1.85 mmol N $m^{-2}d^{-1}$ is obtained at 126 meters. The model fluxes yield 1.72 mmol N $m^{-2}d^{-1}$ for the same period of the year in 1989 which corresponds surprisingly well with these observational estimates. The model flux uncertainties are likely to be restricted to shallower depths. Zooplankton fecal pellets are believed to play a significant role for the annual nitrogen export (Lenz et al. 1993). This can be well supported by the optimised model results. In fact, the largest export flux in the model is associated with zooplankton. About 30% of annual primary production is grazed by zooplankton and a large fraction then enters the detritus pool, being responsable for the deep export of PON.

Because of large interannual variations, the monthly averages contain huge fluctuations. As an example for these interannual variations, the zooplankton biomass of 1989 and 1992 are shown in 35 meters, the depth where the modelled zooplank-

ton becomes maximal in summer, Figure (3.32). Model results yield the earliest raise in zooplankton in the year 1992 whereas 1989 and 1993 are latest. Such interannual variations should be remembered when evaluating the typical seasonal cycles obtained from model simulations.

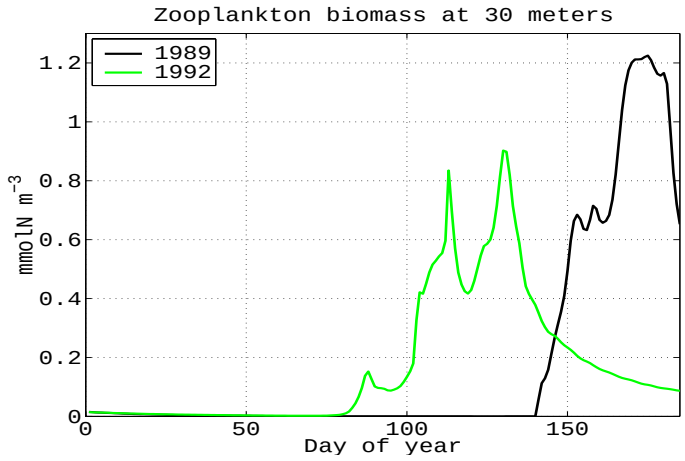

Figure 3.32: Modelled zooplankton biomass at 47^{o}N 20^{o}W in 30 meter depth. The timing of zooplankton initial growth differ among the years of simulation (e.g. 1989 and 1992).

A deviation of the model results from the observational data is obtained during summer. At that time the simulated DCM has penetrated down to 70 meters while the available observations in July and August show the DCM between 10 and 30 meters. However, the simulated distribution of nitrate during the summer period remain reliable. The vertical and temporal extentions of nutrient depletion differ only slightly from the observed and can also be attributed to interannual variability.

For the period of intensive measurements during the spring bloom in 1989 the model captures the basic characteristics of the bloom phases as interpreted in the literature. During the summer period the model results deviate from observations, mainly with regard to the distribution of the DCM. Generally, the model's flux estimates are in good agreement with observations during the spring bloom.

OWS-INDIA (59^{o}N 19^{o}W)

In contrast to the BATS and NABE locations the literature seems rather scarce for OWS-INDIA with respect to nitrogen or carbon budgets. The discussion is therefore restricted to the more general characteristics that can be attributed to this site.

Among the three model locations the site of the OWS-INDIA is the most northern one. The oceanographic region around OWS-INDIA is mainly influenced by the North Atlantic Current system, transporting subtropical water towards the Arctic Ocean. This particular site belongs to the southern part of the Atlantic Subarctic Province (SARC). Generally, winter mixing is deep, reaching depths between 300 and 600 meters. The stratification commences in March and a continuous stabilization of

the water column is established by the begining of May. Figure (3.5) shows that the model's timing of continuous stratification is in agreement with the observations. The most evident mismatch between modelled and observed physics are the maximum mixing depths in winter. It has been mentioned that the years of observations (1971-1974) fell into a low index phase for the North Atlantic Oscillation (NAO). On the other hand, the ECMWF forcing (1989-1993) covers a period with a relatively high NAO index. Simulations under different NAO conditions (Oschlies 2001) revealed decreased mixing in the region of OWS-INDIA for low NAO periods due to weakened westerly winds. Hence, the mismatch in mixing depths between observations and model can to some extent be attributed to different NAO conditions. Discrepancy in the winter mixing depths would not seem too critical because in both cases mixing reaches far below the euphotic zone. With respect to the nitrate input to the upper layers there should also be no difference because the respective vertical profile yield constant nitrate concentrations of approximately 15 mmol N m^{-3} below 300 meters.

The observed chlorophyll concentrations suggest early phytoplankton growth in March and April. Apparently, the physical processes which are not sufficiently resolved by the model may be the origin of such an early biological response. For instance, diurnal changes of the mixed layer depths are not resolved in the model. However, a similar temporal model mismatch in initiating phytoplankton growth was reported by Wolf and Woods (1988), following the approach of Woods and Onken (1982) who could resolve diurnal mixed layer variations. Having short-termed bloom events (ephemeral blooms) as major reason for an early chlorophyll increase has been suggested by Longhurst (1998), referring to observations made by Williams (1988) and Dickey (1994). A deep excursion of high chlorophyll concentrations at the end of April and in May was observed in all four years (Williams 1988) but is not resolved by the model. It is suggested that the observed deep chlorophyll concentrations have their origin in phytoplankton cells which remain ungrazed and sink though the water column (Longhurst 1998). Another possibility to export chlorophyll to great depths are episodical mixing events. Williams (1988) documented interannual variations for the timing of chlorophyll peaks for April and May. Typical integrated chlorophyll concentrations (upper 50 meters) yield maxima ranging from 166 mg CHL m^{-2} in 1971 to 258 mg CHL m^{-2} in 1973. Interannual variations in initiating the bloom are retrieved from the model results as well. Maxima in the model are rather between 120 and 140 mg CHL m^{-2}. The integrated chlorophyll concentrations vary only between end of June and begining of July and therefore interannual variations cannot explain the data-model discrepancies in May and June.

The model's dominant export flux is accounted for by zooplankton, similar to the results at the NABE station. Since the export flux of phytoplankton is likely to be underestimated the model export fluxes should be considered as too small for the OWS-INDIA site. In addition, large uncertainties exist with respect to the zooplankton distribution. The SARC region exhibits complex life cycles of zooplankton. Some copepods, such as *Calanus finmarchicus* and *Pareuchaeta norvegica*, go through several growth stages and comprise overwintered populations. According

to these complexities the zooplankton in the NPZD-wW model must be considered as a very crude approximation. Most recent model investigations with the focus on zooplankton were performed by Carlotti and Wolf (1998). They successfully utilized a Lagrangian ensemble model with elaborated copepod life cycles together with an ecosystem model.

To conclude, model uncertainties remain for the resolution of initial chlorophyll concentrations at great depths in April and May when growth, mixing and sinking processes of phytoplankton are considerably important. Modelled export fluxes further indicate a tight coupling to zooplankton abundances.

4

Summary and conclusions

The ultimate aim of this study is to relate the performance of ecosystem models to existing observations in the North Atlantic. This is achieved by a synthesis of observational data with model results, applying data-assimilation methods. The approach presented here is based on the assumption that the ecosystem models need to be formulated as simple as possible but must resolve the most relevant processes in order to maintain reliable predictive skills for marine biogeochemical fluxes. All investigations in this study are regarded as hindcast experiments and were performed with nitrogen-based ecosystem models. The optimisation results retrieved in this work support the reliability of ecosystem models that are vertically resolved and comprise at least four state variables (NPZD-model). Although knowing that the models are far from being a realistic representation of a marine ecosystem they already capture dominant biogeochemical fluxes. Keeping the models simple as possible is still suggested after these investigations.

Data-assimilation techniques were utilized to identify the optimal parameter values of different ecosystem models, an NPZ-model for the upper ocean's mixed layer and a one-dimensional NPZD-model respectively. Optimal sets of parameter values were retrieved by minimising a cost function which described least square misfits between observations and model results. Measurements from time-series studies, mainly collected during international JGOFS programs, entered the data-assimilative investigations.

Performance of optimisation algorithms and credibility of parameter estimates — Two optimisation methods were applied to assimilate BATS observations into an NPZ-ecosystem model of the upper ocean's mixed layer (Chapter 2). One method relied on an adjoint model which provided gradient information of the cost function for parameter optimisation with a gradient search algorithm. The second method was based on the usage of a stochastic evolutionary search algorithm, the micro-genetic algorithm (μGA). It has been shown that the cost function's hyper-surface contained regions which were not well suited for a gradient search algorithm. For example, flat plateau regions of the cost function existed which yielded low or no sensitivities to parameter variations. Thus, for assimilating observational data into an ecosystem

model, the application of the adjoint method or any other gradient search method for parameter optimisation is not recommended, because the solutions can depend on initial parameter guesses. Under these circumstances several hundreds of optimisations need to be performed, starting from different initial parameter values in order to give reliable optimal estimates. The performance of the μGA was clearly superior to the gradient search method. It provided the lowest cost function value for the NPZ-model at the BATS site. In particular the μGA coped with plateau regions and provided robust estimations of the parameter values. As long as computional costs for the evaluation of the model remain relatively low it is suggested to apply a stochastic search algorithm such as the μGA for parameter optimisation in ecosystem models.

The robustness of the μGA could be confirmed when applying a bootstrap approach to approximate the errors of the parameter estimates (Chapter 3). Additional optimisations were performed with resampled data sets. Therefore more than one optimal parameter solution was obtained. In this study the additional bootstrapped parameter estimates were close to those optimised parameter values which were obtained from the original data set. Despite the fact that the bootstrap method, applied here, must be regarded as a "quick and dirty" approach it was very informative with respect to the robustness of the entire optimisation process and hence the credibility of the parameter estimates.

In general data-assimilation experiments comprise a misfit function where data and model results are compared to each other in a least square sense. Two types of cost functions were defined here. In the first case the data-model comparision was done on a daily base (Chapter 2). That is, an observation was compared with the model counterpart at the date of measurement. It must be emphasized that such comparisions on a daily base are delicate in particular when model results comprise temporal delays or preceedings. Therefore it is recommended to introduce a temporal weighting term to the cost function which accounts for short term mismatches between observation and model result. For the second cost function, monthly averages were introduced in order to reduce the impact of "higher order effects", such as mesoscale variability, on the optimisation results (Chapter 3). In addition, the cost function accounted for the vertical distribution of the biota. The informations entering the cost function were sufficient to constrain the model's parameters well. Solely the effect of interannual variations must be better regarded when periods of intense observations cover only one particular year while the modelled monthly averages are retrieved from several years of simulation.

Simultaneous optimisation and model performance — An NPZD-model with vertical resolution was optimised at three locations in the North Atlantic (Chapter 3). The objective for assimilating data at three site simultaneously is simply to estimate an optimal set of model parameters for large-scale simulations, at least on a basin-scale

in the North Atlantic. Observations from different biogeochemical provinces were regarded for the determination of a best guess of parameter values. The physical boundary conditions used for the one-dimensional model were derived from three-dimensional model simulation which assured some degree of compatibility. Therefore, this work links together local process studies with large-scale biogeochemical modelling efforts.

The simultaneous optimisation was achieved by minimising a cost function which combined the data-model misfits from those sites where time-series observations were available. Data from BATS and NABE were utilized as well as measurements from the OWS-INDIA. The observational data were collected during international JGOFS process studies, with data from OWS-INDIA being the only exception. The measurements of the OWS-INDIA site covered a period of 1971 through 1974 whereas NABE and BATS data were from 1989 and 1989-1993 respectively. Optimisation results could be compared with model simulations that accounted for a parameter set usually suggested for large-scale simulations (referred to as *a priori* parameters). The improvements of the cost function were within 30-47%, if compared with the *a priori* model simulations. Substantial differencies exist between *a priori* and optimised nitrogen fluxes, indicating rapid remineralization. It became evident that the "new" parameter estimates yielded a better model performance at all three locations of interest.

The cost function for the simultaneous optimisation included a simple scaling of the least square misfits at every location. This was necessary in order to assure that the misfits at the respective sites contribute to the cost function in the same order of magnitude. Otherwise, the biology at the BATS site can become extinct because differences between zero and observed values are likely to remain smaller than differences at other locations. A simple scaling approach was proposed which could overcome that particular problem. It only considers averaged observational values and their prescribed error variances. Regarding attempts to assimilate observational data simultaneously at several locations, this or a similar scaling is recommended. An appropriate scaling is of particular importance when the sites comprise large differences in observed values (e.g. combining oligotrophic with eutrophic regions).

The parameter estimates obtained from the simultaneous optimisation can be regarded as the best representatives for the NPZD-model on a basin-scale when covering distinct biogeochemical regions in the ocean. Nevertheless, the optimal parameter set retrieved is a compromise among the observational sites. Local optimisations do yield a different parameter set, as discussed for the BATS location. A full intercomparison of local results with those obtained from the simultaneous optimisation is beyond the scope of this study. However, preliminary results suggest a further refinements are possible regarding the misfits. If compared with the *a priori* costs the improvements that result from local optimisations range between 51% through 63%.

Future work will include such an intercomparison and it is proposed to analyse the distinctions among the optimal parameter estimates.

The seasonal cycles of the optimal model results were analysed at the three locations, mainly referring to monthly averaged variables. Primary production rates, the chlorophyll concentrations and the export fluxes were examined in particular. In general, the optimised NPZD-model could capture characteristic features at the different locations. Distinctions could be attributed to the role of zooplankton on the export fluxes of PON. At the oligotrophic BATS site the modelled zooplankton biomass remained very low (approximately 0.04 mmol N m^{-3}) and the export flux of organic matter from the euphotic zone was mainly associated with turbulent mixing of phytoplankton biomass and detritus. This was contrary to the model solutions obtained at the NABE and OWS-INDIA sites where the dominant export fluxes were due to detritus that was contineously supplied from zooplankton nitrogen, such as fecal pellets. The modelled export flux out of the euphotic layers at OWS-INDIA and the NABE site were about 25% and 38% of the total primary production. Near Bermuda only 6% could be exported by the model because a large fraction of organic material was rapidly remineralized.

The optimised model results yielded large fluxes of organic nitrogen back to its inorganic dissolved form, with phytoplankton being the dominant organic source. This flux appeared to be most important for the oligotrophic BATS site since observed primary productivities are relatively high despite low nutrients concentrations. It actually implies that dissolved organic matter (DOM) produced by phytoplankton plays an important role for primary production in the model. Since this simulated flux was considerably high it must be better analysed or constrained by additional data. In the model the direct link between phytoplankton and nutrient is rudimentary. Naturally, many processes must be attributed to this linkage, such as the release of dissolved organic nitrogen (DON) and bacterial activity. It cannot be stated which location contributed most to constrain the parameter responsible for this increased flux. To figure this out, some subsequent optimisations need to be performed with the locations being successively omitted. For model investigations of the mentioned flux it is advisable to implement DON as an additional state variable by simply resolving the process of DON formation and its transformation with a constant decay rate, assuming a combination of the labile and semi-labile fractions. As a consequence, bacterial activity would be specified by the decay parameter and bacteria need not be introduced explicitely to the model. To start data-assimilation experiments and hence to estimate the additional DON decay parameter, it is possible to use data of total organic nitrogen (TON), as it is provided by BATS. The DON simulations could be combined with those of PON to comprise one model counterpart to the TON observations.

The simulated chlorophyll concentrations were in fair agreement with observa-

tions at the BATS site but with inceasing latitudes the model's performance with respect to chlorophyll became poorer. Although the initiating of the bloom was well resolved by the model at the NABE site the predicted chlorophyll concentrations exhibited a deep chlorophyll maximum during the summer period much deeper than observed. Model refinements are necessary mainly with regard to the chlorophyll to nitrogen ratio. The variable ratio in the model relied on constants determined from fits to experimental results. For future data-assimilation studies it is therefore recommended to consider these constants as free parameters and let them vary and be optimised as well. For constraining these chlorophyll parameters it is useful to introduce radiation data to the assimilation process since the ratio is very sensitive to variations in the light field. Vertical profiles of photosynthetic available radiation (PAR) are best suited. At high latitudes (OWS-INDIA) the model revealed uncertainties with respect to the timing of stratification and hence the development of the spring bloom. Short-termed (ephemeral) bloom events which were observed mainly in April and May could not be resolved by the model. It is suggested that during this period short-termed stratifications are necessary in combination with a rapid biological response (presumably under low light conditions) in order to mix chlorophyll to great depths. Thus, the physical-biological interactions should be better regarded at the OWS-INDIA site. To some extent model discrepancies in spring at OWS-INDIA can be assigned to interdecadel variabilities and hence differences in heat fluxes and mixing. To better specify and extract errors during spring the effect of interdecadel variability on the model results is required to be analysed in detail.

Data of primary production derived from measurements of ^{14}C fixation into organic material can deviate from nitrogen based productivity in models. Major data-model deficiencies appeared immediately after dissolved inorganic nitrogen became depleted, as already evident from the NPZ-model simulations of the upper mixed layer at the BATS site (Chapter 2). In all five years of simulation the model did not capture the temporal maxima in the carbon based productivity. The data-model misfit was therefore identified as a systematic error. Similar conclusions were drawn from one-dimensional simulations with the NPZD-model (Chapter 3). Here, the vertical distribution of the observed and modelled primary production differed likewise after nitrate exhaustion, in particular at the BATS and NABE sites. Observed primary production was always maximal near the ocean's surface at high light intensities. In contrast the modelled primary production followed the deepening of the the nutricline. This feature was not detectable from integrated primary productivities, which were actually in good accordance with the observations. Because carbon and nitrogen dynamics exhibited different temporal and spatial distributions it is suggested that primary produtivity may not be adequately represented by the model when a constant nitrogen to carbon conversion factor is assumed.This particular problem should be addressed in future studies, since primary production is a key factor in biogeochemical flux studies.

Bibliography

Alldredge, A. L. and C. Gotschalk (1989). Direct observations of mass flocculation of diatom blooms; characteristics, settling velocities and formation of diatom aggregates. *Deep-Sea Research I 36(2)*, 159–171.

Alldredge, A. L., U. Passow, and B. E. Logan (1993). The abundance and significance of a class of large, transparent organic particles in the ocean. *Deep-Sea Research I 40*, 1131–1140.

Altabet, M. A. (1989). A time-series study of the vertical structure of nitrogen and particle dynamics in the Sargasso Sea. *Limnology and Oceanography 34*, 1185–1201.

Anderson, T. and P. B. Williams (1999). A oone-dimensional model of dissolved organic carbon cycling in the water column incorporating combined biological-photochemical decomposition. *Global Biogeochemical Cycles 13(2)*, 337–349.

Antia, N. ., C. McAllister, T. Parsons, K. Stephens, and J. Strickland (1963). Further measurements of primary production using a large-volume plastic sphere. *Limnology and Oceanography 19*, 166–183.

Banse, K. (1994). Uptake of inorganic carbon and nitrate by marine plankton and the Redfield ratio. *Global Biogeochemical Cycles 4*, 81–84.

Bard, Y. (1974). Methods of estimation. In Y. Bard (Ed.), *Nonlinear Parameter estimation*, pp. 341. Academic Press, Inc., London.

Bissett, W., J. Walsh, D. Dieterle, and K. Carder (1999). Carbon cycling in the upper waters of the Sargasso Sea: I. Numerical simulations of different carbon and nitrogen fluxes. *Deep-Sea Research I 46*, 205–269.

Blanke, B. and P. Delecluse (1993). Variability of the tropical Atlantic Ocean simulated by a general circulation model with two different mixed-layer physics. *Journal of Physical Oceanography 23*, 1363–1388.

Brock, T. D. (1981). Calculating solar radiation for ecological studies. *Ecological Modelling 14*, 1–19.

Broecker, W. and T.-H. Peng (1992). Interhemisperic transport of carbon dioxide by the ocean circulation. *Nature 356*, 587–589.

Carlotti, F. and K. U. Wolf (1998). A lagrangian ensemble model of *calanus finmarchicus* coupled with a 1-d ecosystem model. *Fishery Oceanography 7:3/4*, 191–204.

Caron, D. A., H. G. Dam, P. Kremer, E. J. Lessard, L. P. Madin, T. C. Malone, J. M. Napp, E. R. Peele, M. R. Roman, and M. J. Youngbluth (1995). The contribution

of microorganisms to particulate carbon and nitrogen in surface waters of the Sargasso Sea near Bermuda. *Deep-Sea Research I 42*, 943–972.

Carroll, D. L. (1996). Chemical Laser Modeling with Genetic Algorithms. *American Institute of Aeronautics and Astronautics 34*, 338–346.

Cloern, J. E., C. Grenz, and L. Vidergar-Lucas (1995). An empirical model of the phytoplankton chlorophyll:carbon ratio —the conversion factor between productivity and growth rate. *Limnology and Oceanography 40(7)*, 1313–1321.

Conkright, M. E., S. Levitus, and T. B. Boyer (1994). Nutrients, Natl. Environ. Satell. Data and Inf. Serv. In N. Oceanic and A. Administration (Eds.), *World Ocean Atlas 1994*, pp. 1994. Silver Spring, Md.

Dickey, T. (1994). Bio-optical and physical variability in the subarctic north atlantic ocean during the spring of 1989. *Journal of Geophysical Research 99*, 22541–22556.

Doney, S. C., D. Glover, and R. Najjar (1996). A new coupled, one-dimensional biological-physical model for the upper ocean: Applications to the jgofs bermuda atlantic time-series study (bats) site. *Deep-Sea Research II 43*, 625–651.

Ducklow, H. W. (1983). Production and fate of bacteria in the oceans. *Bioscience 33*, 494–501.

Ducklow, H. W. and R. P. Harris (1993). Introduction to the jgofs north atlantic bloom experiment. *Deep-Sea Research II 40*, 1–8.

Dugdale, R. and J. Goering (1967). Uptake of new and regenerated forms of nitrogen in primary productivity. *Limnology and Oceanography 12*, 196–206.

Efron, B. (1994). The Bootstrap. In B. Efron (Ed.), *The jackknife, the Bootstrap, and Other Resampling Plans (Sixth printing)*, pp. 91. Capital City Press, Montpelier, Vermont, USA.

Ekman, V. W. (1927). Eddy-viscosity and skin-friction in the dynamics of winds and ocean-currents. *Mem. R. Meteorol. Soc. 2*, 161–171.

Engel, A. (2000). The role of transparent exopolymer particles (TEP) in the increase in apparent particle stickiness during the decline of a diatom bloom. *Journal of Plankton Research 22*, 485–497.

Eppley, R. W. (1972). Temperature and phytoplankton growth in the sea. *Fishery Bulletin 17*, 15–24.

Eppley, R. W. and B. Peterson (1979). Particulate organic matter flux and planktonic new production in the deep ocean. *Nature 282*, 677–680.

Evans, G. T. (1999). The role of local models and data sets in the joint global ocean flux study. *Deep-Sea Research I 46*, 1369–1389.

Evans, G. T. and V. C. Garçon (1997). One–dimensional models of water column biogeochemistry. Technical Report 23, JGOFS Bergen, Norway.

Evans, G. T. and J. S. Parslow (1985). A model of annual plankton cycles. *Biological Oceanography. 3*, 328–347.

Fasham, M. J. R. (1995). Variations in the seasonal cycle of biological production in subarctic oceans: A model sensitivity analysis. *Deep-Sea Research I 42*, 1111–1149.

Fasham, M. J. R., H. W. Ducklow, and S. M. McKelvie (1990). A nitrogen-based model of plankton dynamics in the oceanic mixed layer. *Journal of Marine Research 48*, 591–639.

Fasham, M. J. R. and G. T. Evans (1995). The use of optimization techniques to model marine ecosystem dynamics at the JGOFS station at 47^{o}N 20^{o}W. *Philosophical Transactions of the Royal Society of London B348*, 203–209.

Fasham, M. J. R. and G. T. Evans (2000). Advances in ecosystem modelling within JGOFS. In R. B. Hanson, H. W. Ducklow, and J. G. Field (Eds.), *The Changing Ocean Carbon Cycle*, pp. 417–446. Cambridge University Press.

Fasham, M. J. R., J. L. Sarmiento, R. D. Slater, H. W. Ducklow, and R. Williams (1993). Ecosystem behaviour at bermuda station "s" and ocean weather station "india": A general circulation model and observational analysis. *Global Biogeochemical Cycles 7(2)*, 379–415.

Fennel, K., M. Losch, J. Schroeter, and M. Wenzel (2001). Testing a marine ecosystem model: Sensitivity analysis and parameter optimization. *Journal of Marine System 28*, 45–63.

Fletcher, R. and M. Powell (1963). A rapidly convergent descent method for minimization. *Computer Journal 6*, 163–168.

Gardner, W. D. (1997). The flux of particles to the deep sea: Methods, measurements, and mechanisms. *Oceanography 10*, 116–121.

Gaspar, P., Y. Gregoris, and J. M. Lefevre (1990). A simple eddy kinetic energy model for simulations of the oceanic vertical mixing: tests at station Papa and Long–Term Upper Ocean Study site. *Journal of Geophysical Research 95*, 16179–16193.

Goldberg, D. E. (1989). *Genetic Algorithms in Search, Optimization and Machine Learning*. Addison-Wesley, Reading, MA.

Grasshoff, K., K.Kremling, and M. Ehrhardt (1999). *Methods of Seawater Analysis*. Third edition, Wiley-VCH, Weinheim, Germany.

Gunson, J. R. and P. M. Malanotte-Rizzoli (1996). Assimilation studies of open-ocean flows: 2. Error measures with strongly nonlinear dynamics. *Journal of Plankton Research 101(C12)*, 28473–28488.

Gunson, J. R., A. Oschlies, and V. Garcon (1999). Sensitivity of ecosystem parameters to simulated satellite ocean color data using a coupled physical-biological model of the North Atlantic. *Journal of Marine Research 57*, 613–639.

Harmon, R. and P. Challenor (1997). A Markov chain Monte Carlo method for estimation and assimilation into models. *Ecological Modelling 101*, 41–59.

Herbland, A., A. L. Bouteiller, and P. Raimbault (1985). Size Structure of phytoplankton biomass in the equatorial Atlantic Ocean. *Ecological Modelling 101*, 41–59.

Holland, J. H. (1975). *Adaptation in Natural and Artificial Systems*. A Bradfford Book, The MIT Press, Cambridge, MA.

Hood, R., N. Bates, D. Capone, and D. Olson (2001). Modeling the effect of nitrogen fixation on carbon and nitrogen fluxes at BATS. *Deep-Sea Research II in press*, 000–000.

Hurtt, G. C. and R. Armstrong (1996). A pelagic ecosystem model calibrated with BATS data. *Deep-Sea Research II 43*, 653–683.

Hurtt, G. C. and R. Armstrong (1999). A pelagic ecosystem model calibrated with BATS and OWSI data. *Deep-Sea Research I 46*, 27–61.

Isemer, H. J. . and L. Hasse (1987). *The Bunker Climate Atlas of the North Atlantic Ocean Vol.2*. Springer Verlag.

Jenkins, W. a. J. G. (1985). Seasonal oxygen cycling and primary production in the sargasso sea. *Journal of Marine Research 43*, 465–491.

Jung, T., E. Ruprecht, and F. Wagner (1998). Determination of cloud liquid water path over the oceans from Special Sensor Microwave/Imager (SSM/I) data using neural network. *Journal of Applied Meteorology 37*, 832–844.

Kaehler, P. and W. Koeve (2001). Marine dissolved organic matter: can its C:N ratio explain carbon overconsumption? *Deep-Sea Research I 48*, 49–62.

Karl, D., D. Hebel, K. Bjorkman, and R. Letelier (1998). The role of dissolved organic matter exudation in the productivity of the oligotrophic North Pacific Gyre. *Limnology and Oceanography 43*, 1270–1286.

Kawamiya, M., M. J. Kishi, and N. Suginohara (2000). An ecosystem model for the North Pacific embedded in a general circulation model Part I: Model description and characteristics of spatial distribution of biological variables. *Journal of Marine Systems 25*, 129–157.

Keeling, D. C., T. Whorf, M. Wahlen, and J. van der Plicht (1995). Interannual extremes in the rate of rise of atmospheric carbon dioxide since 1980. *Nature 375*, 666–670.

Kirkpatrick, S., C. D. Gelatt, and M. P. Vecchi (1983). Optimization by simulated annealing. *Science 220*, 671–680.

Krishnakumar, K. (1989). Micro-genetic algorithms for sationary and non-stationary function optimization. *Intellegent Control and Adaptive Systems 1196*, 289–296.

Krüger, J. (1993). Simulated Annealing: A tool for Data Assimilation into an Almost Steady Model State. *American Meteorological Society 23*, 679–688.

Lafore, J. P. e. a. (1998). The Meso-NH atmospheric simulation system, I, Adiabatic formulation and control simulations. *Annual Geopysics 16*, 90–109.

Lawson, L. M., E. E. Hofmann, and Y. H. Spitz (1996). Time series sampling and data assimilation in a simple marine ecosystem model. *Deep-Sea Research II 43*, 625–651.

Lenz, J., A. Morales, and J. Gunkel (1993). Mesozooplankton standing stock during the north atlantic spring bloom study in 1989 with evaluation of its potential grazing pressure: a comparision between low, medium and high latitutes. *Deep-Sea Research II 40*, 559–572.

Lochte, K., H. W. Ducklow, M. J. R. Fasham, and C. Stienen (1993). Plankton succession and carbon cycling at 47^oN 20^oW during the JGOFS North Atlantic Bloom Experiment. *Deep-Sea Research II 40*, 91–114.

Lohrenz, S. E., G. A. Knauer, V. L. Asper, M. Tuel, A. F. Michaels, and A. H. Knap (1992). Seasonal and interannual variability in primary production and particle flux in the northwestern Sargasso Sea: U.S. JGOFS Bermuda Atlantik Time-series Study. *Deep-Sea Research I 39*, 1373–1391.

Longhurst, A. (1998). *Ecological Geography of the Sea*. Academic Press.

Mahadevan, A. and D. Archer (2000). Modeling the impact of fronts and mesoscale circulation on the nutrient supply and biogeochemistry of the upper ocean. *Journal of Geophysical Research 105(C1)*, 1209–1225.

Malone, C. M., S. E. Pike, and C. J. Conley (1993). Transient variations in phytoplankton productivity at the JGOFS Bermuda time series station. *Deep-Sea Research I 40(5)*, 903–924.

Marra, J. and C. Ho (1993). Initiation of the spring bloom in the northeast Atlantic (47^oN, 20^oW): a numerical simulation. *Deep-Sea Research II 40*, 55–73.

Marshall, J. C., A. J. G. Nurser, and R. G. Williams (1993). Inferring the Subduction Rate and Period over the North Atlantic. *American Meteorological Society 23*, 1315–1329.

Martin, J. H., S. E. Fitzwater, R. M. Gordon, C. N. Hunter, and S. J. Tanner (1993). Iron, primary production and carbon-nitrogen flux studies during the JGOFS North Atlantic Bloom Experiment. *Deep-Sea Research II 40*, 115–134.

Matear, R. J. (1995). Parameteroptimization and analysis of ecosystem models using simulated annealing. *Journal of Marine Research 53*, 571–607.

McGillicuddy, D., R. Johnson, D. A. Siegel, A. F. Michaels, N. R. Bates, and A. H. Knap (1999). Mesosclae variations of biogeocchemical properties in the Sargasso Sea. *Journal of Geophysical Research 104(C6)*, 13381–13394.

McGillicuddy Jr., D. J., A. R. Robinson, D. A. Siegel, H. W. Jannasch, R. Johnson, T. D. Dickey, J. McNeil, A. F. Michaels, N. R. Bates, and A. H. Knap (1998). Influence of mesoscale eddies on new production in the sargasso sea. *Nature 394*, 236–266.

Metropolis, N., A. W. Rosenbluth, M. N. Rosenbluth, A. H. Teller, and E. Teller (1953). Equation of state calculations by fast computing machines. *Journal of Chemical Physics 21*, 1087–1092.

Michaels, A. and A. Knap (1996). Seasonal patterns of ocean biogeochemistry at the U.S.JGOFS Bermuda Time-Series Study site. *Deep-Sea Research II 43*, 157–198.

Michaels, A. a. A. K., R. Dow, K. Gunderson, R. Johnson, J. Sorenson, A. Close, G. Knauer, S. Lohrenz, V. Asper, M. Tuel, and B. Bidigare (1994). Seasonal pat-

terns of ocean biogeochemistry at the U.S.JGOFS Bermuda Time-Series Study site. *Deep-Sea Research I 41*, 1013–1038.

Morel, A. (1988). Optical modeling of the upper ocean in relation to its biogenous matter content (Case I waters). *Journal of Geophysical Research 93*, 10749–10768.

Navon, I. (1997). Practical and theoretical aspects of adjoint parameter estimation and identifiability in meteorology and oceanography. *Dynamics of Atmosphere and Oceans 27*, 55–79.

Ono, S., R. G. Najjar, and N. Bates (2001). Shallow remineralization in the Sargasso Sea estimated from seasonal variations in oxygen, dissolved inorganic carbon and nitrate . *Deep-Sea Research II in press*, 000–000.

Oschlies, A. (2001). Nao-induced long-term changes in nutrient supply to the surface waters of the north atlantic. *Geophysical Research Letters in press*, 000–000.

Oschlies, A. and V. Garçon (1999). An eddy-permitting coupled physical-biological model of the north atlantic. 1.sensitivity to advection numerics and mixed layer physics. *Global Biogeochemical Cycles 13(1)*, 135–160.

Oschlies, A., V. Garçon, and W. Koeve (2000). An eddy-permitting coupled physical-biological model of the north atlantic. 2. ecosystem dynamics and comparision with satellite and jgofs local studies data. *Global Biogeochemical Cycles 14(1)*, 499–523.

Pacanowski, R., K. Dixon, and A. Rosati (1991). The g. f. d. l modular ocean model users guide version 1. Technical Report 2, Geophys. Fluid. Dyn. Lab., Princeton, N. J. .

Press, W., B. Flannery, S. Teukolsky, and W. Vetterling (1992). *Numerical recipes*. Cambridge University Press, Cambridge, USA.

Prunet, P. a. J. M., D. Ruiz-Pino, and I. Dadou (1996). Assimilation of surface data in a one-dimensional physical-biochemical model of the surface ocean. I. Method and preliminary results. *Global Biogeochemical Cycles 10*, 111–138.

Redfield, A. C., B. H. Ketchum, and F. A. Richards (1963). The influence of organisms on the composition of seawater. In: The Sea. Vol. 2, M. N. Hill (edit.), Interscience, New York, p. 1-34.

Reed, R. K. (1977). On estimation insolation over the ocean. *Journal of Physical Oceanography 7*, 482–485.

Richardson, K. (1991). Comparison of ^{14}c primary production determinations made by different laboratories. *Marine Ecology Progress Series 72*, 189–201.

Robinson, A. R., D. J. McGillicuddy, J. Calman, H. W. Ducklow, M. J. R. Fasham, F. E. Hoge, W. G. Leslie, J. J. McCarthy, S. Podewski, D. L. Porter, G. Saure, and J. A. Yoder (1993). Mesoscale and upper ocean variability during the 1989 JGOFS bloom study. *Deep-Sea Research II 40*, 213–225.

Sambrotto, R. N., G. Savidge, C. Robinson, P. Boyd, T. Takahashi, D. Karl, C. Langdon, D. Chipman, J. Marra, and L. Codespoti (1993). Elevated consumption of carbon relative to nitrogen in the surface ocean. *Nature 363*, 248–250.

Sarmiento, J. L., R. D. Slater, M. J. R. Fasham, H. W. Ducklow, J. R. Toggweiler, and G. T. Evans (1993). A seasonal three-dimensional ecosystem model of nitrogen cycling in the North Atlantic euphotic zone. *Global Biogeochemical Cycles 7*, 417–450.

Schartau, M., O. Oschlies, and J. Willebrand (2001). Parameter estimates of a zero-dimensional ecosystem model applying the adjoint method. *Deep-Sea Research II in press*, 000–000.

SCOR (1996). *Protocolls for the Joint Global Ocean Flux Study (JGOFS) Core Measurements (Report No.19)*. International Oceanographic Commission.

Siegel, D. A., D. J. McGillicuddy, and E. A. Fields (1999). Mesoscale eddies, satellite altimetry, and new production in the Sargasso Sea. *Journal of Geophysical Research 104(C6)*, 13359–13379.

Siegel, D. A., A. F. Michaels, J. C. Sorensen, M. C. O'Brien, and M. A. Hammer (1995). Seasonal variability of light availability and utilization on the Sargasso Sea. *Journal of Geophysical Research 100(C5)*, 8695–8713.

Smedstad, O. and J. J. O'Brien (1991). Variational data assimilation and parameter estimation in an equatorial Pacific Ocean model. *Progress in Oceanography 26*, 179–241.

Sorensen, J. and D. Siegel (2001). Variability of the Effective Quantum Yield for Carbon Assimilation in the Sargasso Sea. *Deep-Sea Research II in press*, 000–000.

Spitz, Y. H., J. R. Moisan, M. R. Abbott, and J. G. Richman (1998). Data assimilation and a pelagic ecosystem model: parameterization using time series observations. *Journal of Marine Systems 16*, 51–68.

Steele, J. H. and E. W. Henderson (1992). The role of predation in plankton models. *Journal of Plankton Research 14*, 157–172.

Thacker, W. (1987). In E. report GKSS 87/E/65 (Ed.), *Three lectures on fitting numerical model to observations*.

Thacker, W. (1989). The role of the Hessian matrix in fitting models to measurements. *Journal of Geophysical Research 94*, 6177–6196.

Tomczak, M. and J. S. Godfrey (1994). *Regional Oceanography: An Introduction*. Pergamon.

Vallino, J. J. (2000). Improving marine ecosystem models: Use of data assimilation and mesocosm experiments. *Journal of Marine Research 58*, 117–164.

Verity, P. G., D. K. Stoecker, M. E. Sieracki, and J. R. Nelson (1993). Grazing, growth and mortality of microzooplankton during the 1989 north atlantic spring bloom at 47^on 18^ow. *Deep-Sea Research I 40*, 1793–1814.

Volk, T. and M. Hoffert (1985). Ocean carbon pumps: analysis of relative strengths and efficiencies in ocean-driven atmospheric CO_2 changes. In Sundquist, E. T. und W. S. Broecker (Ed.), *The Carbon Cycle and Atmospheric CO_2: Natural Variations Archean to Present*, pp. 99–110. Geophysical Monograph 32, American Geophysical Union, Washington, D.C.

von Liebig, J. (1840). *Organic Chemistry in its Applications to Agriculture and Physiology*. Taylor and Walton, London.

Wagner, F. and C. Lovelace (1971). Phase shift analysis of $\pi^- p \rightarrow k1^b$. *Nuclear Physics 25B*, 411–427.

Wells, M. (1998). A neglected dimension. *Nature 391*, 530–531.

Williams, R. (1988). Spatial heterogenity and niche differentiation in oceanic zooplankton. *Hydrobiologia 167/168*, 151–159.

Wolf, K. U. and J. D. Woods (1988). Langragian simulation of primary production in the physical environment–The deep chlorophyll maximum and thermocline. In B. J. Rothschild (Ed.), *Towards a Theory of Biological-Physical Interactions in the Worlds Ocean*, pp. 51–70. Reidel, Dordrecht.

Woods, J. D. and R. Onken (1982). Diurnal variation and primary production in the ocean- preliminary results of a lagrangian ensemble model. *Journal of Plankton Research 4*, 735–756.

Wright, P. W. (1988). An atlas based on the coads data set: field of mean wind, cloudiness and humidity at the surface of the global ocean. Technical Report 14, Max-Planck-Institut für Meteorologie, Hamburg Germany.

A

Appendix

A.1 NPZ-equations for ecosystem model of the upper mixed layer

Dissolved inorganic nitrogen (N)

$$\frac{dN}{dt} = [-\mu u + \gamma \Phi_P]\, P + [(1-\beta)\, G + \Phi_h]\, \Omega Z + \mathcal{F}_N \tag{A.1}$$

Phytoplankton biomass (P)

$$\frac{dP}{dt} = \left[\mu u - \Phi_P - \frac{m_r + w_e}{M}\right] P - GZ - \Phi^*_{\mathbf{P}}\mathbf{P^2} \tag{A.2}$$

Herbivorous zooplankton (Z)

$$\frac{dZ}{dt} = \left[\beta G - \Phi_Z - \frac{m_r + w_e}{M}\right] Z - \Phi^*_{\mathbf{Z}}\mathbf{Z^2} \tag{A.3}$$

with the entrainment velocity $w_e = max(\frac{dM}{dt}, 0)$. It denotes entrainment with mass conservation when the mixed layer deepens and a conservation of the nitrogen concentration when stratification occurs. The last term of equation (A.1) corresponds to the turbulent flux of dissolved nitrogen at the bottom of the mixed layer. The quadratic loss terms ($\Phi^*_{\mathbf{P}}\mathbf{P^2}$ and $\Phi^*_{\mathbf{Z}}\mathbf{Z^2}$) are optional, see Experiment II and III in Chapter 2.

The daily, depth-averaged chlorophyll to carbon ratio in the dimensions [mg CHL mg C^{-1}] was calculated as follows:

$$\begin{aligned} CHL:C =& 0.003 + 0.0154 \cdot (\exp(0.050 \cdot T)) \\ & \cdot \left[\exp\left(\frac{-0.059 \cdot PAR\,(1 - \exp(-\kappa M))}{\kappa M}\right)\right] \cdot u \end{aligned} \tag{A.4}$$

with the temperature T [^{o} C] and the nutrient availability for growth $u = N/(k+N)$. In equation (A.4) PAR is in the units [mol quanta m^{-2} d^{-1}], (for PAR 1.0 W m^{-2} ≈ 0.4mol quanta m^{-2} d^{-1}). For a given constant molar C:N Redfield ratio of 106:16 then 1 mg C is equivalent to $12.58 \cdot 10^{-3}$mmol N and the chlorophyll to nitrogen ratio for the model counterpart in the dimensions [mg CHL mmol N^{-1}] becomes $r_{chl}\,(T, PAR, M, u) = 79.5\,(CHL:C)$.

A.1.1 The adjoint model

The extension of the cost function J by adding the product of Lagrange multipliers with the strong constraints gives a *Lagrange*-function :

$$\mathcal{L} = J(\mathbf{y}, \mathbf{z}^{obs}, \mathbf{p}_0, \mathbf{p}^{est}) + \int \boldsymbol{\lambda}^T \left(\frac{d\mathbf{y}}{dt} - F(\mathbf{y}, \mathbf{p}^{est}) \right) dt \tag{A.5}$$

which satisfies the relation

$$\frac{\delta \mathcal{L}}{\delta \vec{y}} = \frac{\partial \mathcal{L}}{\partial \mathbf{y}} - \frac{d}{dt} \frac{\partial \mathcal{L}}{\partial \mathbf{y}'} = 0 \tag{A.6}$$

when the optimal parameters p_ν are found. Solving equation (A.6) for the Lagrange multipliers gives the adjoint equations:

$$-\frac{d}{dt}\boldsymbol{\lambda} = \boldsymbol{\lambda}^T \cdot \frac{\partial F}{\partial \mathbf{y}} - \frac{\partial J}{\partial \mathbf{y}} \tag{A.7}$$

for a time dependent model. The gradients of $\mathcal{L}$ with respect to the parameters p_i were calculated after integrating equation (A.7) and solving for the Lagrange multipliers. New parameter values p_ν^{est} were estimated by supplying a variable metric algorithm with the values of $\frac{\partial \mathcal{L}}{\partial p_\nu}$, p_ν, and $\mathcal{L}$. The cost function J was minimised when the gradients had converged to zero.

The Lagrange function

The Lagrange function formulated for the discrete prognostic equations :

$$\begin{aligned}
\mathcal{L} = J &+ \sum_i \lambda_i^P \left[\frac{1}{\tau} (P_{i+1} - P_i) - (\mu u_i - \Phi_P - h) P_i + G(P_i) Z_i \right] \\
&+ \sum_i \lambda_i^Z \left[\frac{1}{\tau} (Z_{i+1} - Z_i) - (\beta G - \Phi_z - h) Z_i \right] \\
&+ \sum_i \lambda_i^N \left[\frac{1}{\tau} (N_{i+1} - N_i) + (\mu u_i - \gamma \Phi_P) P_i - [(1-\beta) G + \Phi_z] \Omega Z_i - h(N_D - N_i) \right]
\end{aligned} \tag{A.8}$$

with $h = \dfrac{m_r + w_e}{M}$.

The adjoint NPZ-equations

Derivatives with respect to the state variable P_i:

$$\begin{aligned}
\frac{\partial \mathcal{L}}{\partial P_i} = \frac{\partial J}{\partial P_i} &+ \frac{1}{\tau} \left(\lambda_{i-1}^P - \lambda_i^P \right) - \lambda_i^P \left(\frac{\partial \mu}{\partial P_i} u_i P_i + \mu u_i - \Phi_P - h + \frac{\partial G}{\partial P_i} Z_i \right) \\
&- \lambda_i^Z \beta \frac{\partial G}{\partial P_i} Z_i + \lambda_i^N \left(\frac{\partial \mu}{\partial P_i} u_i P_i + \mu u_i - \gamma \Phi_P - \Omega (1-\beta) \frac{\partial G}{\partial P_i} Z_i \right) = 0
\end{aligned} \tag{A.9}$$

The Lagrange multipliers need to be integrated backward in time starting from the date of the last observation :

$$\begin{aligned}\Longrightarrow \lambda_{i-1}^{P} = &\left[-\frac{\partial J}{\partial P_i} + \lambda_i^P \left(\frac{\partial \mu}{\partial P_i} u_i P_i + \mu u_i - \Phi_P - h - \frac{\partial G}{\partial P_i} Z_i\right) + \lambda_i^Z \beta \frac{\partial G}{\partial P_i} Z_i\right] \tau \\ &- \left[\lambda_i^N \left(\frac{\partial \mu}{\partial P_i} u_i P_i + \mu u_i - \gamma \Phi_P - \Omega\,(1-\beta)\,\frac{\partial G}{\partial P_i} Z_i\right)\right] \tau + \lambda_i^P\end{aligned}$$

Derivatives with respect to the zooplankton (herbivores) Z_i:

$$\begin{aligned}\frac{\partial \mathcal{L}}{\partial Z_i} &= \frac{\partial J}{\partial Z_i} + \frac{1}{\tau}\left(\lambda_{i-1}^Z - \lambda_i^Z\right) + \lambda_i^P \\ &\quad - \lambda_i^Z\left(\beta G - \Phi_z - h\right) - \lambda_i^N \Omega\left(\left(1-\beta\right) G + \Phi_z\right) = 0 \\ \Longrightarrow \lambda_{i-1}^{Z} &= \left[-\frac{\partial J}{\partial Z_i} - \lambda_i^P G + \lambda_i^Z\left(\beta G - \Phi_z - h\right) + \lambda_i^N\left(\Omega\left(1-\beta\right) G + \Phi_z\right)\right] \tau + \lambda_i^Z\end{aligned} \tag{A.10}$$

Derivatives with respect to N_i:

$$\begin{aligned}\frac{\partial \mathcal{L}}{\partial N_i} &= \frac{\partial J}{\partial N_i} - \lambda_i^P \mu \frac{\partial u_i}{\partial N_i} P_i + \frac{1}{\tau}\left(\lambda_{i-1}^N - \lambda_i^N\right) \\ &\quad + \lambda_i^N \sigma \frac{\partial u_i}{\partial N_i} + \lambda_i^N h = 0\end{aligned} \tag{A.11}$$

with $\dfrac{\partial u_i}{\partial N_i} = \dfrac{k}{\left(k+N_i\right)^2}$

$$\Longrightarrow \lambda_{i-1}^{N} = \left[-\frac{\partial J}{\partial N_i} + \left(\lambda_i^P - \lambda_i^N\right) \mu \frac{k P_i}{\left(k+N_i\right)^2} - \lambda_i^N h\right] \tau + \lambda_i^N$$

Derivatives of the cost function J with respect to the state variables:

$$\frac{\partial J}{\partial P} = \frac{\partial J^{\mathcal{PP}}}{\partial P} + \frac{\partial J^{CHL}}{\partial P} \tag{A.12}$$

$$\frac{\partial J^{\mathcal{PP}}}{\partial P} = \frac{1}{\sigma_{\mathcal{PP}}^2}\left(R\mu u P - \mathcal{PP}_{obs}\right) \cdot \left(R \cdot \frac{\partial \mu}{\partial P} u P + R \mu u\right) \tag{A.13}$$

$$\frac{\partial J^{CHL}}{\partial P} = \frac{1}{\sigma_{chl}^2}\left(r_{chl} P - CHL_{obs}\right) \cdot r_{chl} \tag{A.14}$$

$$\frac{\partial J}{\partial N} = \frac{\partial J^{N}}{\partial N} + \frac{\partial J^{\mathcal{PP}}}{\partial N} + \frac{\partial J^{CHL}}{\partial N} \tag{A.15}$$

$$\frac{\partial J^{\mathcal{PP}}}{\partial N} = \frac{1}{\sigma_{\mathcal{PP}}^2}\left(R\mu u P - \mathcal{PP}_{obs}\right) \cdot R \mu P \cdot \frac{\partial u}{\partial N} \tag{A.16}$$

$$\frac{\partial J^{CHL}}{\partial N} = \frac{1}{\sigma_{chl}^2}\left(r_{chl} P - CHL_{obs}\right) \cdot \frac{\partial r_{chl}}{\partial N} \cdot P \tag{A.17}$$

$$\frac{\partial J^{N}}{\partial N} = \frac{1}{\sigma_{din}^2}\left(N - \left(NO_3 + NO_2\right)^{obs}\right) \tag{A.18}$$

A.2 NPZD-equations for one-dimensional simulations

Dissolved inorganic nitrogen

$$sms(N) = -J(z,\mu,u) + \Phi_p P + \Phi_z Z + \gamma D \tag{A.19}$$

Phytoplankton biomass

$$sms(P) = J(z,\mu,u) - \Phi_p - \Phi_p^* P^2 - G(\epsilon,g)Z \tag{A.20}$$

Herbivorous zooplankton

$$sms(Z) = [\beta G(\epsilon,g) - \Phi_z - \Phi_z^* Z]\, Z \tag{A.21}$$

Detritus

$$sms(D) = [(1-\beta)G(\epsilon,g) - \Phi_z^* Z]\, Z + \Phi_p^* P - \gamma D - w_s \frac{\partial D}{\partial z} \tag{A.22}$$

with the nutrient uptake rate $u = \frac{N}{k_{DIN}+N}$.

A Holling type III function is utilized for simulating the grazing:

$$G(\epsilon,g) = \frac{g\epsilon P^2}{g+\epsilon P^2} \tag{A.23}$$

The growth function $J(z,\mu,u)$ uses the minimum principle of von Liebig (1840):

$$J(z,\mu,u) = min(\overline{\mu}(z), V_p \cdot u) \tag{A.24}$$

with the analytical solution for the depth integrated light-limited growth $\overline{\mu}(z)$ according to Evans and Parslow (1985), integrating over the vertical grid box at depth z (Oschlies and Garçon 1999).

The maximal phytoplankton growth rate is temperature (T[^{o}C]) dependent and is calculated as follows:

$$V_p = \mu_m \cdot {q_{10}}^{cT}, \tag{A.25}$$

as used in Sarmiento et al. (1993) and Fasham et al. (1993).

VERTICAL LAYERS OF THE NPZD-MODEL			
Model Level	Depth of Grid Point	Depth of Grid Box Bottom	Thickness of Grid Box
1	5.50	11.00	11.00
2	17.00	23.00	12.00
3	29.00	35.00	12.00
4	41.00	47.00	12.00
5	53.00	59.00	12.00
6	65.50	72.00	13.00
7	78.50	85.00	13.00
8	91.50	98.00	13.00
9	104.50	111.00	13.00
10	118.50	126.00	15.00
11	140.50	155.00	29.00
12	179.55	204.09	49.09
13	232.60	261.10	57.01
14	295.03	328.95	67.85
15	370.21	411.47	82.52
16	462.51	513.54	102.07
17	577.37	641.19	127.65
18	721.47	801.74	160.55
19	900.89	1000.04	198.30
20	1125.04	1250.04	250.00
21	1375.04	1500.04	250.00
22	1625.04	1750.04	250.00
23	1875.04	2000.04	250.00
24	2125.04	2250.04	250.00
25	2375.04	2500.04	250.00
26	2625.04	2750.04	250.00
27	2875.04	3000.04	250.00
28	3125.04	3250.04	250.00
29	3375.04	3500.04	250.00
30	3625.04	3750.04	250.00
31	3875.04	4000.04	250.00
32	4125.04	4250.04	250.00
33	4375.04	4500.04	250.00
34	4625.04	4750.04	250.00
35	4875.04	5000.04	250.00
36	5125.04	5250.04	250.00
37	5375.04	5500.04	250.00

Table A.1: Vertical Levels of the Numerical Model. The units are given in meters

A.3 Algorithms and artificial objective– cost function

Preliminary studies were performed to simply suggest which optimisation algorithm together with its tuning parameters should be applied. The subject of the following experiments is to evaluate different optimisation algorithms and their configurations. An artificial cost function was designed such that certain criteria are fulfilled. First of all, the function must remain very simple and differentiable. Second, the dimensionality of the function should be increasable without any additional programming effort. Finally, the function needs to provide a variety of local minima solutions with different characteristics, e.g. deep narrow valleys with values that are close to the global minimum value, Figure (A.1).

$$\mathcal{J}_{14D}(p_i) = \sum_{i=1}^{i=14} c_i \left(\frac{1}{f_i + \frac{1}{a_i + f_i}} + f_i \right) - 10 \tag{A.26}$$

with

$$f_i = (p_i - b_i)^2 = (p-b)_i^2, i = 1, \ldots, 14 \tag{A.27}$$

And the derivatives of $\mathcal{J}$ with respect to the parameters are:

$$\frac{\partial \mathcal{J}}{\partial p_i} = 2 \cdot (p-b)_i \cdot \left[\frac{c_i \left(u_i^{-2} - 1 \right)}{\left(f_i + u_i^{-1} \right)^2} + 1 \right] \tag{A.28}$$

with

$$u_i = a_i + f_i, i = 1, \ldots, 14 \tag{A.29}$$

Depending on the different factors a_i, b_i and c_i it is possible to construct, besides the global minimum, a variety of local minimum solutions. For each additional parameter there exist three local minima. As the dimensions (the number of parameters) are increased to fourteen, the total number of possible local minima solutions becomes $3^{14} - 1 = 4782968$. In real data-assimilation experiments with ecosystem models it is expected that the total number of local minima will not exceed the one for this artificial cost function.

The local minima can be very different in shape and "depth". Keeping the different factors within a given range, the local solutions can be either in narrow "valleys" or within a large "plane". Such different characteristics of the cost function are a challenge for the minimization algorithm.

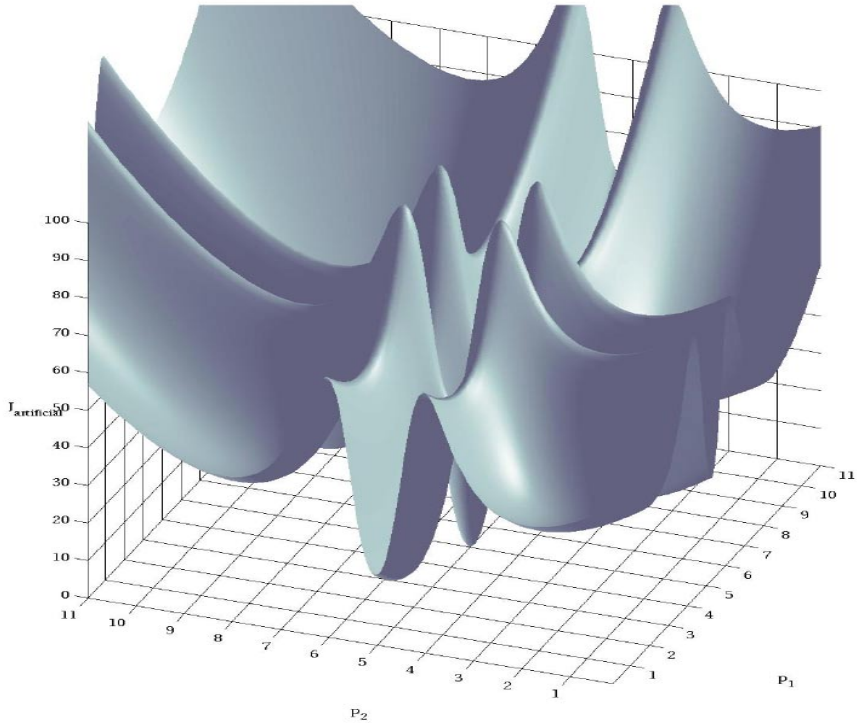

Figure A.1: Artificial cost function in two dimensions. The global minimum is, in this case, located in the centered valley ($b_1 = 5, b_2 = 5$). The scaling is chosen to be constant $c = 100$, while the coefficients are $a_1 = 0.1$ and $a_2 = 0.01$. The choice of the coefficients a_i determine the slopes within the narrow vallies, nearby the global minimum. The graphic also shows flat spots which should simulate cost function areas with very low sensitivity.

A.3.1 Methods tested for parameter optimisation

The descriptions, given here, are very brief and it is strongly suggested to read the original literature referred to.

Simulated annealing (SA)

Some aspects of the sound theory of statistical mechanics were adopted for the development of a heuristic optimisation method, known as simulated annealing (SA). (Kirkpatrick et al. 1983) constructed this algorithm for large and complex optimisation problems, describing its analogy with annealing in solids. The annealing is a stochastic, probabilistic process and can be simulated with a Metropolis algorithm (Metropolis et al. 1953). Originally, the Metropolis procedure simulates the thermal motion of atoms within a heat bath at a given temperature. Changes in energy are evaluated for small variations in the atom's positions. A set of these "positions" can be considered as one configuration. Any new configurations which decrease the energy level are unconditionally accepted. In the case of an increased energy level their

exists a probability that the configuration is retained, otherwise the original configuration will be utilized again for the next step. As the temperature slowly decreases, the probability of accepting configurations which produced an energy increase will become less. As stated by (Kirkpatrick et al. 1983), for an optimisation problem it is straightforward to apply this Metropolis procedure by substituting the energy with a cost function and replacing the configuration of atoms with a set of parameters. Hence, the temperature then becomes a control variable in the units of the cost function. In general, the strategy of the simulated annealing can be stated as:

- Initialization: Determine an initial temperature T_0 (or initial control variable) and produce an initial set of parameter values
- Iteration: Generate a series of random changes to the parameter's values (new configuration)
- Evaluate the cost functions for the series of parameter values
- Apply the Metropolis procedure
- Decrease temperature
- Restart iteration until stopping criterion is fullfilled

The origin of the computer code used for these preliminary investigations is unknown. Several tests and modifications were done before it could be succesfully applied. Major modification was due to the calculation of the initial temperature. Here, the best performance was achieved when the initial temperature is determined according to

$$T_0 = \frac{< \triangle J^+ >}{ln\, P} \tag{A.30}$$

as it was originally proposed by (Kirkpatrick et al. 1983). $< \triangle J^+ >$ is the average increase in costs when starting from an initial set of parameter guesses. P is the probability of simulations with higher costs to be accepted. In this study it was set to P=0.8. A similar approach was applied by Krüger (1993) who was the first to use the SA for oceanographic data-assimilation experiments.

Genetic and micro-genetic algorithm (GA and μGA)

The FORTRAN source code (used here) for the genetic and micro-genetic algorithm was originally developed to optimise the perfomance of a chemical laser model by Carroll (1996). The genetic algorithm follows evolutionary concepts such as selection, recombination and mutation (Holland 1975, Goldberg 1989). Selection accounts for the principle of "survival of the fittest". The algorithm comprises a population of size n which is initialized by a random selection of parameters in the parameter space. A set of parameters is represented by chromosomes of one indivdual of the population.

The initial population is regarded as the first generation. Four operations are performed when creating a new generation of individuals (parameter sets):

1) Fitness: The cost function is evaluated for each individual, representing one set of parameters (individual fitness=f_i). This is done for the whole population of size n, yielding a total fitness which is simply the sum of all ($\sum_i^n f_i$).

2) Selection: Two types of mechanisms are normally used, "expected value" and "tournament" selection respectively. Tournament selection is applied by randomly selecting pairs of individuals and the "fittest" of the pairs is allowed to mate (to recombine). The expected value selection accounts for the individual fitness and relates it to the total fitness. For maximizing the cost function the probability for recombination (or mating) is $p_i = f_i / \sum_i f_i$ whereas for minimising the costs it becomes $p_i^* = 1 - p_i = f_i / \sum_i f_i$.

3) Crossover: Crossover is part of the recombination process. The fittest individuals are to combine their chromosome informations (the parameter sets). For example, if one selected individual has the chromosomes 'abcde' and another has 'ABCDE' then the crossover point determines where informations of the pair are exchanged, mapping it into a child. A child may then contain chromosomes 'abCDE', having informations from both parents (from two parameter sets).

4) Mutation: There exists a small probability that one or more of the child's chromosomes become mutated. That is, the chromosomes may become 'XbCDE', where X is does not come from either of the parents.

The tournament selection and single-point crossover are used in this preliminary work and the selection/crossover process goes on until a new generation of size n is formed which then becomes subject to the mutation operation. Having a new generation of individuals (parameter sets), the four operations are repeated, yielding a new (better) generation of parameter sets. Here, the population size is 100 with maximal 260 generations. The crossover probability is 0.7 and the mutation probability is set 0.01. Furthermore, an elitism operator is applied which simply assures that the entire information (chromosomes) of the very best individual is retained in the optimisation process, avoiding that its 'good' chromosomes get lost during the tournament selection process.

The μGA is based on the above mentioned operations except that it does not contain the mutation operation and a probability of 1.0 is chosen for crossover. The major difference is due to the size of the population. A very small population is utilized for the μGA, if compared to the GA. Krishnakumar (1989) introduced the μGA for being able to optimise non-stationary functions. The principle functioning is briefly described. The μGA starts with a small population (here n=13) and evolves similarly to the GA but converges within few generations. The best individual, after convergence, is considered for recombination with a new random population. This process is repeated several times. Hence, while general convergence is achieved the whole parameter space is explored. This avoids premature convergence and introduces a greater variety of parameter combinations.

TESTS: 14D-optimisation

The following Figures show some results of some preliminary investigations performed with a fourteen dimensional artificial function as described before. Two dimensional parameter cross-sections are presented for the SA, GA, μGA and the gradient search algorithm (as utilized for the adjoint method).

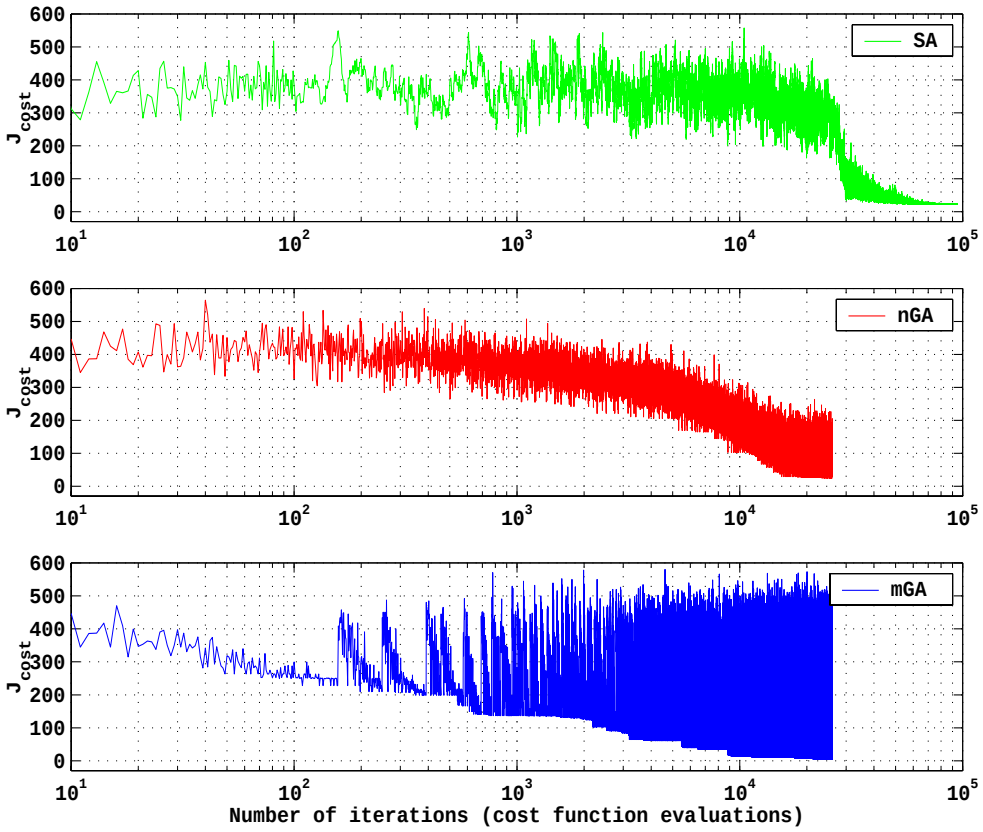

Figure A.2: Cost function values over number of iterations. TOP: Simulated annealing, MIDDLE: normal GA and BOTTOM: μGA

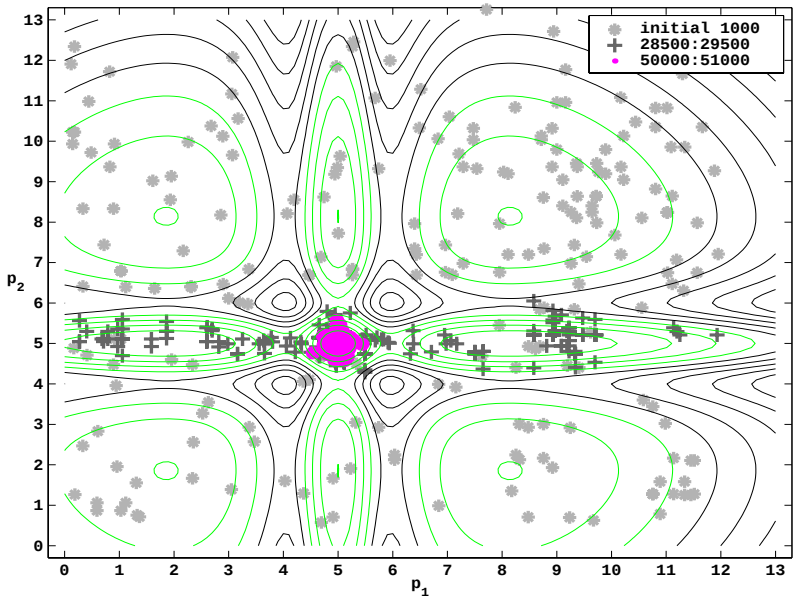

Figure A.3: Two dimensional cross-section of the parameter estimates during the search course with a simulated annealing algorithm. Each circle represents parameter values within the two dimensional parameter subspace. The markers refer to a certain range of iterations: Light gray '$*$' =iterations 1 to 1000, '+' = iterations 28500 to 29500 and '$\cdot$' =50000 to 51000 (black). Note, that 15 iterations happen within a loop with constant stepsizes for each parameter, which apparently reduces the number of parameter combinations in two dimensions.

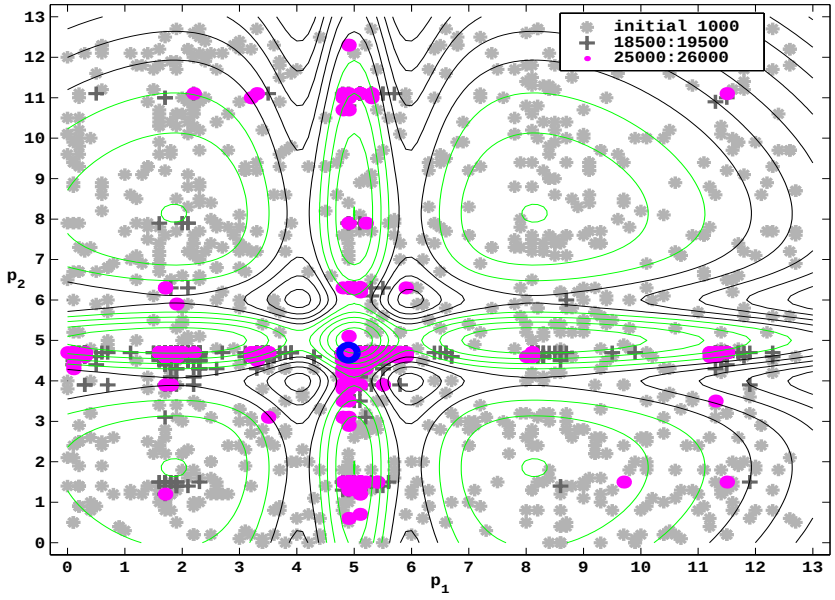

Figure A.4: Two dimensional cross-section of the parameter estimates during the search course with a normal GA. The markers refer to a certain range of iterations, see legend.

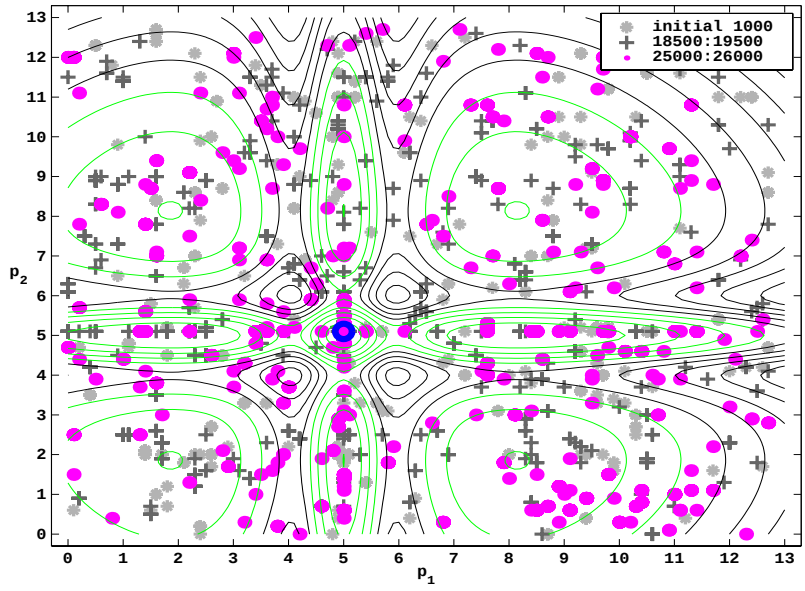

Figure A.5: Two dimensional cross-section of the parameter estimates during the search course with a μGA. The markers refer to a certain range of iterations, see legend. The μGA explores the entire parameter space until final convergence.

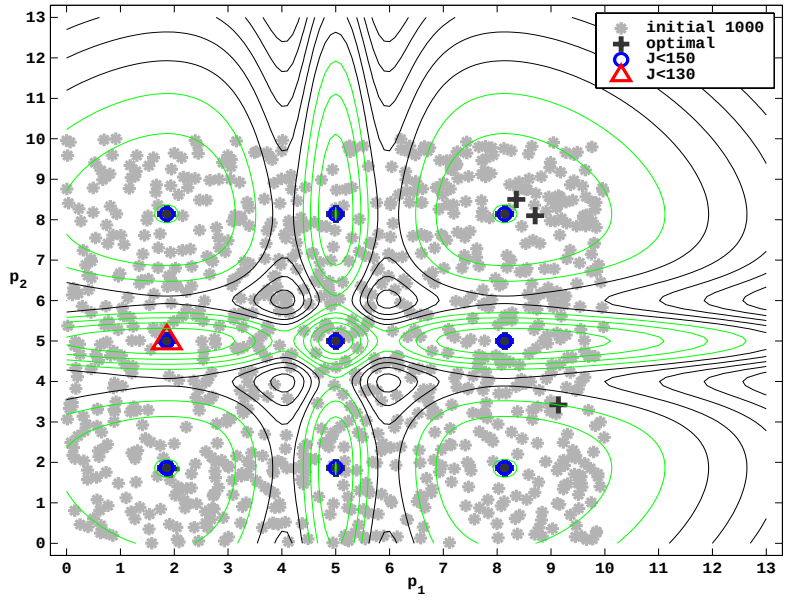

Figure A.6: Starting from different initial parameter values the gradient search (here variable metric algorithm) ends and the nearest local minimum.

Danksagung

Ich danke Prof. Dr. Jürgen Willebrand für die Idee, das Angebot zur Umsetzung dieser interdisziplinären Doktorarbeit und deren Betreuung.

Mein besonderer Dank richtet sich an Dr. Andreas Oschlies für seine Unterstützung und die Beantwortung vieler Detailfragen. Es waren insbesondere seine Motivation und Geduld die mir das nötige Vertrauen in diese Arbeit gegeben haben. Vielen Dank Andreas.

Als hilfreiche Partnerin begleitete mich Dr. Anja Engel durch die Welt der marinen Biologie. Sie verstand es, gute und verwertbare Ratschläge zu geben. Manche Vorschläge konnten auch in dieser Doktorarbeit berücksichtigt werden. Ich möchte mich dafür besonders bedanken.

Ich danke Dr. Christoph Völker für Korrekturvorschläge. Christoph ist ein wichtiger Diskussionpartner gewesen und ich freue mich auf eine weitere Zusammenarbeit.

Gleichermaßen danke ich Dr. Michio Kawamiya, der mir stets mit guten Tips zur Seite stand.

Weiterhin danke ich Dr. Wolfgang Koeve für die Bereitstellung von Beobachtungsdaten von der Station 47^{o}N 20^{o}W und Dr. Iris Kriest für ihre zahlreichen Erklärungen zu bestimmten biologischen Prozessen.

Ich danke Dr. Geoff Evans für Vorschläge zum zweiten Kapitel und für die Motivation, auf diesem Gebiet weiter zu arbeiten.

Ich danke den vielen Personen der Bereiche Theorie und Modellierung und biologische Ozeanographie, für ihre Bereitschaft zur Diskussion und den oftmals nötigen Anregungen, sowie den Mitarbeitern des Rechenzentrums IfM, für ihre Unterstützung.